Optimizing Patient Protection During Diagnostic Procedures -Developing Diagnostic Reference Levels at the Dr George Mukhari Hospital

M.Sc. Med (Medical Physics)

K E DUMELA

2010

OPTIMIZING PATIENT PROTECTION DURING DIAGNOSTIC PROCEDURES - DEVELOPING DIAGNOSTIC REFERENCE LEVELS AT THE DR GEORGE MUKHARI HOSPITAL

by

KHOMBO EUNICE DUMELA

RESEARCH DISSERTATION

Submitted in fulfillment of the requirements for the degree of

MASTER OF SCIENCE

in

MEDICAL PHYSICS

in the

FACULTY OF MEDICINE

at the

UNIVERSITY OF LIMPOPO

SUPERVISOR: Ms M.M. Jordaan
CO-SUPERVISOR: Dr A. C. Chamberlain

2010

DECLARATION

I declare that the dissertation hereby submitted to the University of Limpopo, for the degree of M.Sc (Medicine) Medical Physics has not previously been submitted by me for a degree at this or any other university; that it is my work in design and in execution, and that all material contained herein has been duly acknowledged.

KE Dumela (Miss) **30 April 2010**

200515686

ACKNOWLEDGEMENTS

I would like to thank the following people:

- Ms M. M. Jordaan from the Department of Medical Physics at the University of Limpopo (Medunsa Campus) for introducing me to radiology and her assistance and guidance throughout the study.

- Dr. A. C. Chamberlain from the Department of Medical Physics at the University of Limpopo (Medunsa Campus) for his assistance and guidance.

- Neo Kwanele Kgame for her assistance in editing the thesis.

- The Radiology department at the Dr George Mukhari Hospital for the use of the X-ray units and the radiographers who helped during data collection.

- Sellinah Dumela for her moral support throughout the study.

- Kulani Khosa for her moral support throughout the study.

- Petro van der Westhuizen for her moral support throughout the study.

- Sehloho Ntlamele for his support throughout the study.

- D. F Langa, R. Mhlonga, Dr M.S Sithole from the Department of Physics at the University of Limpopo (Medunsa Campus) for their assistance throughout the study.

The study was supported partially by the National Research Foundation (NRF).

Dedicated to my mom, Anicky Vulani; dad, James; my sisters, Talent and Vongani; my brothers: Akani, Mukondleteri, Amukelani and Ponani; my nieces: Vukona and Vuthsila.

ABSTRACT

Key words: Diagnostic reference levels (DRL**),** entrance surface dose (ESD), thermoluminescence dosimetry (TLD)

Introduction: Diagnostic reference levels (DRL's) are defined as a dose level set for standard sized patients or standard phantoms and are not for individual exposures and individual patients and are an efficient standard for optimizing the radiation protection of patients and are practically useful for more common examinations. The International Atomic Energy Agency (IAEA) recommends entrance surface dose (ESD) as DRL's in diagnostic radiology and are establish using a TLD on a patient/phantom surface.

Aim: To estimate entrance surface dose for different X-ray procedures.

Objectives: The objective of this study is to develop the diagnostic reference levels by assessing the dose received by a patient in radiographic exposure. This was achieved using different X-ray techniques to estimate the entrance surface dose for different examinations.

Method: The study was conducted at the Dr George Mukhari hospital using 5 different X-ray machines. Before the study commenced quality assurance was done on the machines. The following examinations were considered: Cervical spine (AP), cervical spine (LAT), Skull (AP), Skull (PA), Abdomen (AP), Pelvis (AP), Lumber spine (AP), Lumber spine (LAT), Chest (PA) and Chest (LAT). Thermoluminescence lithium fluoride (LiF) (TLD-100, 3.16 X 3.16 X 0.9 mm^3, Harshaw) and the Rando phantom were used to estimate the ESD's in mGy. Three TLD's were mounted on the top of the phantom in the centre of X-ray beam, external to the organ/tissue being imaged. The average dose was calculated for each radiograph and for each examination. The following technique factors were recorded: tube kilovoltage, focus-to-surface distance, focus-to-film distance, time and mA.

Results: The mean ESD's measured at the centre of X-ray beam on the surface of the phantom for the following examinations are: Cervical spine (AP), 2.99 (± 0.26) mGy; Cervical spine (LAT), 3.23 (± 0.34) mGy; Skull (PA), 3.50 (±0.37) mGy; Skull (LAT), 2.60 (± 0.26) mGy; Abdomen (AP), 4.18 (± 0.40) mGy; Pelvis (AP), 3.96 (± 0.33) mGy; Lumber spine (APS), 4.72 (± 0.39) mGy; Lumber spine (LAT), 8.56 (± 0.67) mGy Chest (PA), 0.72 (± 0.27) mGy and Chest (LAT), 1.03 (± 0.45) mGy.

Conclusion: The results of the individual exposure and the overall results of each examination were lower than reported in the literature except for the chest (PA). The determination of patient dose and the comparison with the international DRL's are an important factor in the optimization process in diagnostic radiology and it is of special concern for the patient's protection. The baseline of diagnostic reference levels for the Dr George Mukhari hospital has been established and the results obtained could be useful for future patient dose measurements in diagnostic radiology Department at the Dr George Mukhari hospital.

TABLE OF CONTENTS

LISTS OF TABLES

PAGE

LISTS OF FIGURES

PAGE

Chapter 1

RADIATON PROTECTION

1.1 Introduction

Since the discovery of X-rays in 1895 [Chougule, 2005], the use of X-rays has given tremendous benefit to societies worldwide. The increase in the medical application of X-rays has since given rise to the growing concern of potential health hazards associated with such. Medical imaging fulfils a crucial role in the diagnostic process. In diagnostic radiology, X-rays create images that help to diagnose the patient's medical condition [Seeram and Brennan, 2006] and are also useful in detecting some disease processes in soft tissue. Examples of such X-ray examinations are the common chest X-ray examinations, which can be used to identify lung cancer or pulmonary edema and abdominal X-ray examinations, which can detect ileas (blockage of the intestine), free air (from visceral perforations) and free gall stones or kidney stones.

Fluoroscopy is an image technique commonly used by physicians to obtain real time moving images of the internal structures of a patient through the use of a fluoroscope. X-ray of a person can be used to detect any abnormalities like broken bones, cancerous growths and tooth decay. [Capps III, 2006]. The increase in use of X-rays in hospitals has made medical exposure an important source of radiation in the collective dose of the population. However, in light of all the benefits of this discovery, it is to be noted that a radiation excess dose of X-rays is harmful to human beings. [Martin, 2007].

X-rays are ionizing radiation, which can potentially damage cells within the body. [Martin, 2007]. Ionizing radiation is known to cause harm. High radiation doses tend to kill cells, while low doses tend to damage or alter the genetic code of deoxyribonucleic acid (DNA) of irradiated cells. [Andreassi, 2004]. Radiation can cause cancer and there are no dose limits for patients receiving medical exposure as

part of their treatment or diagnosis**,** because the exposure must be justified by a net benefit to the patient and hence the clinical necessity supersedes any dose limitation. There is no dose below which there is a zero risk. [Cousins and Sharp, 2004]. Energy from ionising radiation breaks chemical bonds, releasing free radicals and ions that can damage DNA and proteins, short term radiation damage includes burns and hair loss. A long term effect of radiation injury includes cancer induction and cataract formation. [Furlow, 2004].

The biological effects fall into two categories: Stochastic effects refer to effects whose probability increases with increasing dose and for which there is no threshold dose (D_T) and tissue reactions are those in which the severity of the effect, rather than the probability, increases with increasing dose and for which there is a threshold dose. [Seeram and Brennan, 2006]. The International Commission on Radiological Protection (ICRP report No 60, 1990) recommends that all medical exposures should be subjected to the radiation safety principle of justification and optimization as stated by Obed *et al*, 2007. Diagnostic radiological procedures are justified if the benefits to the individual patient from the radiological image outweigh the individual detriment the exposure may cause. Once medical exposure has been justified, the principle of optimization is applied that is, the radiological examination must be carried out with equipment and exposure parameters that ensures doses to patients are as low reasonably practicable consistent with the intended diagnostic purposes. [Freitas and Yoshimura, 2009].

A dose assessment must be done to avoid unnecessary radiation during X-ray imaging or guidance must be given on dose levels. Physical parameters differ across populations therefore a specified procedure must be followed when imaging both small and large patient's volume. DRL's are an important method of minimizing radiation dose and radiation dose variation at a minimal cost to the radiology department. [Seeram and Brennan, 2006]. Dose measurement is acknowledged to be a vital part of the quality assurance process in diagnostic radiology and thermoluminescent dosimetry (TLD) is the recommended method of entrance dose measurement for "simple examinations". [Obed *et al*, 2007]. DRL's or reference levels (RV's) have been proposed by the International Commission on Radiological Protection (ICRP). [Vano *et al*, 2002].

DRL's are defined as a dose level set for standard procedures, for a group of standard sized patients or a standard phantom [Vano *et al*, 2002; Workman *et al*, 2009; Matthews and Brennan, 2008] and are not for individual exposures and individual patients. The European Union in 1997 introduced the use of DRL's as an efficient standard for optimizing the radiation protection of patients. [Compagnone *et al*, 2005]. DRL's are practically useful for more common examinations, or examinations which may involve high doses or are frequently performed such as chest posterior (PA) and lateral (LAT), lumber spine anterior posterior (AP), lateral (LAT), which give relatively high doses and pelvis, abdomen, skull posterior and lateral and cervical spine anterior posterior (AP) and lateral (LAT) which are frequently performed. [Frigran, 1999].

The International Atomic Energy Agency (IAEA, 1996) recommends Entrance Skin/Surface Dose (ESD) as dose descriptor for guidance levels in diagnostic radiography because it provides an indication of maximum skin dose and is useful for periodic checking of patient dose as stated in Obed *et al*, 2007. DRL's can be established using a TLD on the patient's skin or phantom's surface to measure the ESD including backscatter. An alternative method is to measure the dose-area-product (DAP) using a DAP meter. [Medical Council, 2004]

1.2 Ionizing radiation interactions with tissue

When ionization radiation, such as X-rays, interacts with living tissue, it is the breaking of molecular bonds that causes damage. If the radiation passes through the tissue without absorption, there would be no biological effects and no radiological image would be produced. Whenever radiation is absorbed, chemical changes are produced virtually immediately and subsequent molecular damage follows in a short space of time (seconds to minutes). It is after this, during a much longer time span of hours to decades, which the biological damage becomes evident [Farr, 1997] as shown in Figure 1.1.

Human skin includes three main layers: from shallow to deep they are in sequence epidermis, basal layer and dermis. The epidermis is mostly composed of dead cells

and their function is mainly for protection. The thickness of the epidermis varies at different sites of the human body: approximately 4–5 $mg.cm^{-2}$ thick on the head, neck, trunk and upper parts of limbs, 10-15 $mg.cm^{-2}$ at the back of hands and feet and 30–40 $mg.cm^{-2}$ on the palm and soles. The basal layer, located at the lowest part of the epidermis, is the skin cell provider and is considered to be where the skin damage occurs while receiving a radiation dose. [Lin *et al*, 2001]

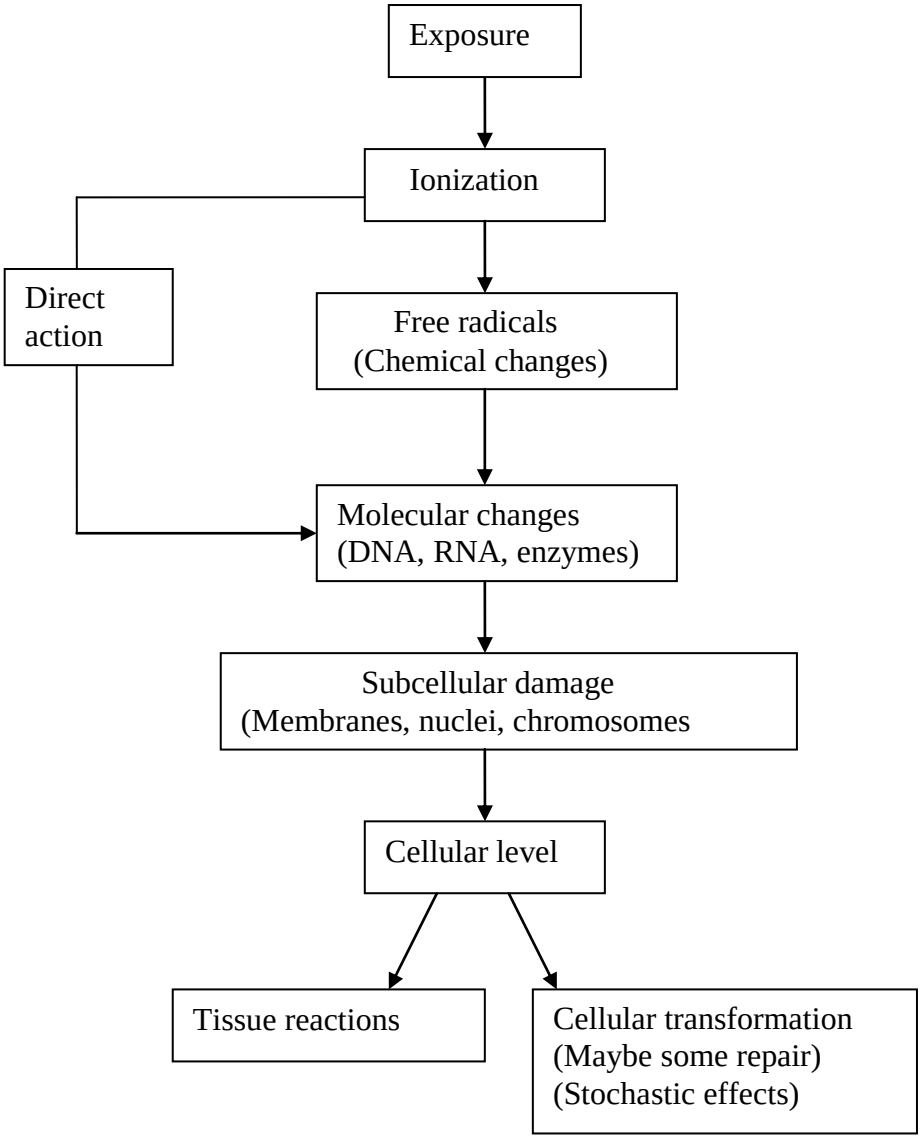

Figure 1.1: Chain of events following exposure to ionization radiation. [Farr, 1997].

Energy from ionizing radiation breaks chemical bonds, releasing free radicals and ions that can damage deoxyribonucleic acid (DNA) and proteins. [Furlow, 2004]. A free radical is an atom or molecule carrying an unpaired orbital electron in the outer

shell. An orbital electron does not only revolve around the nucleus of an atom but also spins around its own axis. The human body is comprised of 80% of water and the interaction with an X-ray photon or charged particle will occur mainly in the water molecules. The hydrolysis of water is brought about by the transfer of energy from alphas, betas or electrons to the water molecules.

$$H_2O \rightarrow H_2O^+ + e^- \qquad 1.1$$

H_2O^+ is an ion radical. An ion is an atom or molecule that is electrically charged because it has lost or gains an electron. Free radicals contain an unpaired electron in an outer shell making them highly reactive. H_2O^+ is charged and has an unpaired electron; consequently, it is both an ion radical and a free radical. The ion radical reacts with another water molecule to form the highly reactive hydroxyl radical ($OH^\bullet$) [Hall and Graccia, 2006]:

$$H_2O + H_2O^+ \rightarrow H_3O^+ + OH^\bullet \qquad 1.2$$

The biological effects of ionization radiation come primarily from the damage to the DNA. At the molecular level, damage to the DNA can occur by either of two processes. With direct attack, a high-velocity electron ionizes or excites part of the DNA molecule itself into a chemically unstable state:

$$DNA + energy \rightarrow DNA^\bullet \qquad 1.3$$

Alternatively, the damage can be caused by indirect attacks from chemically reactive free radicals that exist briefly, but long enough to diffuse into the vicinity of the DNA. The hydrolysis product most effective in damaging DNA molecules is the hydroxyl radical. [Wolbarst, 1993]. DNA carries genetic information and any DNA damage to a somatic cell, if not repaired, can be transmitted to the daughter cells. According to Eggermont *et al* [2006], there is evidence that cellular responses can include genetic change because they can continue to occur (genetic instability) for longer periods over many cell generations.

The number of illnesses in which genetics plays a role is high and there are numerous studies that show radio sensitivity is linked to cancer that depends on the individual's genetic history. Genetic effects are the result of a mutation produced in the reproductive cells of an exposed individual that are passed on to their children. These effects may show up as birth defects or other conditions in the future to the children of the exposed individual and succeeding generations. [Andreassi, 2004].

1.3 Biological effects

The biological effects of radiation can be broadly grouped as stochastic effects and tissue reactions (nonstochastic effects).

1.3.1 Stochastic effects

Stochastic affects occurs if an irradiated cell is modified rather than killed and then subsequently reproduces. Stochastic effects refer to effects whose probability increases with increasing dose for which there is no threshold dose (D_T). [King *et al*, 2002]. Any dose, no matter how small, has the potential to cause harm. When harm occurs and the damage becomes apparent years after exposures, it is called late effects. ICRP defines stochastic effects as a lethal cancer or a mutation expressed in the first two post-irradiation generations. [Osibote and de Azeredo, 2008]. Examples of stochastic effects are leukaemia, hereditary or genetic effects and cancer induction. [Seeram and Brennan, 2006].

1.3.2 Tissue reactions

Tissue reactions is when the number of cells lost in an organ or tissue is so great that there is a loss of tissue function [King *et al*, 2002] and which the severity of the effect, rather than the probability, increases with increasing dose and for which there is a threshold dose. [Seeram and Brennan, 2006]. There is no harm below this threshold. [King *et al*, 2002]. The effects are also called early effects and involve high exposures, which with the exception of interventional procedures are unlikely to occur

in diagnostic radiology. Examples of tissue reactions are ulceration, cataracts, epilation, hemalogic damage and skin erythema. [Seeram and Brennan, 2006; King *et al*, 2002].

1.4 Protection

The goal of radiation protection in the radiology department is to prevent tissue reactions by ensuring that radiation doses are kept well below relevant threshold doses and to minimize the probability of stochastic effects. [Seeram and Brennan, 2006].

1.4.1 The principle of protection

The radiation protection system for patients subjected to medical exposures in diagnostic radiology is governed by the principles of justification and optimization, including the consideration of diagnostic reference levels. [Freitas and Yoshimura, 2009].

1.4.1.1 Justification principle

In diagnostic medical exposures, patient dose has to be kept to the minimum necessary to achieve the required diagnostic objective, taking into account norms of acceptable image quality established by appropriate professional bodies and relevant levels for medical exposure. This means that exposures resulting in doses above clinical acceptable minimum doses must be avoided as any decision that alters the radiation exposure situation should do more good than harm. Diagnostic radiological procedure is justified to the individual patient from the medical diagnosis obtained with the radiological image balancing the individual detriment the exposure may cause. Once a medical exposure has been justified, the radiological examination must be carried out with equipment and exposure parameters that ensure doses to patients are as intended for the specified diagnostic purpose. [Freitas and Yoshimura, 2009].

1.4.1.2 Optimization principle

Optimization in medicine is an important tool to avoid unnecessary high doses. Optimization of protection does not mean dose reduction but that diagnostic information should be the deciding factor. [Reference Levels in Diagnostic X-rays, 2006]. Optimized images have to be established based on the characteristics of the image receptor, the patient habitus and the purpose of the radiological examination. There are no dose limits for patients and the goal of radiation protection is to shield patients from unnecessary exposure. The principle of optimization is the essential control mechanism used for this purpose. [Seeram and Brennan, 2006].

There is considerable scope for the reduction of dose without loss of diagnostic information. Optimization is paramount that the image obtained contains the diagnostic information as intended and the strategies for the reduction of patient doses, without loss of diagnostic accuracy, are therefore of great interest to society and have been focused on general terms by the ICRP (ICRP 1996). In accordance with the recommendations of the ICRP, it is often useful in the management of the operation to establish values of measured quantities above the same specific action or decision should be taken. [Reference levels in diagnostic X-rays, 2006]. Patient dose measurement is widely considered as an important quality control tool in medical radiology. Quality assurance in diagnostic radiology provides a satisfactory (lowest achievable level) result. [Mortazavi *et al*, 2004].

Because diagnostic medical procedures are usually for the direct benefit of the patient, less attention has been given to optimization of protection in medical exposures. [Reference levels in diagnostic X-rays, 2006]. The ICRP publish dose limits for the general public and for occupationally exposed workers that remove the probability of tissue reactions and hold the risk of stochastic effects. [Matthews and Brennan, 2008; Seeram and Brennan, 2006].

ICRP 60 IR(ME)2000 recommendations requires dose constraints or diagnostic reference levels to be established. A tool in radiology to optimize radiation protection of the patient is the DRL. [King *et al*, 2002]. Once a medical test exposure of ionizing radiation has been decided, the corresponding exposure must be optimized: the radiation dose which is delivered must be kept as low as reasonably achievable (ALARA principle). [Bourguignon, 2009].

1.5 A tool for optimization: Diagnostic reference levels (DRL's)

The DRL is a measure of patient dose and serves as a quantitative guide to optimize patient protection. DRL's for diagnostic medical exposures represent thresholds for the internal investigation of potentially poor practice within radiology departments. [Shrimpten *et al*, 1999]. DRL's are supplement to professional judgment and do not provide a dividing line between good and bad medicine. DRL's apply to medical exposure, not to occupational and public exposure. They have no link to dose limits or dose constraints. [Gray *et al*, 2005].

The existing international DRL's are set after international trials in many hospitals as shown in Table 1.1, which were set by collecting the mean dose of each hospital and placed them in increasing order, a horizontal line marks the point below which three quarters of the hospitals' values occur and the value at the third quartile or 75^{th} percentile line became the reference level. [Seeram and Brennan, 2006; Vano *et al*, 2002].

DRL's were introduced to reduce patient exposure and to increase image quality and the most important purposes of the introduction of DRL's in clinical practice is to verify that the DRL used is below the defined European values. [Compagnone *et al*, 2005]. The overall goal of DRL's is to manage patient dose in diagnostic radiology using the principle of optimization of radiation protection. [Seeram and Brennan, 2006].

Table 1.1: Reference values of entrance surface dose for adult patients. [ICRP, 2001]

Examination	Projection	Entrance surface dose (mGy)
Skull	AP/PA	5
	LAT	3
Chest	PA	0.4
	LAT	1.5
Abdomen	AP	10
Pelvis	AP	10
Lumber spine	AP/PA	10
	LAT	30
Cervical spine	AP	1.25[a]
	LAT	

Note: [a] is from U.S. (AAPM 1999), PA: posterior-anterior projection; LAT: lateral projection; AP: anterior-posterior projection.

The existing ICRP guidelines for DRL's are that they are:

- An easily measured dose quantity such as absorbed dose in air or entrance surface dose for a tissue equivalent phantom or representative patient.
- An investigation level, which, if exceeded, should lead to a review of procedures and equipment in order to evaluate whether the approaches to optimizations are adequate and to indicate when consideration of dose reducing measures should be made.
- Intended for use as a simple test for identifying situations where the level of radiation dose to patients are unusually high.
- Supplementary to professional judgment. [Seeram and Brennan, 2006].
- DRL's promote progression toward an optimum range of dose values for a particular examination and reduce the number of high or low dose exposures. [Matthews and Brennan, 2008].

1.5.1 Local diagnostic reference levels

Local diagnostic reference levels (LDRL's) can be established by comparing the values with international or national DRLs. The DRL's concept can be adopted to calculate new ESD values that are to be used locally (i.e. inside the hospital) as LDRL's. The study of LDRL's is encouraged as a further step in patient dose optimization, beyond the simple use of national or international (European) DRL's. [Compagnone *et al*, 2005].

Where a national or European DRL's is not available for an examination type, there is no requirement to set a DRL's locally for that particular examination. [Pillai and Jain, 2004]. Any relevant local patient dosimetry data should be reviewed to identify examinations where established local practice will support the adoption of a DRL's value lower than the equivalent national or European DRL's. [Pillai and Jain, 2004; Workman *et al*, 2009].

When assessing local performance, mean dose from a group of people with a weight close to 70 kg or experiments with phantoms can be compared with the DRL (ESD per radiography). In order to obtain meaningful values a significant number of patients (10 is a minimum) or experiments with phantoms are required. Thus for each given procedure, the average of these measurements can be considered as the local dose indicator of the department. [Bourguignon, 2009].

1.5.2 Setting DRL's

DRL's can be established using TLD's on the patient skin to measure entrance surface dose (ESD) including the backscatter. An alternative method is to use a dose area product (DAP) meter. [Medical Council, 2004].

1.5.2.1 Guiding principles for setting a DRL are:

- The national, regional or local objectives are clearly defined, including the degree of specification of clinical and technical conditions for the medical imaging task.
- The DRL selected is drawn from relevant regional, national or local data.
- The DRL value can be obtained with ease.
- The DRL quantity is indicative of the relative change in patient risk for the given medical imaging task.
- The intended application of the DRL is clear. [Matthews *et al*, 2008]..

After the DRL's have been established, to produce an image of film with an acceptable level of contrast, the exposure must be within a relatively narrow range of doses. The exposure factors used will be optimized through the experience of the radiographers and charts employed for each X-ray unit. The chart provides a guide to the best factors for different examinations for patients of standard build. However, adjustments will need to be made for patients of different physical parameters (for example weight and height). [Rampado and Ropolo**,** 2004]

1.6 Patient dose monitoring methods

The estimate of organ and effective doses can be made from entrance surface dose measurements. [Shrimptan *et al*, 1999]. Average skin entrance dose measurements can provide an estimate of the skin entrance dose to typical patients, and one can use receptor entrance dose measurements to scale doses from the different imaging modes. The estimate can be improved to some extent by recording the average kilovoltage peak and tube current (milliampere) for patient and appropriate scaling of the skin entrance dose. [Mahesh, 2001].

1.6.1 Entrance surface dose (ESD)

Entrance surface dose (ESD) in mGy is the important parameter in assessing the dose received by a patient in a single exposure. The European Union has defined this physical parameter as one to be monitored as a diagnostic reference level in hope of optimizing patient dose. It is possible to evaluate ESD either by direct measurement on a suitable phantom using ionisation chambers or thermoluminescent dosimeters (TLD's) on a patient [Compagnone *et al*, 2005] or a phantom. [Seeram and Brennan, 2006]. The reason for assessing the skin doses is that the dose is greater at the surface, where radiation enters the body, and the skin is the main organ for which the possibility of tissue reaction may occur. [Martin *et al*, 1999].

Martin [2007] defined ESD as the dose to the skin at the point where an X-ray beam enters the body and includes both the incident air kerma (kinetic energy released in a medium) and radiation backscattered from the tissue.

1.7 Methods for estimating entrance skin dose

There are currently a number of methods available by which one can estimate or measure the patient skin dose. They may be classified as direct or indirect methods.

1.7.1 Direct method

The direct method of skin dose estimation involves use of small detectors placed on the patient's skin or phantom's surface at the beam entrance location. Types of detectors used for direct method are: thermoluminescence dosimetry (TLD's), photographic film and diodes or metal-oxide semiconductor field-effect transistor (MOSFET). Use of TLD's is potentially the most accurate way of determining actual skin dose and the dosimeters are taped to the patient's skin or phantom's surface. [Rampado and Ropolo**,** 2004; Mahesh, 2001].

1.7.2 Indirect method

The most convenient and widely used method for indirect monitoring is the DAP. [Mahesh, 2001]. The DAP is the product of dose in air (kerma) within the X-ray beam and the beam area, and is therefore measure of the radiation that enters a patient. [Martin, 2007]. It can be measured using an ionization chamber fitted to the X-ray tube as shown in figure 1.2 and does not depend on the distance from the X-ray tube.

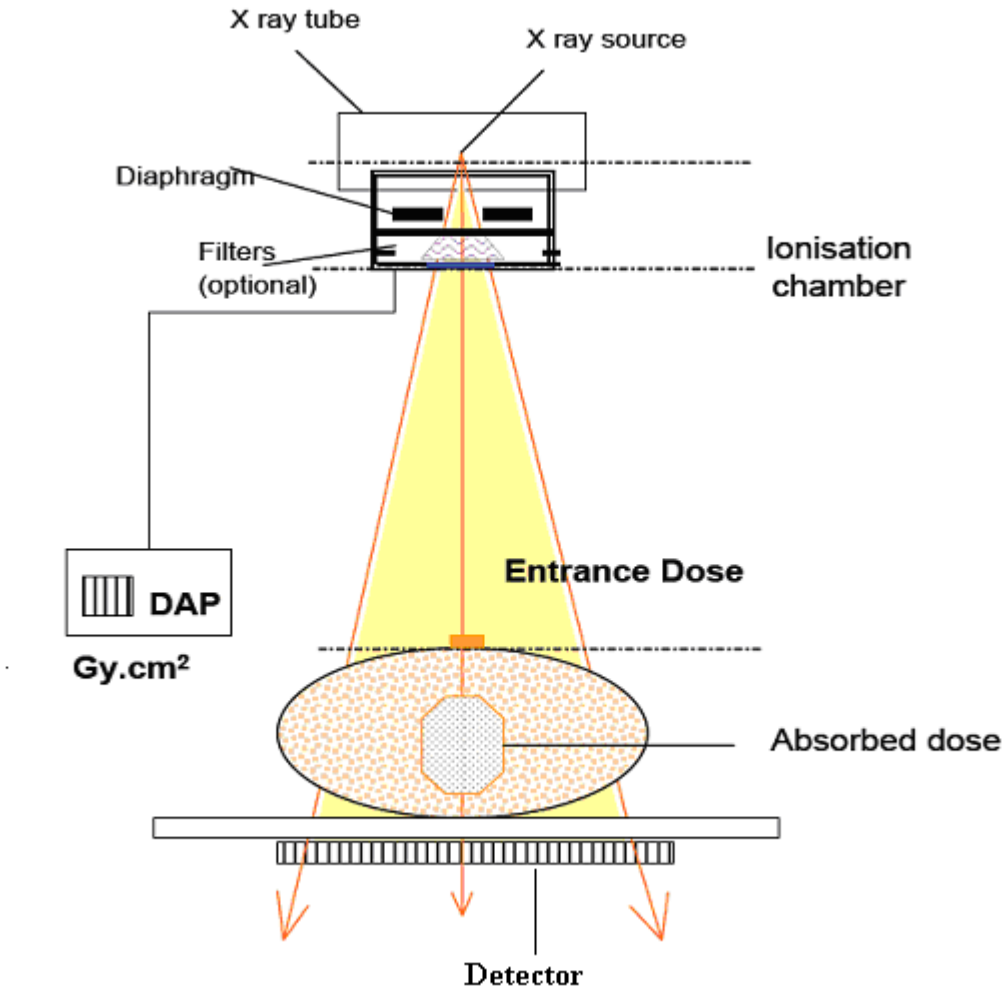

Figure1.2: Typical setup of measuring the DRL's. [Bourguignon, 2009]

From the DAP ($Gy.m^{-2}$), the ESD is obtained by:

$$ESD = (DAP / area).f.BSF \qquad 1.4$$

Where area is the irradiated area of the patient (cm^2), f is the ratio of the mass absorption coefficients of muscle and air, and BSF is backscatter factor. [Ruiz-Cruces *et al*, 2000]. The disadvantage of a DAP meter is that they do not measure backscatter radiation which increases patient dose because the measuring device is located at the X-ray tube rather than at the patient or phantom. [Seeram and Brennan, 2006].

1.8 Options for investigating entrance surface dose (ESD)

Two options are available for establishing examination specific dose values: using phantoms or patients.

1.8.1 Patient investigation

The number and types of patients sampled within each radiology centre is important if the values are to be representative. In early work on adult DRL's, it was recommended that a minimum of 10 patients with a mean sample weight of 70 kg (± 5 kg) participate. However, weight depended on the individual patient within any particular state or region. [Seeram and Brennan, 2006].

1.8.2 Phantom investigation

For the study involving phantoms, the phantom must be of a specific size and type and an anthropomorphic Rando phantom is ideal for this purpose as it represents a tissue equivalent adult human with anatomical structures, so image quality can be monitored to some extent. The advantage of phantom based studies over patient studies is that patient variability is eliminated and fewer measurements are required. Phantom studies allow for quicker investigation, a rapid and thorough examination of equipment-based variability and regular updates or reference levels and also eliminates the problem of globally defining the "standard-sized patient". [Seeram and Brennan, 2006].

1.9 Exposure factors in diagnostic radiography

The exposure factors are:

- Tube voltage expressed in kilovoltage.
- Tube current expressed in milliampere.
- Duration of exposure expressed in seconds.
- Focus film distance and focus skin distance.
- Focal spot size.

The minimum patient dose is generally obtained at high kilovoltage with corresponding low milliampere. The X-ray intensity decreases with distance from the focal spot according to the inverse square law. The dose at the position of the patient skin is greater than the dose at position of the film by the factor $(FFD/FSD)^2$, where FSD is the focus-skin/surface distance. As the ratio of the FFD to FSD is decreased the entrance skin to film-plane dose ratio is increased. The X-ray beam is collimated to the region of interest as the dose increases with an increase in field size.

Chapter 2

BASICS OF X-RAY PRODUCTION

2.1 Introduction

X-rays are electromagnetic radiation and were discovered in 1895 by Wilhelm Conrad Roentgen in experiments where beams of electrons moving in an evacuated glass tube struck the wall of the tube, some invisible, mysterious rays were emitted that caused a faint luminosity (fluorescence) on the nearby sheet of paper impregnated with chemicals. He also found that these rays could darken photographic film and also recognized the possible medical application of these rays for making images of the tissues inside the human body, especially by bones.

2.2 Productions of X-rays

X-rays are produced by energy conversion when a fast moving stream of electrons is suddenly decelerated in the target (anode) of an X-ray tube. X-rays for medical procedures or research purposes are produced in the standard way**,** are generated by an X-ray tube, a vacuum tube that uses a high voltage to accelerate electrons released by a hot cathode to a high velocity. The high velocity electrons collide with a metal target, the anode, creating the X-rays.

A medical X-ray tubes target is usually tungsten (95%) or more the crack-resistance alloy of tungsten rhenium (5%). Tungsten is chosen as the target material because it satisfies the requirement of the anode material for the production of X-rays. It has a high atomic number 74, which makes it more efficient for the production of X-rays. It has a high melting point; it is able to withstand the high temperature produced. Tungsten melts at 3370°C. Tungsten is a good material for the absorption of heat and for the rapid dissipation away from the target area. [Curry *et al*, 1990].

2.2.1 Characteristic X-rays

Characteristic X-rays are the result of an interaction where a high speed electron of kinetic energy E_o interacts with one of the atom's orbital electrons such as K, L or M electron, leaving the atom ionized. The original electron will move from the collision with energy $E_O - \Delta E$, where ΔE is the energy of given to the orbiting electron. [Khan, 2003].

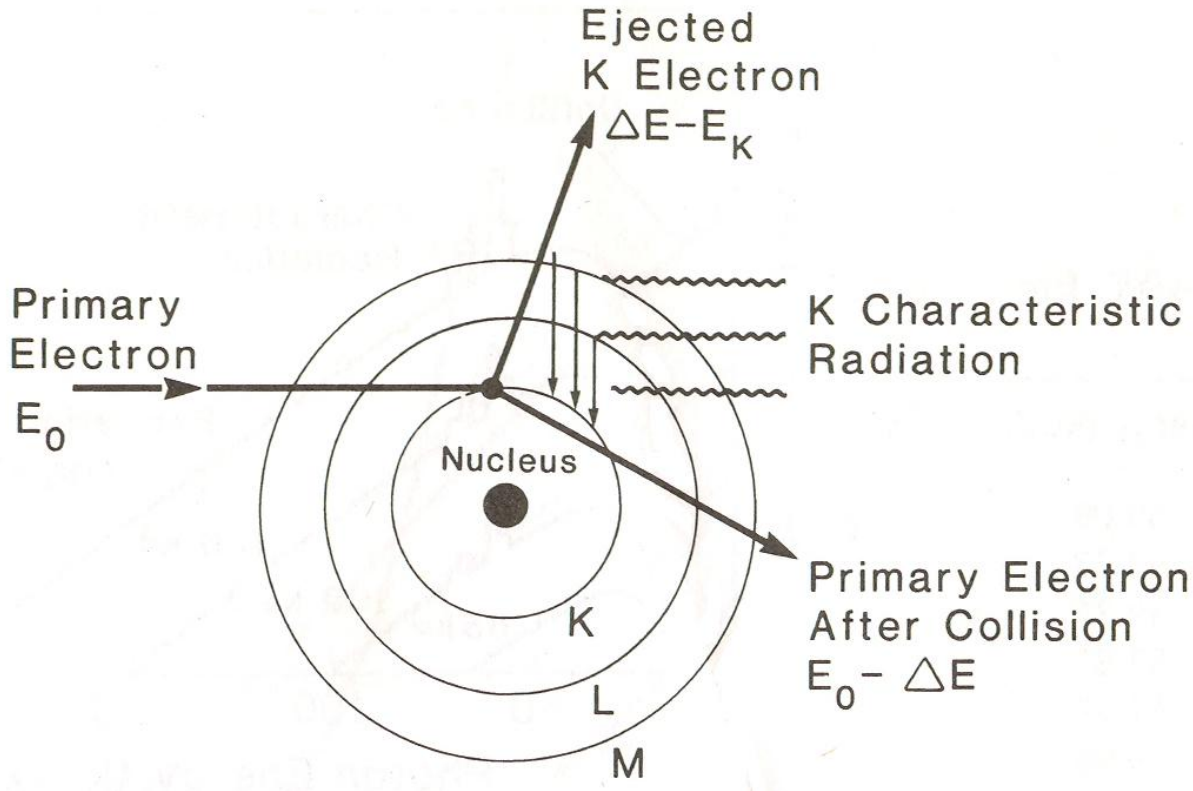

Figure 2.1: Illustrating the production of characteristic radiation. [Khan, 2003].

If ΔE is greater than E_K, the binding energy of the orbiting electron, it will be ejected, leaving a vacancy in the electron shell of the atom. The atom, left with net positive charge will pull in another electron from the outer shell, to fill the vacancy. Energy lost as an electron falls from the outer orbit down into an inner orbit is emitted as a characteristic X-ray. Characteristic radiation makes only a small portion overall of an X-ray beam, but since it can possess high energies that penetrate through the patient to the film, it is important in producing a radiographic image. [Carroll, 2003].

2.2.2 Bremsstrahlung X-rays

If the electron passes near the atomic nucleus, the positive attraction of the nucleus will cause it to brake or slow down. This deceleration in the speed of the electron represents a loss of kinetic energy, and that energy which is lost is emitted as an X-ray photon. X-rays produced by this interaction are called Bremsstrahlung (braking radiation) and they account for the vast majority of the total X-ray beam. High speed electrons may pass by the nucleus at various distances from it. The closer an electron approaches the nucleus, the greater its deceleration due to the stronger pull of the nucleus, thus the more energy will be lost and the higher the energy (keV) of the emitted X-ray. [Carroll, 2003].

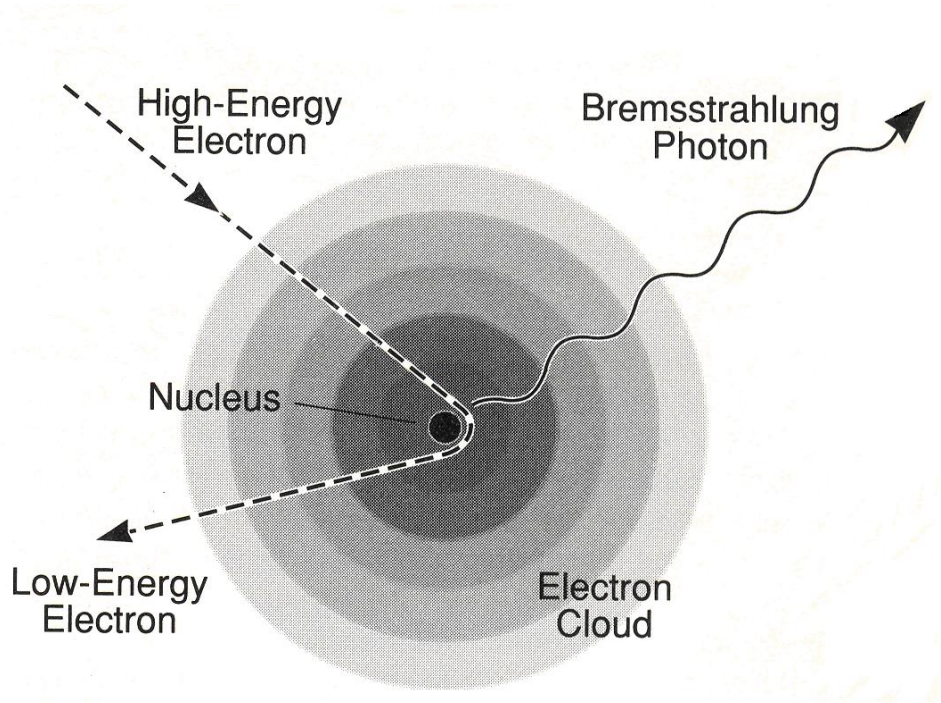

Figure 2.2: Production of Bremsstrahlung photons. [Wolbarst, 1993].

2.2.3 The x-ray spectrum

X-rays generated by diagnostic machines contain a spectrum of photon energies that range up to a maximum determined by the voltage applied across the X-ray tube gap. The peak tube voltage (kVp) determines the maximum photon energy (expressed in kilo electron volts (keV).

2.2.3.1 Continuous X-ray spectrum

The emission spectrum is called a continuous emission spectrum. The energies of the photons emitted may range from zero to a maximum value. The general shape of the continuous spectrum is the same for all X-ray machines. The maximum energy that an X-ray can have is numerically equal to the kVp across the tube. The greatest number of X-ray photons is emitted with energy approximately one-third of the maximum photon energy. The number of X-rays emitted decreases rapidly at very low photon energies and below 5 keV nearly reaches zero.

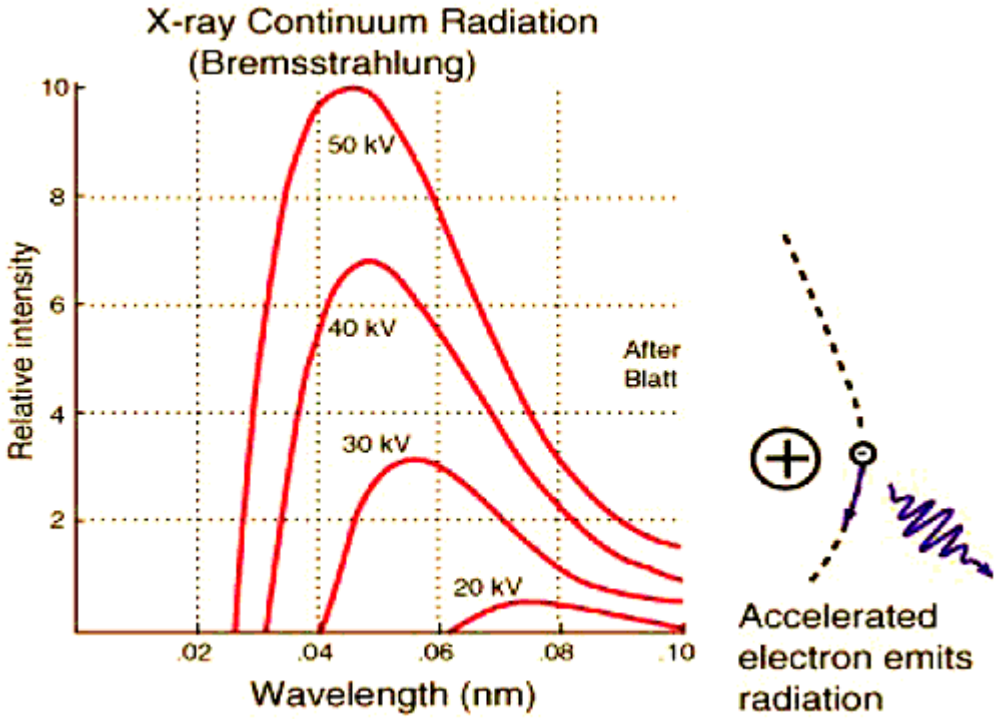

Figure 2.3: The continuous spectrum. [Nave, 2009].

2.2.3.2 The discrete spectrum

Characteristic X-rays are emitted from heavy elements when their electrons make transitions between the lower atomic energy levels. The characteristic X-rays emission which is shown as two sharp peaks in the illustration below occur when vacancies are produced in the n=1 or K-shell of the atom and electrons drop down

from above to fill the gap. The X-rays produced by transitions from the n=2 to n=1 levels are called K- alpha X-rays and those for the n=3 transition are called K-beta X-rays. The continuous distribution of X-rays which forms the base for the two sharp peaks at left is the Bremsstrahlung component. [Nave, 2009].

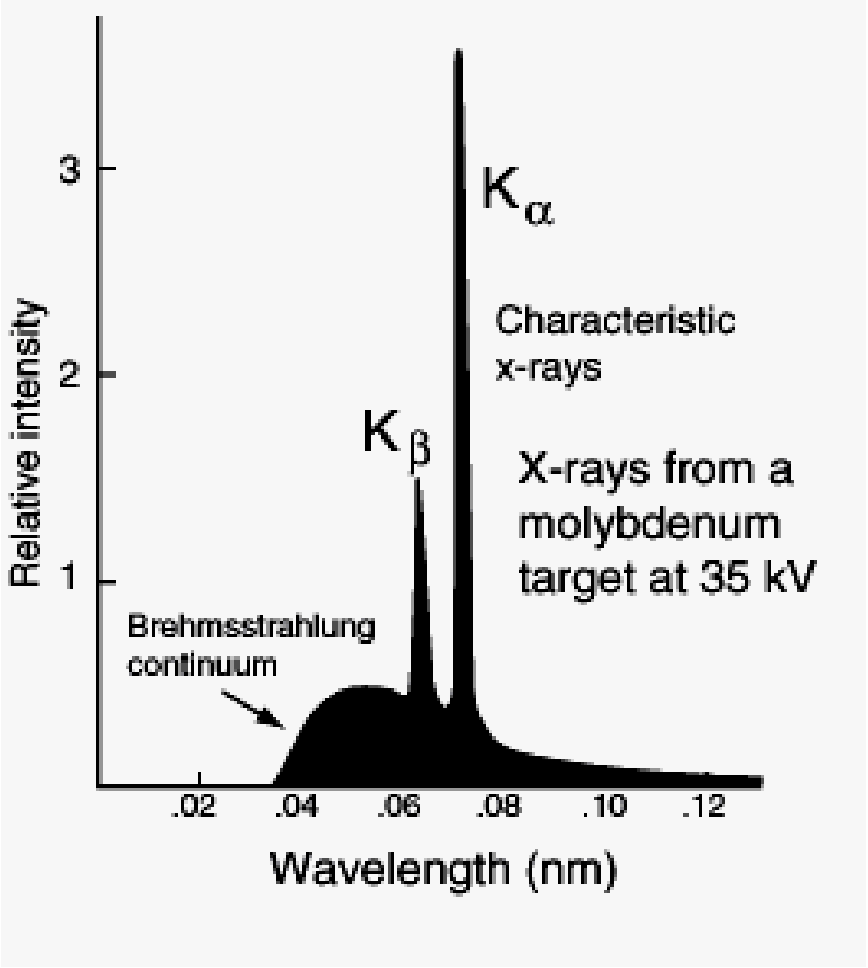

Figure 2.4: Discrete spectrum. [Nave, 2009].

2.3 The X-ray tube

An X-ray tube is an energy converter. It receives electrical energy and converts it into two other forms: X-radiation and heat. The heat is an undesirable by-product. X-ray tubes are designed and constructed to maximise X-ray production and to dissipate heat as rapidly as possible.

2.3.1 Components of X-ray tubes

All X-ray tubes consist of a cathode and anode assembly, placed inside an evacuated glass or envelope as shown in figure 2.5. The cathode assembly consists of a tungsten filament wire which is coiled to form a spiral and mounted in a shallow focusing cup. When the filament is heated, by the application of an electric current, electrons are boiled off the surface of the wire in a process of thermionic emission. If the anode is made positive with respect to the filament, these electrons will be attracted to the anode and will constitute an electron current which can be measured with an external millammeter. This mA meter is usually located on the console of the X-ray machine, along with a meter indicating the accelerating voltage.

The anodes (positive electrodes) of X-ray tubes are of two types, rotating and stationary. The anode material used should satisfy the following requirements:

- High conversion efficiency for electrons into X-ray. High atomic number Z materials are favoured since the X-ray intensity is proportional to Z
- High conductivity so that the heat is removed rapidly
- High melting point so that the large amount of heat released causes minimal damage to the anode
- A low vapour pressure, even at very high temperature, so that atoms are not boiled off from the anode
- Suitable mechanical properties for anode construction

In a stationary anode the target area is pure tungsten (W) (Z=74, melting point 3370ºC) because it satisfies the requirements of the anode material mentioned above and its ability to be shaped into many forms. Originally rotating anodes were made of pure tungsten. However, at the high temperatures generated in the rotating anode, deep cracks developed at the point of impact of the electrons. The addition of 5-10% rhenium (Rh) (Z=75, melting point 3170ºC) greatly reduced the cracking by increasing the ductility of tungsten at the high temperature. [Dendy and Heaton, 1987; 1999].

2.3.2. Anode

2.3.2.1 Stationary anode

The anode of a stationary anode X-ray tube consists of a small plate of tungsten, 2- or 3 mm thick, that is embedded in a large mass of copper. The tungsten plate is square or rectangular in shape, with each dimension usually being greater than 1cm.

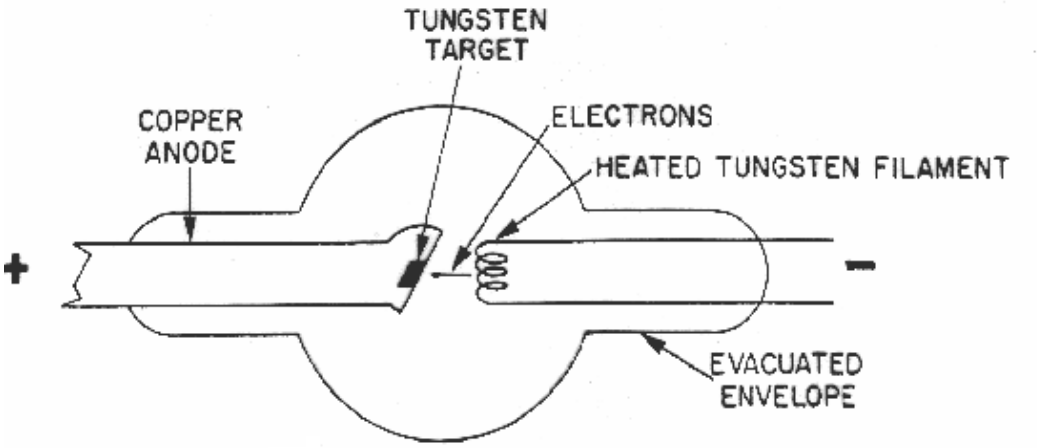

Figure 2.5: The major components of a stationary anode X-ray tube.
[Curry *et al*, 1990].

2.3.2.2 Rotating anode

Rotating anodes have a high rate at which energy deposited in the small target of an X-ray tube heats the target to a very high temperature. Rotating anodes increase the area of tungsten that absorbs energy from impinging electrons, reducing the temperature attained by the anodes. Rotating anodes are also composed of mixture of tungsten with other elements. [Hendee and Ritenour, 1992].

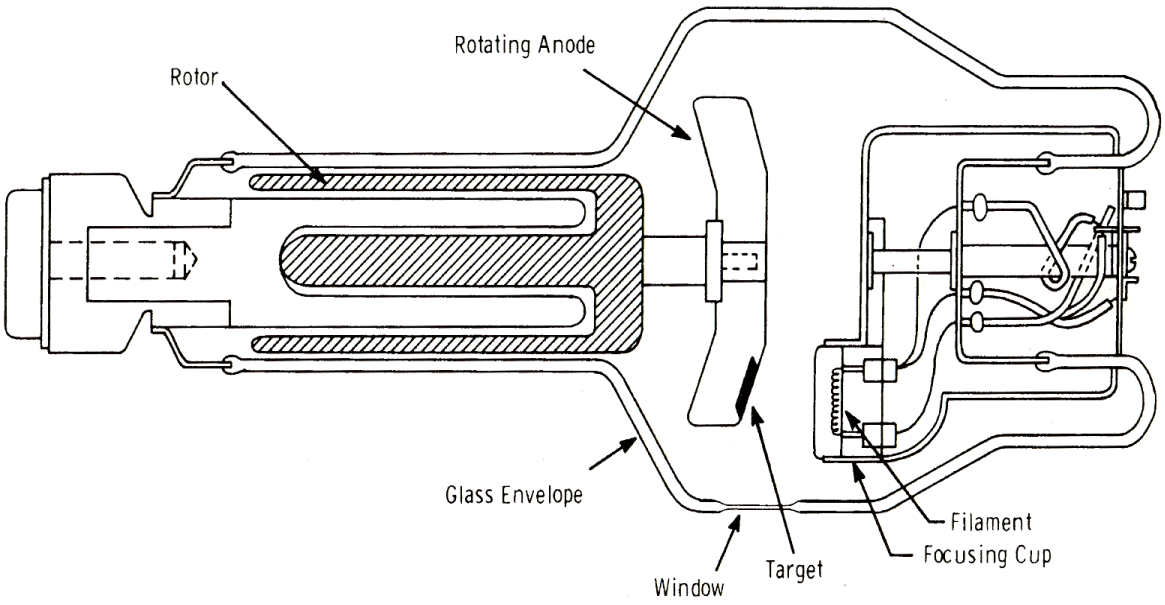

Figure 2.6: The principal parts of a modern rotating anode X-ray tube. [Martin, 2006].

The rotating anode is shaped like a disc and the front surface of the disc is coated with an alloy of tungsten and rhenium. The anode disc is connected to a motor shank which is part of the motor. When the motor is switched on, the shank spins at the same time that the filament is being heated. By spinning the anode disc, the target surface struck by the electron beam is constantly changing. The heat is distributed across a larger surface area and the anode is less likely to melt. [Carroll, 2003].

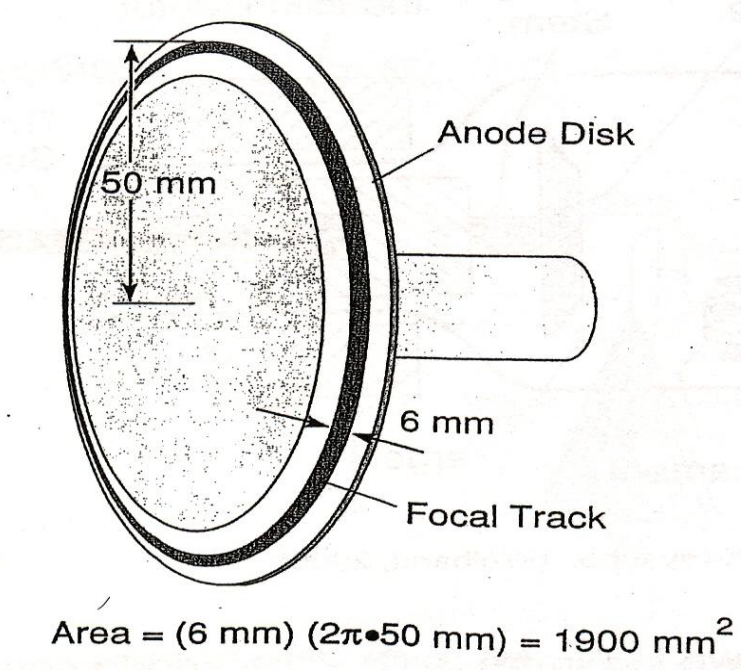

Figure 2.7: Rotating anode disk. [Wolbarst, 1993].

The example of the rotating anode with a larger target area can be illustrated with a simple calculation. Stationary anode, with a focal spot of 6 mm high and 1.5 mm wide has an area of 9 mm^2. A 100 mm diameter rotating anode (Figure 2.7), with a focal track of 6 mm wide and 2π 50 mm = 314 mm long has an area of 190 mm^2. The area of the rotating anode is about 200 times bigger than the area of the stationary tube for electrons to irradiate, with no apparent increase in the focal spot. [Wolbarst, 1993].

2.3.2.3 Target angle

The anode surface of a diagnostic X-ray tube and the stream of electrons from the cathode are not perpendicular to one another. The anode surface is canted by the anode angle. The target angle is typically 10° to 20º, that is, the anode is tilted 10º to 20º away from facing the stream of electrons head-on. When high velocity electrons are incident on a target, the useful Bremsstrahlung X-rays are emitted predominantly in the direction perpendicular to the electron stream and out of the target. (X-ray photons starting off in the opposite direction are fully absorbed by the anode). The angular dependency of Bremsstrahlung production is an important factor in the design of the anode. A thick target aligned perpendicularly to the electron flow would absorb most of the photons created in it. With a target that is overly canted, on the other hand, the focal spot would be too large. The target angle should be close to that which gives rise to the greatest usable X-ray beam intensity. [Wolbarst, 1993].

2.3.2.4 Focal spot size

The focal spot is defined as the area of the tungsten target that is bombarded by electrons to produce X-rays. The focal spot size is determined by the dimensions and position of the filament and construction of the focusing cup. Since less than 1% of the energy carried by the electrons is converted into X-rays, the anode can get very hot and can be damaged unless this bombarding source of heat energy is uniformly distributed over a sizeable area. This need to distribute heat energy conflicts with the fact that the small focal spots are best for producing good radiographic detail because X-rays stream from the target as though from a point source. [Martin, 2006].

2.3.2.5 Line focus principle

Two approaches are used to provide a small focal spot and take advantage of the need for a large impact area to allow greater heat loading: the line focus principle and the rotating anode. X-rays emerging from the tube can be made to appear to emanate from a small area if the anode is constructed with an angle perpendicular to the incident beam. The angles are shown in figure 2.8, range from 10° to 20°. This construction is called the line focus principle, which causes the emitted X-rays to project an apparent focal spot that is considerably smaller than that of the actual area being bombarded. The size of the projected focal spot is directly related to the sine of the angle of the anode. Focal spot size is expressed in terms of the apparent or projected focal spot, and the sizes are typically 0.3, 0.6, 1.0, and 1.2 mm. [Martin, 2006].

2.3.2.6 Heel effect

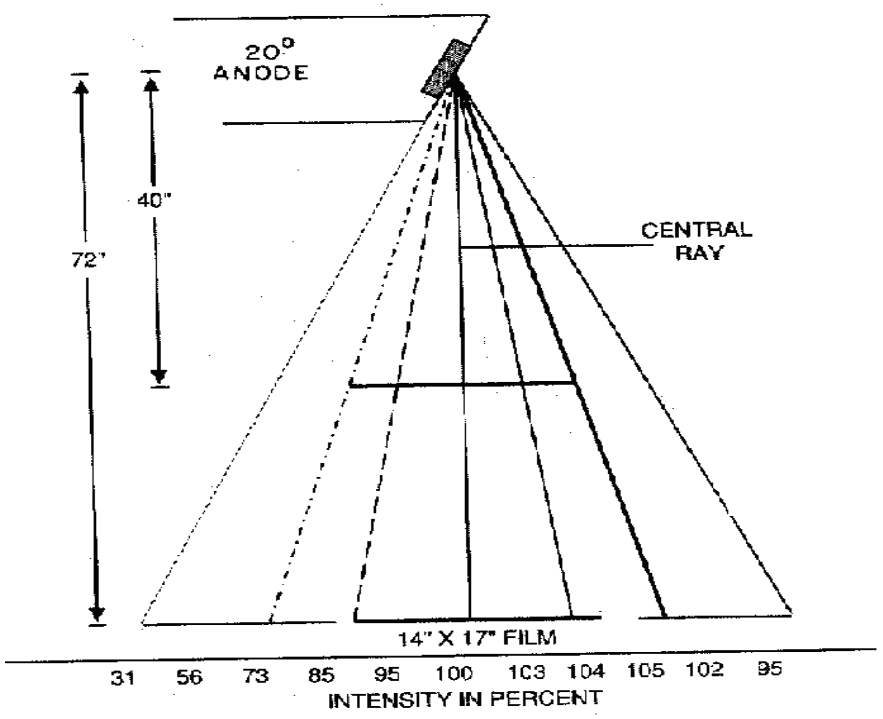

Figure 2.8: Reduction in X-ray intensity due to the heel effect. [Martin, 2006].

Electrons interact with target atoms at various depths into the target. The X-rays that constitute the useful beam are emitted from depth in the target toward the anode side

and must transverse a greater thickness of target material than the X-rays emitted in the cathode direction of the target. The intensity of X-rays emitted through the heel of the target is reduced because they have a longer path through the target to escape and there is an increase in absorption of those rays. This is called the heel effect. Generally the smaller the anode angle, the larger the heel effect. The differences in radiation intensity across the useful beam of an X-ray can vary as much as 45%. [Bushong, 1997].

2.3.3 Tube envelope and housing

The envelope

The envelope is made of thick walled glass and is constructed under very clean conditions to a high precision to provide adequate insulation between cathode and anode. It provides a vacuum seal to the metallic components that protrude through it. At the manufacturing stage, great care was taken to achieve a very high level of vacuum before the tube is finally sealed. If the residual gas molecules are bombarded by electrons, the electrons may be scattered and strike the walls of the glass envelope, thereby X-ray tube will have ceramic insulation between the tube and the anode and cathode connections. The presence of atoms or molecules of gas or vapour in the vacuum will have deleterious effects on the performance of the X-ray tube.

The tube housing

The tube housing is used to:

- Provides an X-ray window-which filters out some low energy X-rays
- Contains the anode rotation power source
- Provides high voltage terminals
- Insulates the high voltage
- Allows precise mounting of the X-ray tube envelope
- Contains the cooling oil. [Dendy *et al,* 1987; 1999].

2.3.4 Cathode assembly

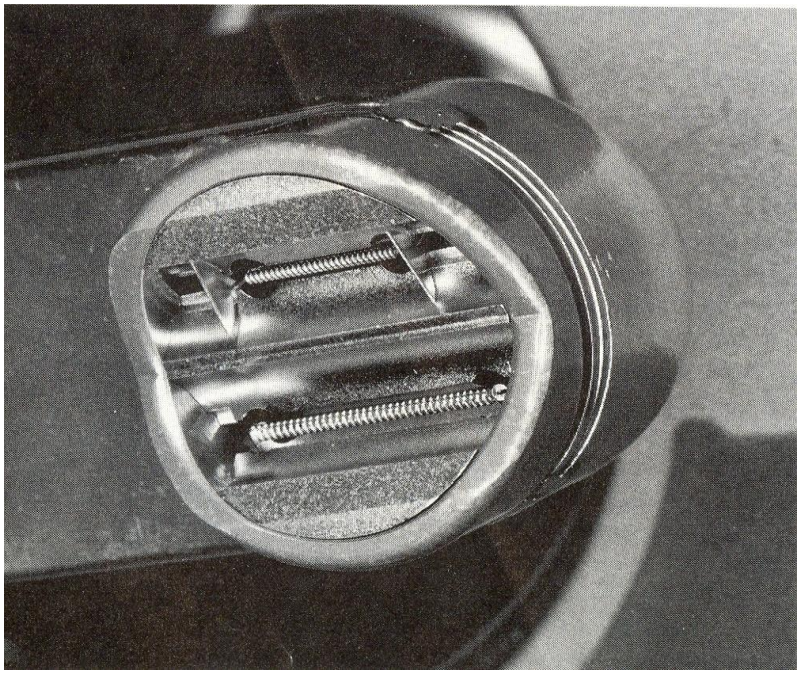

Figure 2.9: The cathode assembly of a dual-focus tube. [Wolbarst, 1993].

The cathode is used to expel electrons from the electrical circuit and focus them into a well-defined beam aimed at the anode. The typical cathode consists of a small coil of wire (filament) recessed within a cup-shaped region. [Sprawls, 1995]. The cathode assembly consists of one or more filaments in a focusing cup as shown in figure 2.9. The small filament is used for high resolution imaging and the larger filament is used when higher intensities are needed. It spreads the heat out over a larger focal region on the anode. [Wolbarst, 1993].

When the current flowing through the filament is sufficiently high, about four amperes and above, the outer-shell electrons of the filament atoms are boiled off and ejected from the filament. This is called thermionic emission. Filaments are made of tungsten. Tungsten provides higher thermionic emission than other metals because of its high melting point compared with 1500°C or less for all other metals. [Bushong, 1997] as discussed in section 2.2 and 2.3.1.

2.3.4.1 Filament size

The filament must be large enough to give a practical electron density but not too large, since this will cause focusing problems. The controlling factors are maximum operating filament temperature and filament size. In practice filament current is not switched on and off after each exposure but is kept on standby mode (about 5 mA) and increased to operating current (4.5 to 5.5 A) for exposures. When an exposure is made, a preparation switch is first depressed which starts the anode rotating and increases the filament temperature from standby mode. [Dowsett *et al*, 1998].

2.3.4.2 Electron focusing

During the X-ray exposure, the anode of the X-ray is positively charged and the cathode is negatively charged. As a result of this, the electron space charge is emitted from the negative cathode and attracted to the positive anode. The situation which would arise if both the cathode and anode were flat plates is shown on Figure 2.10

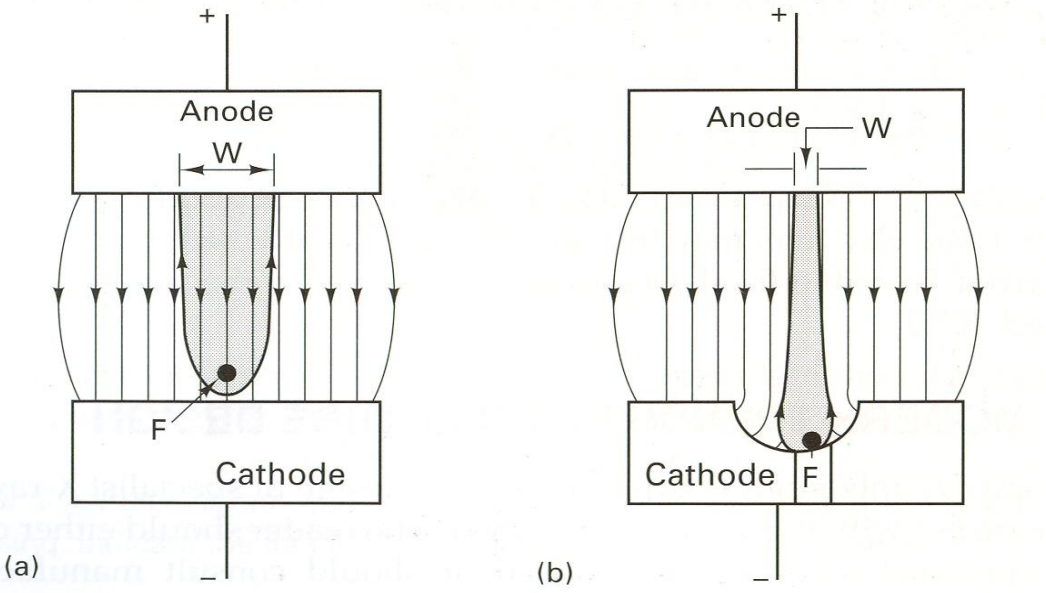

Figure 2.10: Simplified explanation of the focusing of electrons in the X-ray tube. [Graham, 1996].

Figure 2.10(a) shows the result of no focusing cup on the cathode and in Figure 2.10(b) the concave focusing cup directs the electrons from the thermionic emitter F

towards the central axis, so that they strike smaller area (W) on the anode. The electric force field consists of parallel lines starting at the anode and finishing at the cathode. Electrons are emitted from the filament, F, and are attracted to the positive anode and the electrons repel each other so the plume of electrons will increase in size as it travels across the X-ray tube.

The area W on the anode represents an unacceptably large focal area as this would produce a large geometric bluntness on the resulting radiograph. To overcome this problem, focusing cup is used as shown in Figure 2.10(b). The thermionic electrons from F now experience two forces, the one towards the central axis of the beam is greater than the force of electrostatic repulsion between the electrons and the plume of electrons is focused on to a small area of the anode-W in Figure 2.10(b). [Graham, 1996].

2.3.4.3 Grid-controlled X-ray tubes

Conventional X-ray tubes contains two electrodes (anode and cathode). The switches used to initiate and to stop an exposure with these tubes must be able to withstand the large charges in voltage applied between the cathode and anode. A grid controlled X-ray tube contains its own "switch" which allows the X-ray tube to be turned on and off rapidly. The third electrode is the focusing cup that surrounds the filament. In conventional X-ray tubes a focusing cup is electrically connected to the filament. This focusing cup helps to focus the electrons on the target. [Curry *et al*, 1990].

2.3.5 Saturation voltage

When the filament of an X-ray tube is heated, a space charge is produced. When a potential difference is applied between the cathode and anode, electrons flow from the filament to the anode to produce the tube current. If the potential difference applied across the tube is insufficient to cause almost all electrons to be pulled away from the filament the instant they are emitted, a residual space charge will exist about the

filament. The residual space charge acts to limit the number of electrons available and thus it limits the current flowing in the X-ray tube.

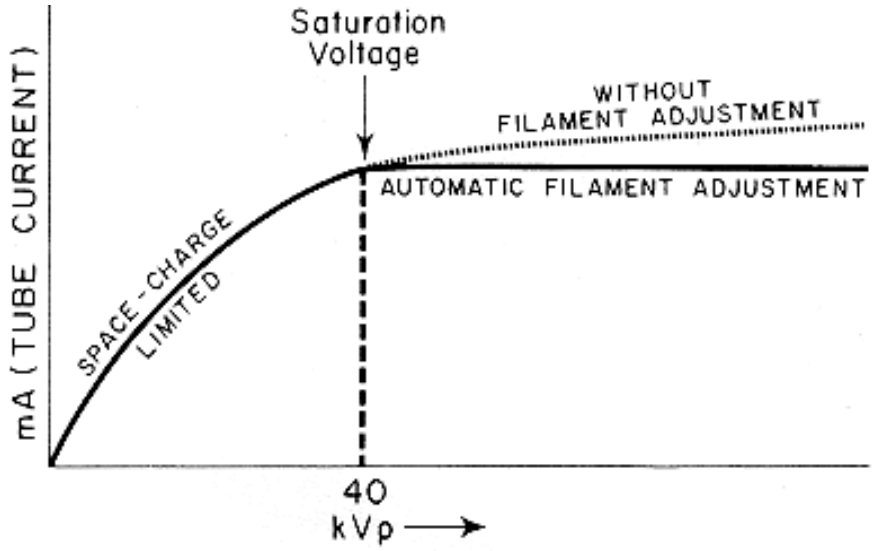

Figure 2.11: Saturation voltage. [Curry *et al*, 1990].

From Figure 2.11, up to about 40 kVp, there is an increase in kilovoltage that produces a significant increase in X-ray tube current even though filament heating remains the same. Above 40 kVp (saturation voltage), further increases in kilovoltage produces very little change in tube current and space charge has no influence on current flowing in the X-ray tube. In this region the current is determined by the number of electrons made available by the heated filament and is said to be emission-limited or temperature-limited. [Curry *et al,* 1990].

2.3.6 X-ray tube kilovoltage and milliampere

Two sources of electrical energy are required and are derived from the alternating current (AC) mains by means of transformers. The figure 2.12 shows:

- The filament heating voltage (about 10 V) and current (about 10 A).
- The accelerating voltage between the anode and cathode. This drives the current of electrons flowing between the anode and cathode (‘tube current’, ‘milliampere’, or ‘mA’).

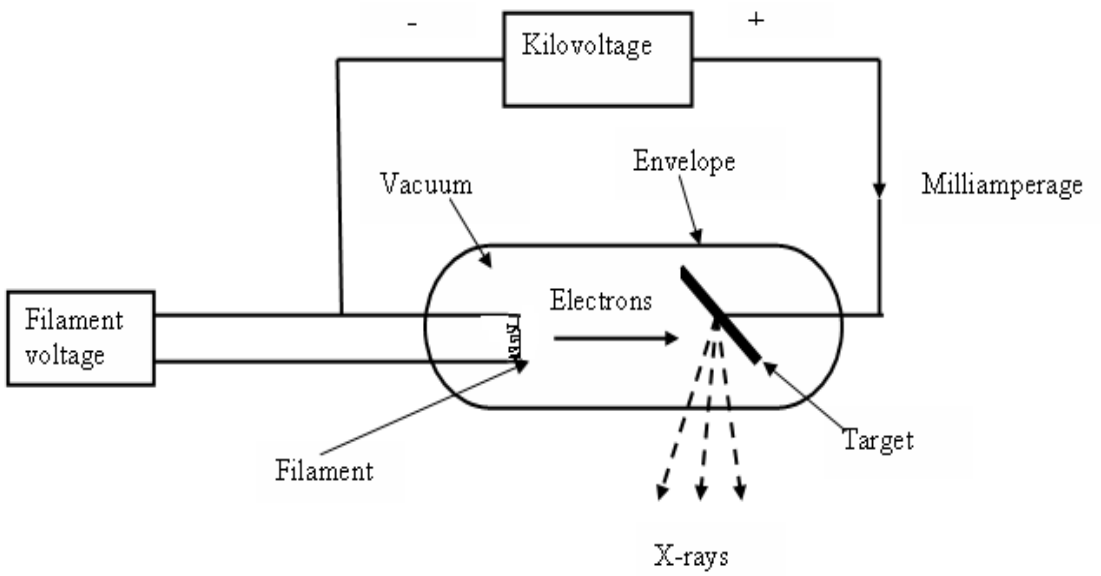

Figure 2.12: An X-ray tube and its power supply. [Farr, 1997].

The mA is controlled by varying the filament temperature. A small increase in filament temperature, voltage or current produces a large increase in tube current. [Farr, 1997].

2.3.7 Tube vacuum

To prevent collision between molecules of air and electrons accelerated between the filament and target, X-ray tubes are evacuated to a pressure of less than 10^{-5} mm Hg. Removal of air reduces deterioration of the hot filament by oxidation. The method of evacuation includes “out gassing” procedures to remove gas occluded in components of the X-ray tube. [Hendee and Ritenour, 1992].

2.4 Rating of X-ray tube

2.4.1 Heat unit

The heat unit is defined as the product of current (mA), kVp and time (sec) for the single phase power supplier. [Curry et al, 1990]. The high rate of energy deposited in

the target of X-ray tubes heats the target to a very high temperature. The maximum-energy ratings are provided for the target, anode, and housing of an X-ray tube. These ratings are expressed in heat units, for single phase electric power.

Number of heat units (HU) = (Tube voltage) (Tube current) (Time)

$$= (Vp)(mA)(sec)$$

If the tube voltage and current are constant, then l HU=1J of energy. For three phase power, the number of heat units is computed as

Number of heat units (HU) = (Tube voltage) (Tube current) (Time) (1.35)

$$= (Vp)(mA)(sec)(1.35)$$

Energy ratings for the anode and the tube housing are expressed in terms of heat storage capacities which indicate the total number of heat units that may be absorbed without damage to these components. To determine whether the target of an X-ray tube might be damaged by a particular combination of the tube voltage, tube current, and the exposure time, rating charts furnished with the X-ray tube should be consulted. [Hendee *et al,* 1992].

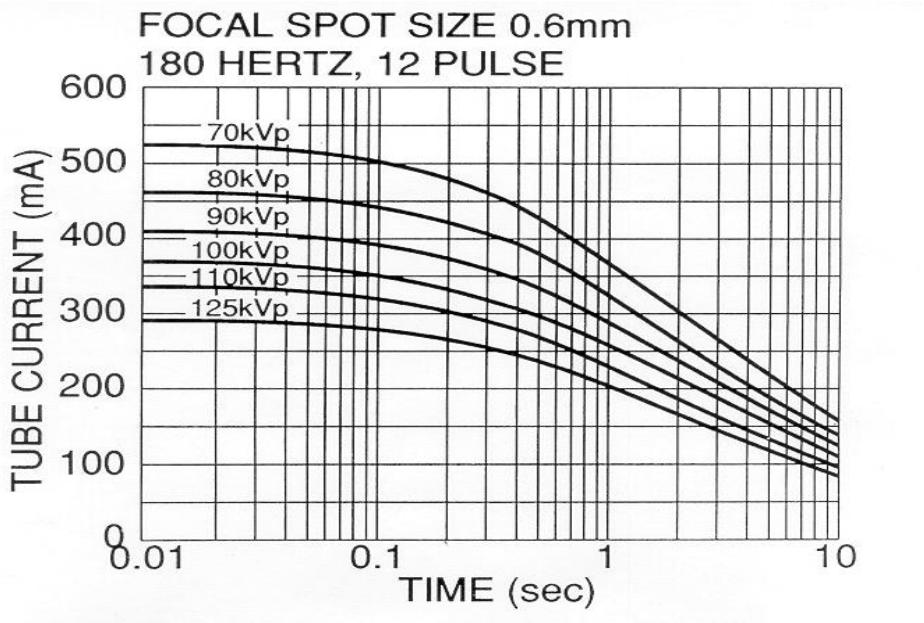

Figure 2.13: An X-ray tube rating chart. [Curry *et al*, 1990].

2.4.2 Cooling curves

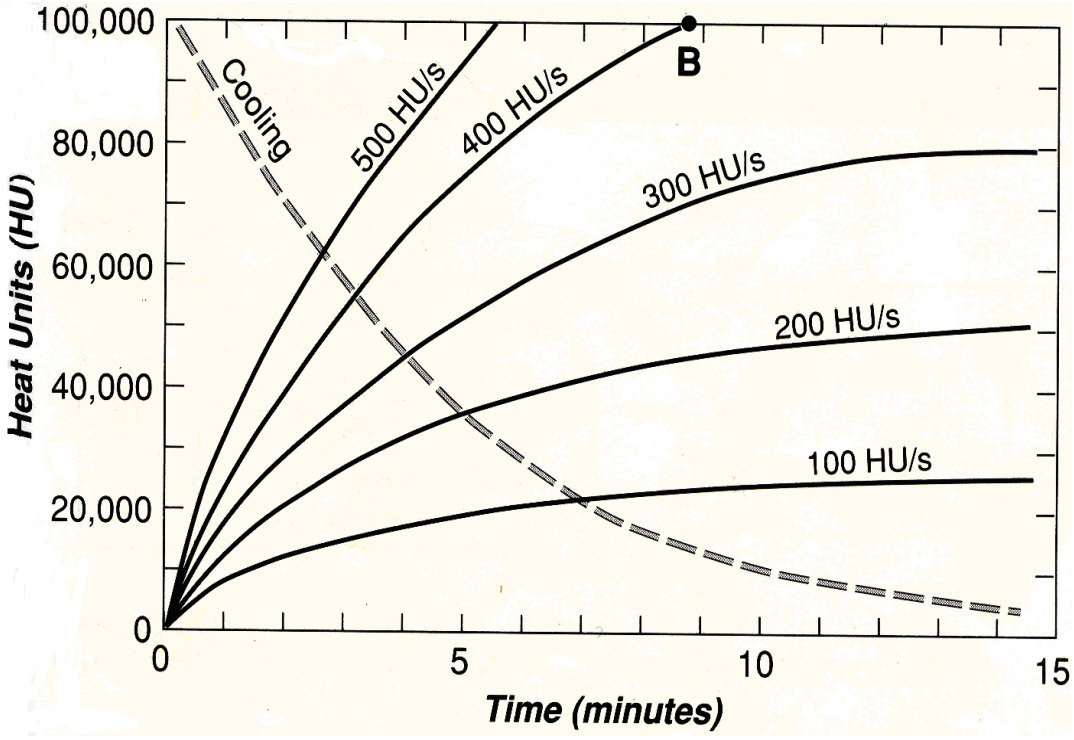

Figure 2.14: Anode thermal characteristics chart for the tube. [Wolbarst, 1993].

A cooling curve reveals the rate at which a hot anode radiates away heat. The curve can be used to determine the time required for an anode that has already absorbed a certain quantity of heat to lose any specified amount of it. [Wolbarst, 1993].

2.5 Energizing and controlling an X-ray tube

To produce X-rays, the X-ray tube must be supplied with electrical energy. An X-ray machine has a number of components that rearrange, control and store electrical energy before it is applied to the X-ray tube. These components are collectively referred to as either the power supply or generator. The function of the generator is not to supply or to generate energy, but to transform it into an appropriate form for X-ray production. The other major function of the generator is to permit the operator to control three quantities namely kV, mA and exposure time. [Sprawls, 1995].

2.5.1 kVp control

2.5.1.1 Single phase generator

There are few components involved in the production of X-rays in the design circuit of a single phase generator. The primary voltage corresponding to the selected kVp is output from the autotransformer and applied to the primary coil winding of the high voltage transformer.

The primary voltage is stepped up through the transformer to the desired secondary high voltage, is converted to DC and then applied to the X-ray tube. From Figure 2.15, the single phase generator is characterized by 100 percent ripple of the DC waveform. Since useful radiation is produced only during the peak portion of the waveform (approximately 33% of each pulse) this type of generator is not very efficient at X-ray production. [Panichello, 1998].

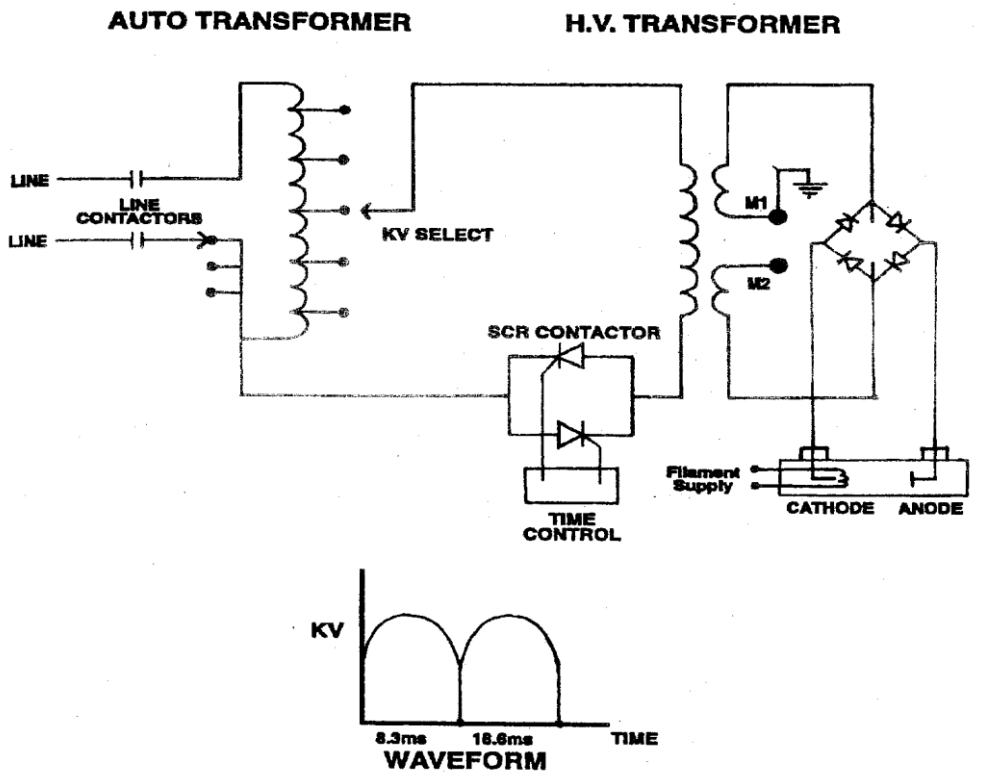

Figure 2.15: Single phase generator and output waveform. [Panichello, 1998].

2.5.1.2 Three phase generator

Three-phase generators deliver more power and are more efficient at producing X-ray radiation and provide better time control. Three phase generators require three different line phases for input power, each phase at 120º out of phase with the other two. These generators have three separate autotransformers, usually motor driven, one for each phase.

The primary voltage that is derived from the autotransformers is applied to the primary of a special three-phase, high voltage transformer. There are two types of three phase, high voltage transformer used in these X-ray generators. The type of transformer, and its corresponding output waveform, depends on the type of secondary winding configuration employed.

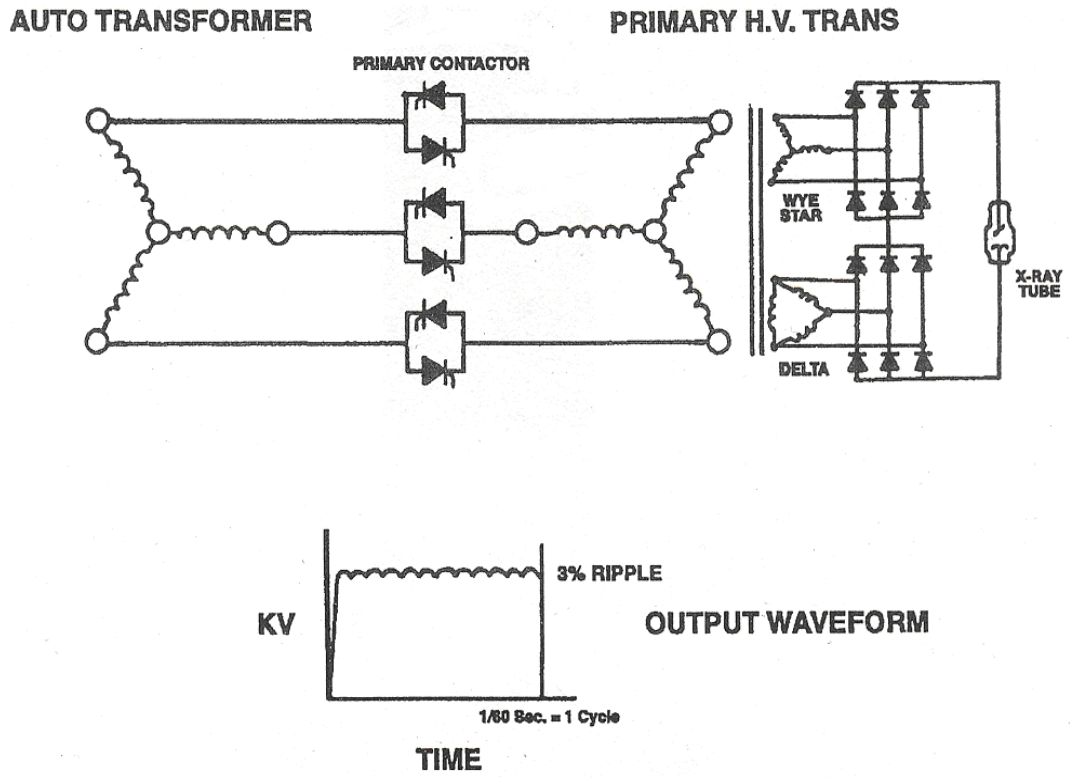

Figure 2.16: Three phase generator and output waveform. [Panichello, 1998].

The secondary could be configured with two separate delta windings, two separate Wye windings, or the secondary could have a delta-Wye configuration. If the same winding configuration is used in the secondary, then it is termed a six-pulse. If the

Delta-Wye winding configuration is used in the secondary, this designates a twelve-pulse generator. A six-pulse generator produces a DC output waveform that has 13.5% ripple. This is a significant improvement over a single phase generator.

Twelve pulse generators produce an output waveform with only 3.4% ripple. Three-phase generator provides many advantages over single-phase units. The increased output efficiency of these generator allows for much shorter exposure times, as compared to a single-phase generator using the same kVp setting and much higher exposure techniques can be used at short exposure time settings with three-phase systems. The exposure time is more accurately controlled in three-phase generator. [Panichello, 1998].

2.5.1.3 Constant potential generator

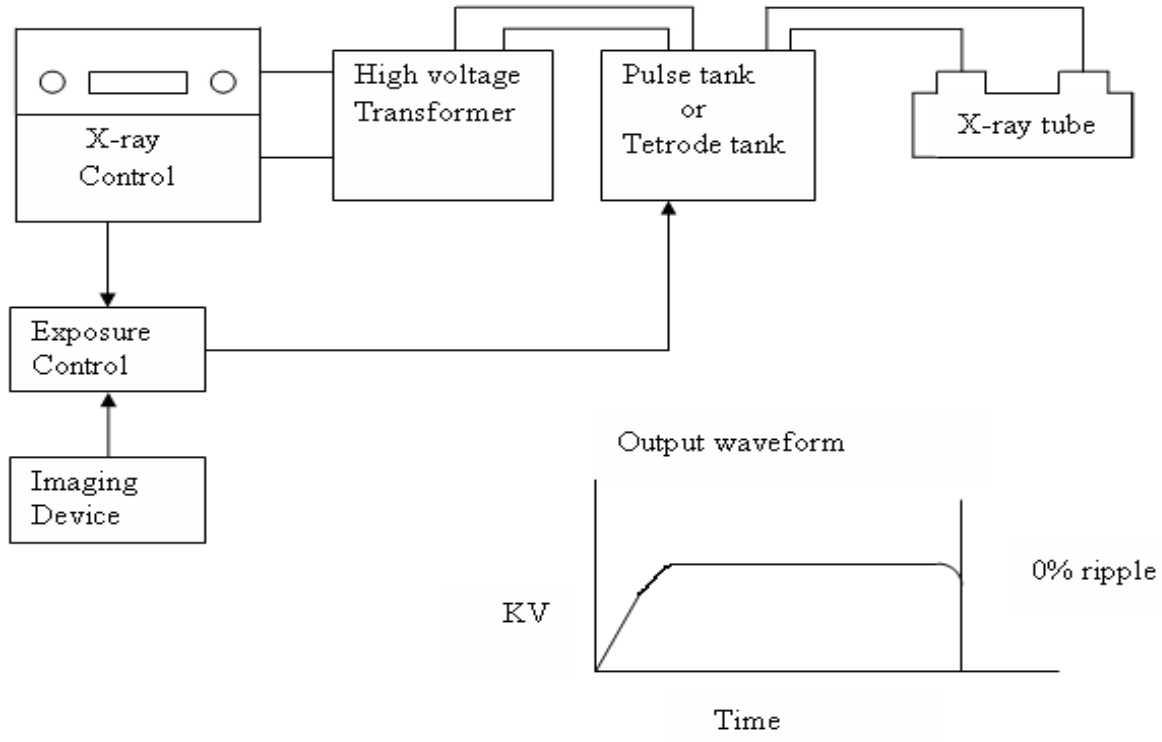

Figure 2.17: Constant potential generator block and its output waveform.
[Panichello, 1998].

This is a special version of a three-phase generator. Additional switching circuitry is employed in the high voltage secondary circuit to achieve the accurate exposure time

control required for high-speed filming applications. Because this type of generator utilizes a high voltage "switch" the exposure times are precisely controlled and the resulting kVp waveform is a DC square wave that is essentially ripple free that is, constant potential produces very little ripple.

With a true square wave output, the kVp remains constant for the duration of the exposure, hence the name constant potential. Fast switching of high voltage is accomplished by the use of tetrodes in the high voltage secondary circuit. The tetrodes, located in a separate tank called the tetrode tank, are wired in series with the X-ray tube. An external exposure signal, sent from an imaging device such as a cine camera or film charger, turns the tetrode "on" and "off" which, in turn, allows the X-ray tube to conduct. [Panichello, 1998].

2.5.1.4 High frequency generator

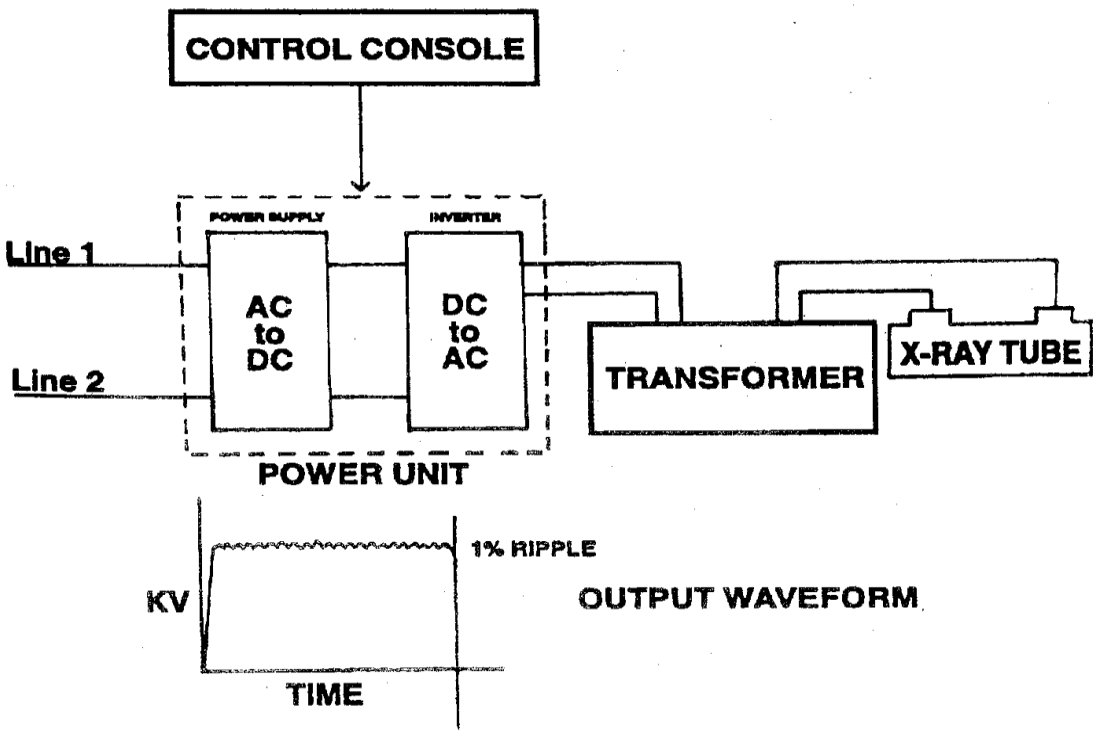

Figure 2.18: High frequency generator block diagram and output waveform. [Panichello, 1998].

The modern high-voltage generator design uses a high frequency circuit. Full wave-rectified power at 60 Hz is converted to a higher frequency usually 500 to 25000 Hz. The generator is small and can be placed within the X-ray tube housing and produce a nearly constant potential voltage waveform which results in improved image quality at lower patient dose. High frequency X-ray generators are grouped by frequency. [Bushing, 1997].

High frequency generators have a unique way of producing high voltage. In this generator the incoming line voltage is immediately converted to DC, providing a constant source to the power inverter section. In the high frequency generators, the high quality DC supply maintains a stable, filtered DC output regardless of inconsistencies with the AC line. The required output from the DC supply is fed directly to the power inverter section of the generator. The inverter is used to convert the DC supply voltage into high frequency pulses, thus simulating an AC waveform. The inverter sends the pulses to the high voltage transformer which then steps up the voltage to the current level of high voltage that will be delivered to the X-ray tube. [Panichello, 1998].

2.5.2 mA control

The cathode is heated electrically by a current from a separate low-voltage power supply. The output of this is controlled by the mA selector. Increasing the mA selector setting passes more heating current through the cathode, thus in turn, increases the temperature, and the increased emission produces an increase in X-ray tube current. There are actually two currents flowing through portions of the X-ray tube: one, the mA, flows from the cathode to the anode and through the high voltage power supply; the other flows only through the filament of the cathode. It is the first current that controls the cathode-to-anode current.

The cathode temperature required to produce adequate thermionic emission, especially at high mA values, is relatively high. The temperature is sufficiently high, in many cases, to produce some evaporation of the tungsten cathode. Because of this it is undesirable to keep the cathode at the high operating temperature except for the

duration of the X-ray exposure. Most of the X-ray equipment operates heating with two levels of cathode heating. When the equipment is turned on, the cathode is heated to a standby level that should not produce significant evaporation. Just before the actual exposure is initiated, the cathode temperature is raised to a value that will give the appropriate tube current. [Sprawls, 1995].

2.5.3 Exposure timer

The exposure is initiated by the equipment operator and then terminated either after a preset time has elapsed or when the receptor has received a specific level of exposure. In fluoroscopy, the exposure is initiated and terminated by the operator, but the timer displays accumulated exposure time and produces an audible signal at the end of each 5-minutes exposure increment. Operator-controlled switches and timers turn the radiation on and off by activating switching devices in the primary circuit of the X-ray generator. [Sprawls, 1995].

2.5.3.1 Manual timer

X-ray equipment with a manual timer requires the operator to set the exposure time before initiating the exposure. The time is determined by personal knowledge, or from a technique chart, after the size of the patient and kV and mA values being used are considered. [Sprawls, 1995].

2.5.3.2 Automatic exposure control

Automatic exposure control (AEC) is an X-ray machine function that terminates the exposure when a specific predetermined amount of radiation reaches the receptor. This function is referred to as phototiming. AEC is used frequently in many general radiographic procedures. [Sprawls, 1995].

2.6 Fluoroscopy

Fluoroscopy is a dynamic radiography, or radiography of motion. The advantage of fluoroscopy is the speed and ease to use.

2.6.1 Image intensifiers

The purpose of an image intensifier tube is to amplify electronically the brightness of an image. Figure 2.19 illustrate the basic operation of the image intensifier. The incoming X-rays are converted into a visible light in the CsI input phosphor layer and this visible light is converted into photoelectrons at the photocathode. The photoelectrons are accelerated and focused by the electrostatic lenses to the output phosphor and converted again into visible light photons. [Kelsey, 1985].

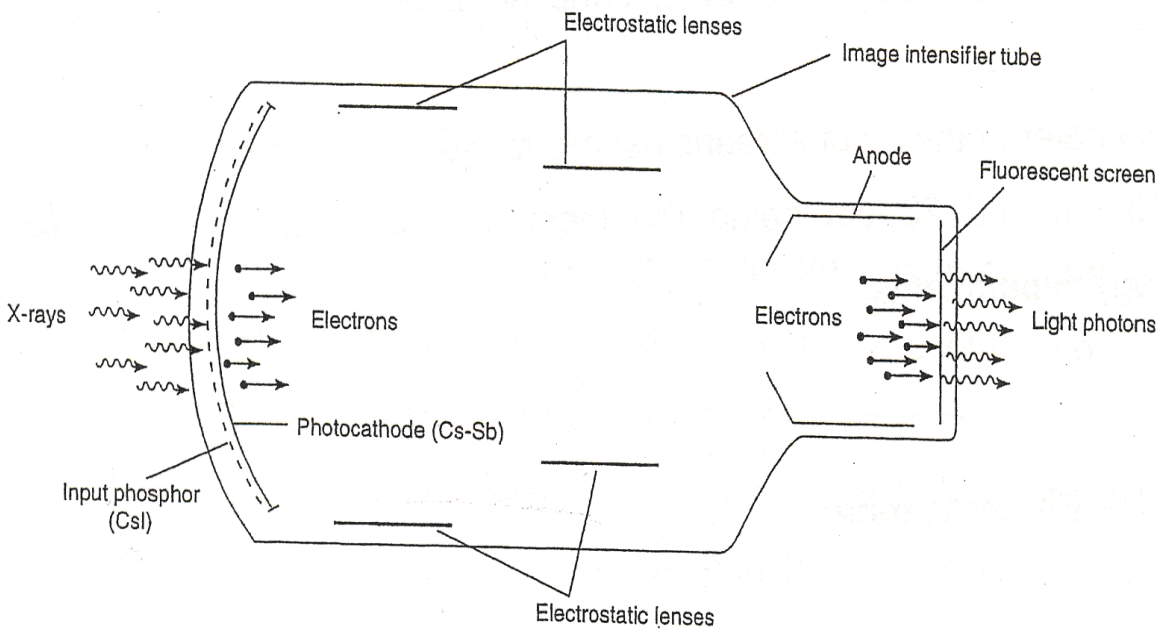

Figure 2.19: Schematic illustration of an image intensifier tube.
[Thompson *et al*, 1994].

2.6.2 Input phosphor

The old input phosphors were (ZnCd)s. Modern image intensifier tubes have CsI input phosphor. CsI has k edges closer to the X-ray beam average energy and can be

vacuum deposited to provide more dense packing and a needle-like crystal shape that channels the light more efficiently onto the cathode and absorbs about 50% of the incident X-rays. [Kelsey, 1985].

2.6.3 Output phosphor

The output phosphor is made of (ZnCd)s because it is more efficient at converting electron energy into visible light and has excellent resolution in thin layers. [Kelsey, 1985].

2.6.4 Fluorescence

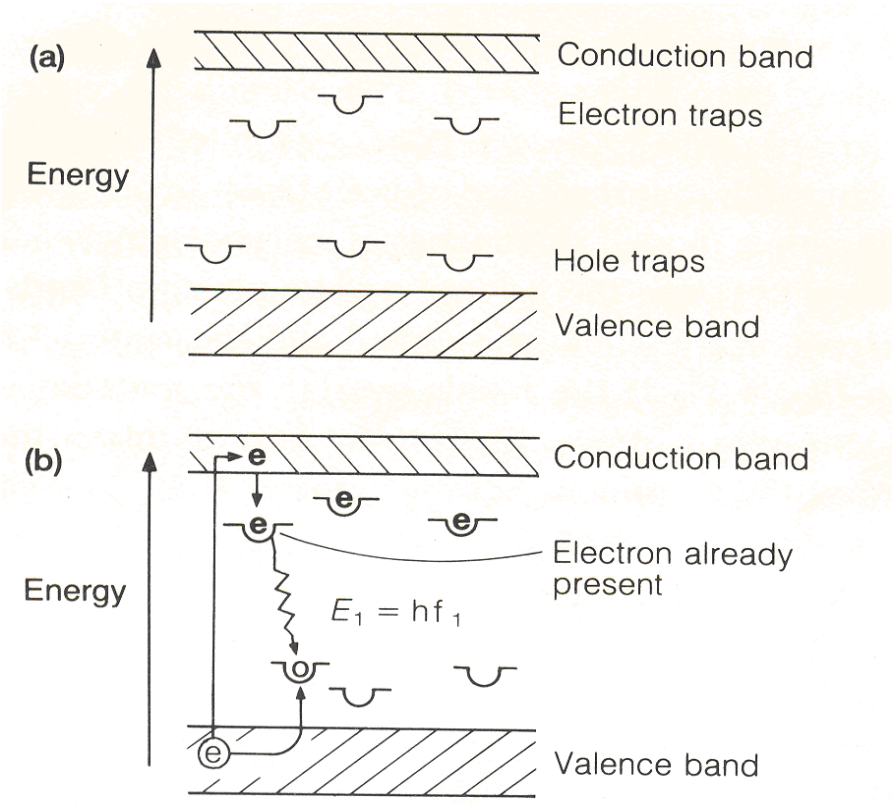

Figure 2.20: Process of fluorescence. [Dendy *et al*, 1987; 1999].

The process of fluorescence is as follows:

- Electron traps are normally filled with electrons (Figure 2.20 (b))

- An X-ray photon interacts by the photoelectric or Compton process to produce a photoelectron which dissipates energy by exciting other electrons to move from the valence band to the conduction band.
- Holes are thus created in the filled valance band.
- The hole, which has a positive charge numerically equal to that of the electron, moves to a hole trap at a luminescent centre in the forbidden band.
- When both an electron and a hole are trapped at a luminescent centre, the electron may fall into the hole emitting visible light of characteristic frequency where $E_1 = hf_1$.
- The electron trap is refilled by an electron that has been excited up into the conduction band.

In fluorescence, the migration of electrons and holes to the fluorescent centre and the emission of a light happen so quickly that it is essentially instantaneous. Not all transitions of electrons are luminescent centres and produce light. [Dendy *et al*, 1987; 1999].

2.6.5 Photocathode

The cathode consists of cesium and antimony (CsSb) metal alloy and is adjacent to the input screen, separated by a thin sheet of transparent, chemically inert material to prevent chemical reactions. Light produced by X-ray photon interactions in the CsI input screens eject photoelectrons from a point on the surface of the photocathode. The rate in which the photoelectrons are released from any point on the surface of the photocathode is proportional to the intensity of the X-rays reaching the input screen, so that the spatial pattern of electron emission is determined by that of the incident X-rays. [Wolbarst, 1993].

2.6.6 Gain

The image is intensified, minified, and converted by the action of the electrons lens. For each X-ray photon absorbed by the input phosphor about 400 light photons are

emitted, producing some 400 photoelectrons, which then cause the output phosphor to emit nearly 4 X 10^6 output photons.

Intensification can be measured in two ways:

$$\text{Brightness gain} = \frac{\text{Brightness of the output phosphor}}{\text{Brightness of the input phosphor}} \quad 2.3$$

The brightness gain tends to deteriorate as an image intensifier ages, thus the patient dose with an old image intensifier tends to be higher than that with a new image intensifier of the same type. The deterioration can proceed at a rate of about 10% per year. The brightness gain from manification produces a reduction in image size. The quantity of the gain is influenced by the relative areas of the input and output screens.

$$\text{Manification gain} = \left(\frac{d_I}{d_O} \right)^2 \quad 2.4$$

Where d_I is the diameter of the input screen and d_o is the diameter of the output screen. [Curry *et al*, 1990]. Flux gain refers to the increase in the number of light photons due to the acceleration and hence gain is proportional to the energy of the electrons, 50-100 times. [Farr, 1997].

The total brightness gain of an image intensifier is the product of the manification and flux gain given by:

$$\text{Brightness gain} = \text{manification gain} \times \text{flux gain} \quad 2.5$$

The other measurement of brightness gain, recommended by the International Commission on Radiologic Units and Measurement (ICRU), is the conversion factor. Farr, [1997] defines conversion factor as a ratio to the luminance of the output phosphor to the input exposure rate:

$$\text{Conversion factor} = \frac{\text{Brightness or luminance of the output phosphor (candela/m}^2\text{)}}{\text{Dose rate in air on the input surface of the intensifier } (\mu Gy/s)} \quad 2.6$$

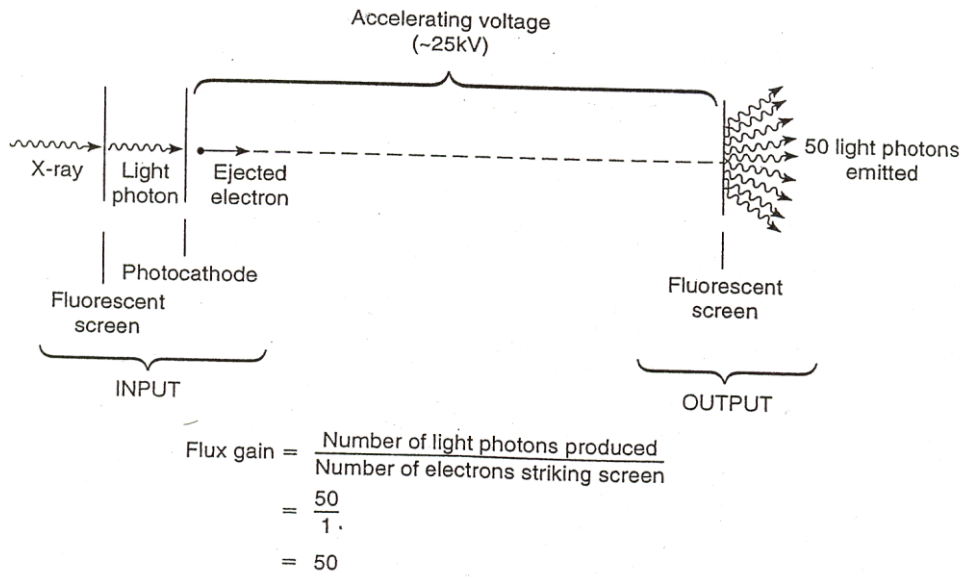

Figure 2.21: Interactions that occur at the input and output screens of an image intensifier tube. [Thompson *et al*, 1994].

2.6.7 Brightness control

Brightness is controlled by adjusting fluoroscopic mA and kVp. The primary factor affecting the brightness of the fluoroscopic image is the size or density of anatomic part because an increase or decrease in size or density reduces or enhances, respectively, the number of photons that reach the phosphor. Image brightness, is maintained by the number (mAs) or the energy (kVp) of photons must be adjusted for changes in part thickness or density. kVp and mA affect the quality of the fluoroscopic image in the same way they affect radiographic images. In general, a relatively high kVp and a low mA are preferred. [Thompson *et al*, 1994].

According to Thompson *et al* [1994], when the method used to maintain the image brightness of the monitor changes the intensity of radiation, mAs and kVp automatically, it is called automatic dose rate control (ADC), when the video signal is adjusted, it is called automatic gain control (AGC) and when the sensitivity of the camera plate is adjusted, it is called automatic brightness control (ABC).

2.7 Image quality

2.7.1 Radiographic image quality

2.7.1.1 Radiographic density

Radiographic density refers to the overall darkness or blackness of the image when viewed on a normal illuminator (view box). The requirements of a good radiographic image include minimal distortion of the body part for a specific radiographic projection and sufficient contrast to reveal each tissue density within the part.

2.7.1.2 Radiographic contrast

Radiographic contrast permits visualisation of details of the various structures in the body part. Bone, muscle or fluid, adipose tissue and gases are the four natural, basic body densities that can be easily demonstrated in a radiographic image. Contrast depends on both the capability of an individual film to display differences in image density (film contrast) and differences in levels of density produced by the degree of penetration of the body part by the X-ray beam (subject contrast).

2.7.1.2.1 Film contrast

Film contrast refers to the capabilities of an individual film to permit the production of image contrast. The factors that affects film contrast is the chemical development process, this includes the processing techniques used, chemical characteristics of the processing solution and the physical of the process (time in each developing solution). [Thompson *et al*, 1994].

2.7.1.2.2 Radiographic subject contrast

Subject contrast is the difference in X-ray intensity transmitted through one part of the subject as compared to that transmitted through another part and this image contrast depends on the penetration of the body part by the X-ray beam. The subject contrast also depends on the tissue thickness, tissue density, tissue electron density, tissue effective atomic number Z, tissue attenuation μ, X-ray energy kV, X-ray filtration and scatter within the tissue. [Dowsett *et al*, 1998].

If an X-ray beam is directed at two different thicknesses of the same material, the number of X-rays transmitted through the thin part will be greater than the number transmitted through the thick part. The tissue density between body tissues is one of the most important factors in causing subject contrast. The greater the density of a tissue, the greater is its ability to attenuate X-rays. Radiation quality is the ability of an X-ray photon to penetrate tissue and depends on its energy, high kVp X-rays have greater energy. Low kVp produces a greater subject contrast than high kVp. [Curry *et al*, 1990].

2.7.2 Fluoroscopic image quality

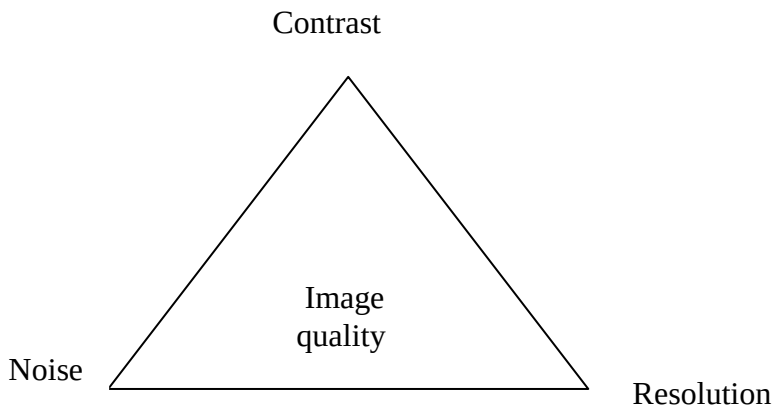

Figure 2.22: Three principal determinates of image quality. [Wolbarst, 1993].

Three important parameters of image quality are: the contrast in light intensity (or in X-ray fluence) corresponding to different parts of the subject, the resolution of fine detail and the level of interfering noise.

2.7.2.1 Contrast

Hendee et al, [1992] describes the contrast of an image as the product of complex interactions among the anatomic and physiologic attributes of the region of interest, the properties of the imaging method and receptor employed and the intercessions by interpreter of the image to influence both the intrinsic properties of the region and its presentation on the display device.

Image contrast is controlled through the amplitude of the video signal. In addition to the scatter radiation and kVp, two factors diminish contrast in image intensifiers.

These are:

- The input screen does not absorb of all photons in the X-ray beams.
- Light scatter resulting in retrograde (backward) light flow in the image intensifier.

Light scatter (reflection and refraction) from the output screen produces a form of fog by retrograde light flow. This light can pass back through the image tube, activating the photocathode and producing a fog that will reduce image contrast. Contrast decreases at the edge of images. The brightness section of the image is at the centre of the image. Contrast tends to deteriorate as image intensifier ages. [Curry *et al*, 1990]. Contrast depends on the object, subject and image contrast.

2.7.2.1.1 Object contrast

Object contrast is proportional to the product of object density and thickness. This quantity represents the mass of object per unit area (cm^2) of the image. The chemical

composition of an object contributes to its contrast only if its effective atomic number Z is different from that of the surrounding tissue. [Sprawls, 1995].

2.7.2.1.2 Subject contrast

The amount of subject contrast produced depend on the physical contrast characteristics which are the atomic number, density and thickness of the object and the penetrating characteristic which is the photon energy spectrum of the X-ray beam. [Sprawls, 1995].

2.7.2.1.3 Image contrast

The contrast in visible fluoroscopic images is in the form of the brightness ratio between various points within the image area. The amount of contrast in a fluoroscopic image depends on the amount of subject contrast entering the receptor system and the characteristics and adjustments of the components (image intensifier tube, video, ect.) of the imaging system. [Sprawls, 1995].

2.7.2.2 Resolution

The factor affecting the geometry (resolution) of the image are the video monitor (the primary factor), magnification gain, electrostatic focal spot, the diameter of the input and output screen, object-to-image receptor distance (OID) and phosphor size and thickness and the result is caused by the repulsion of electrons and the divergence of the primary beam from the focal spot of the X-ray tube.

2.7.2.3 Quantum mottle (Noise)

Quantum mottle is a grainy or blotchy appearance caused by insufficient radiation to produce a uniform image. Mottle is a problem in fluoroscopy because the units operation is based on the minimum number of photons required to activate the

fluoroscopic screen through automatic brightness stabilization. Since the problem is an insufficient amount of radiation, the solution to mottle is to increase the fluoroscopic mA. [Thompson *et al*, 1994].

Chapter 3

RADIATION QUANTITY AND QUALITY

3.1 X-ray beam quantity

A subjective assessment of spectrum shape is given by beam quality. The quantity of X-radiation incident on a surface (e.g. patient) depends on area, time, and energy. Measurements of radiation quantity are important for estimating the sensitivity of imaging devices and calculation dosimetry. The following parameters describe intensity:

- Photon fluence
- Photon flux
- Energy fluence
- Energy flux [Dowsett *et al*, 1998].

Radiation is the energy in transit from one location to another and radiation intensity is the variety of attributes of the output of a radiation source. The beam radiation is shown in Figure 3.1.

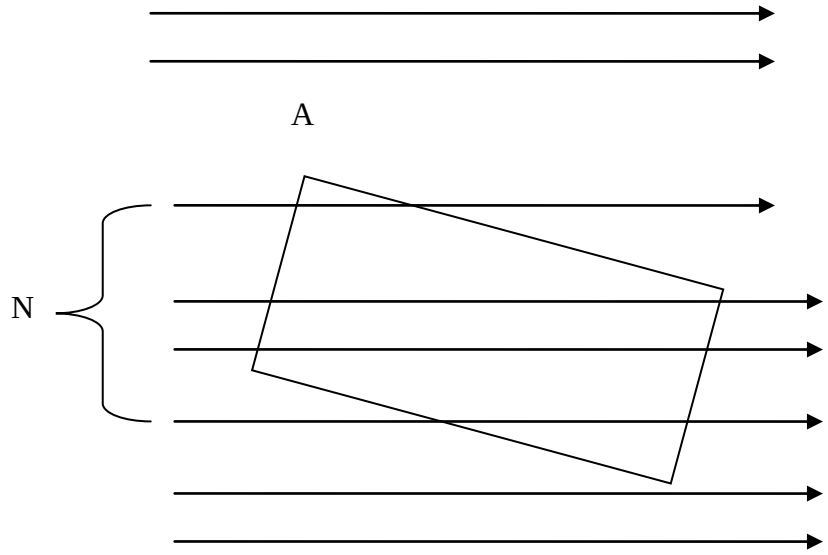

Figure 3.1: The number of particles (N) passing through a unit area A.
[Hendee and Ritenour, 1992].

The photon fluence of the beam Φ is the number of photons N per area A

$$\Phi = \frac{N}{A} \qquad 3.1$$

When the beam is uniform the size of the area A is irrelevant because it is perpendicular to the direction of the beam. When the beam is not uniform over its entire area, the fluence is averaged over the number of a small area or specified separately for each other. The time rate of change of fluence, known as the photon flux ϕ, is

$$\phi = \frac{\Phi}{t} = \frac{N}{A \times t} \qquad 3.2$$

If the fluence varies with the time t, then the flux must be averaged over time. If all photons in the radiation beam possess the same energy, the energy fluence Ψ is the product of the fluence Φ and the energy E per photons

$$\Psi = \Phi E = \frac{NE}{A} \qquad 3.3$$

The photon flux ϕ may be converted to the energy flux ψ, also known as intensity I, by multiplying by the energy E per photon, one can get intensity and is given by [Hendee and Ritenour, 1992]

$$I = \psi = \phi E = \frac{N\mathrm{E}}{A \times t} \qquad 3.4$$

Table 3.1: Fluence and flux (intensity) of the beam radiation. [Hendee and Ritenour, 1992].

Quantity	Symbol	Definitions	Units
Photon fluence	Φ	$\frac{N}{A}$	$photon/cm^2$
Photon flux	ϕ	$\frac{N}{A \times t}$	$photon/cm^2.\sec$
Energy fluence	Ψ	$\frac{NE}{A}$	MeV/cm^2
Energy flux	ψ	$\frac{NE}{A \times t}$	$MeV/cm^2.\sec$

3.2 Attenuation and absorption

Martin [2006] derived the equation of intensity based on Figure 3.2 as follows: The number of photons is expressed mathematically as a decreasing function with thickness of absorber:

$$-\frac{d\mathrm{N}}{dx} = \mu \mathrm{N} \qquad 3.4$$

where the constant of proportionality μ, is the total attenuation coefficient of the medium for the photons of interest. If all of the photons possess the same energy (i.e. the beam is monoenergetic) and if the photons are attenuated under conditions of good geometry (i.e. the beam is narrow and contains no scattered photons), the number N of the photons penetrating an absorber of thickness x (i.e. without interaction in the medium) is found by rearranging and integrating

$$\int_{\mathrm{N}_O}^{\mathrm{N}} \frac{d\mathrm{N}}{\mathrm{N}} = \int_{0}^{x} -\mu dx \qquad 3.5$$

to yield

$$\ln \mathrm{N} - \ln \mathrm{N}_0 = -\mu x \qquad 3.6$$

or

$$\ln \mathrm{N} = -\mu x + \ln \mathrm{N}_0 \qquad 3.7$$

Which is the equation of a straight line with a slope of $-\mu$ and a y-intercept (i.e. with no absorber) of $\ln \mathrm{N}_0$ as shown in Figure 3.2. This can be simplified by the law of logarithms to

$$\ln \frac{\mathrm{N}}{\mathrm{N}_0} = -\mu x \qquad 3.8$$

and since the natural logarithm of a number of exponents to which the base raised to obtain the number, this expression translates to

$$\frac{\mathrm{N}}{\mathrm{N}_0} = e^{-\mu x} \qquad 3.9$$

or

$$\mathrm{N} = \mathrm{N}_0 e^{-\mu x} \qquad 3.10$$

where N_0 is the number of photons of the incident beam, N is the number of photons after traversing a distance x through the absorbing medium and μ, is the linear attenuation coefficient, is the probability of interaction per unit distance in an absorbing medium.

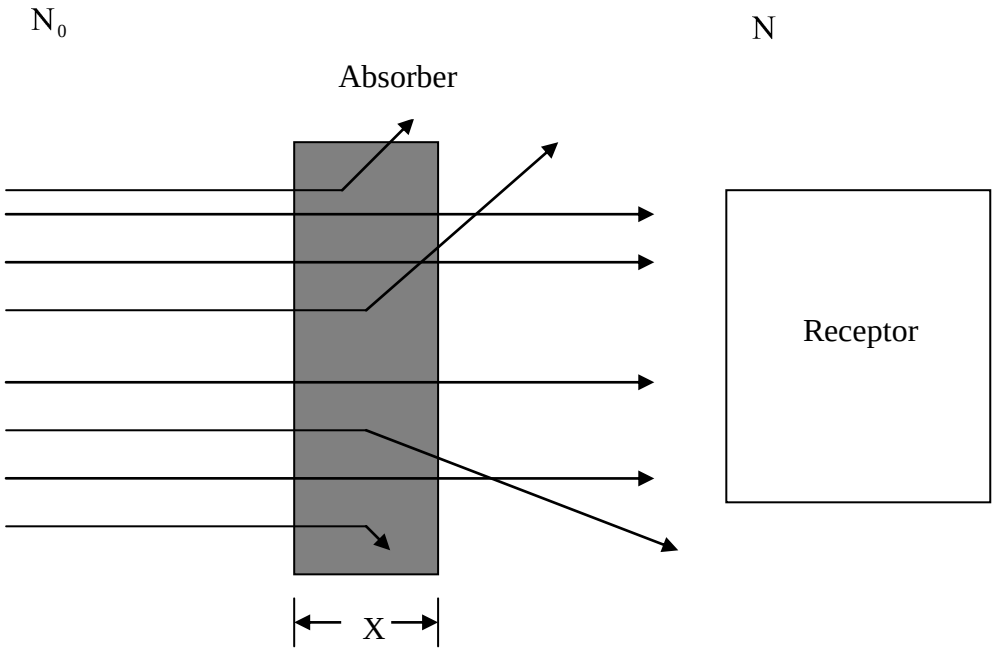

Figure 3.2: Alteration of a beam of photons by attenuation processes. [Martin, 2006].

Substituting equation 3.10 into 3.1, the fluence of the beam becomes

$$\Phi = \frac{\mathrm{N}_0 e^{-\mu x}}{A} = \Phi_o e^{-\mu x} \qquad 3.11$$

The absorption of X-rays by matter depends upon:

- The density of the part.
- The thickness of the part.
- Atomic number of the tissue.
- The energy of the X-ray quanta. [McEntee *et al*, 2004].

The lower the density of the part and atomic number of the tissue are, the more transparent the material is to X-ray. The fact that bones are more opaque than the surrounding flesh, make X-ray photographs possible.

3.3 Coefficients

3.3.1 Linear attenuation coefficient

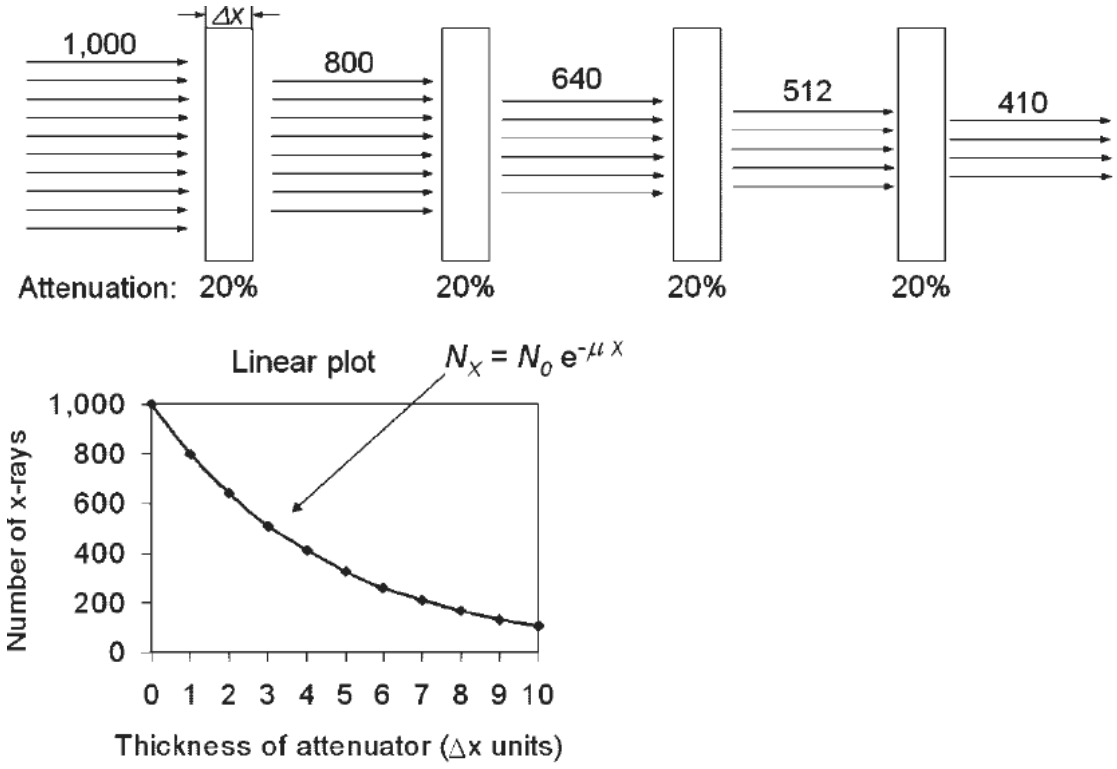

Figure 3.3: Monoenergetic X-ray transmitted through several layers of an attenuator with attenuation coefficient (μ) of 20% per unit thickness. [Seibert, 2005].

Figure 3.3 shows the attenuation of monoenergetic beam. The factors relevant with the transition of radiation are:

- The number of photons is not halved as the thickness is doubled but decreases exponentially with thickness.
- The fraction absorbed depends on the photon energy.
- The linear attenuation coefficient is energy and atomic number Z of the material dependent. [Dowsett *et al*, 1998].

The total linear attenuation coefficient is the sum of the linear attenuation coefficients for the individual interaction mechanisms given by

$$\mu = \tau + \sigma_{coh} + \sigma_c + \kappa \qquad 3.12$$

Where σ_{coh}, τ, σ_c and κ are the attenuation coefficients for coherent scattering, photoelectric effect, Compton effect, and pair production, respectively. The linear attenuation coefficient depends on the atomic number Z, material density ρ, and the photon energy E. [Seibert, 2005].

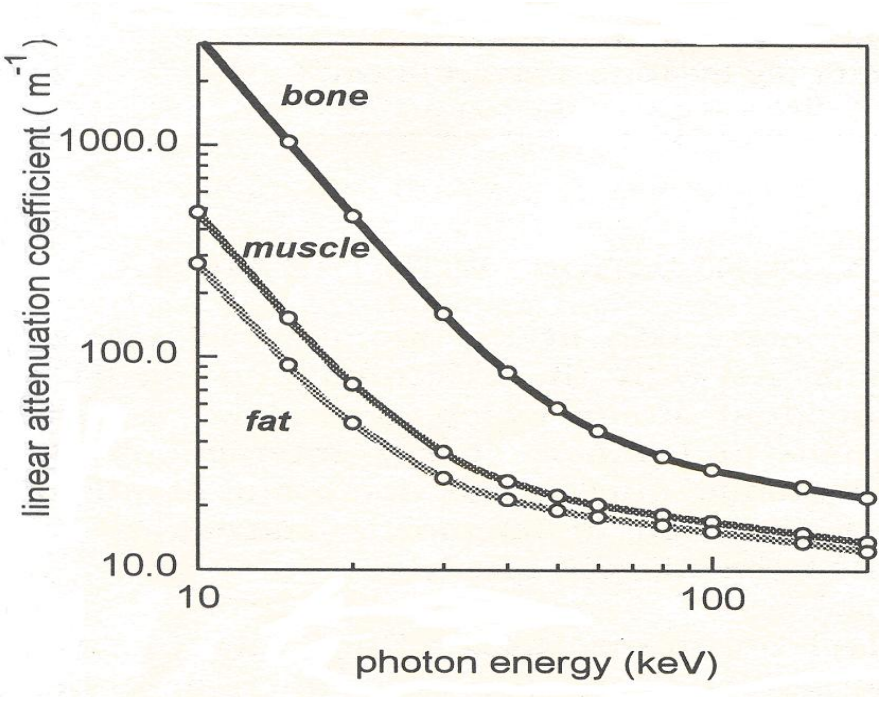

Figure 3.4: The linear attenuation coefficient for bone, soft tissue and fat.
[Dowsett *et al*, 1998].

When comparing muscle, bone and fat, fat has a higher concentration by weight of hydrogen (~11%) and carbon (~57%) and a lower concentration of nitrogen (~1%), oxygen (30%) and high-Z trace elements (<1%). The effective atomic number of fat (Z_{eff} =5.9 to 6.3) is less than that for soft tissue (Z_{eff} =7.4) or bone (Z_{eff} =11.6 to 13.8) and low energy photons are attenuated less rapidly in fat than in an equal mass of soft tissue or bone and attenuated more rapidly in bone than in an equal volume of soft tissue. The absorbed dose is reduced by structure beyond bone. [Hendee and Ritenour, 1992].

3.3.2 Mass attenuation coefficient

The mass attenuation coefficient is denoted by μ/ρ. For the mass attenuation coefficient, "thickness" becomes the product of the density and linear thickness of the material or ρ_x. This is known as the mass thickness with units of $g/cm^3 \times cm = g/cm^2$. The reciprocal of the mass thickness represents the units of mass attenuation coefficient, cm^2/g, and the corresponding Lambert–Beers equation is given by

$$N_x = N_0 e^{-(\mu/\rho)\,\rho x} \qquad 3.13$$

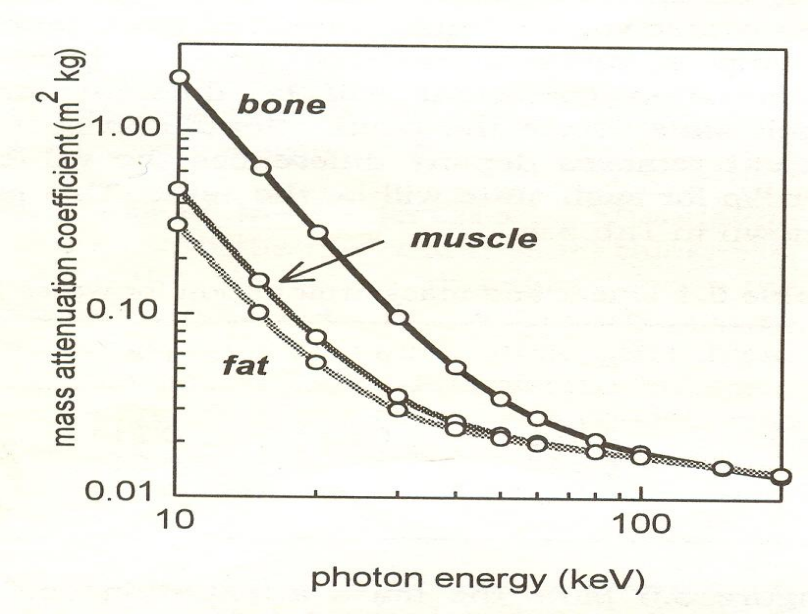

Figure 3.5: The mass attenuation coefficients matching bone, soft tissue and fat for the attenuation coefficients in figure 3.4. [Dowsett *et al*, 1998].

The mass attenuation coefficient for a specific material is a sum of the individual interaction probabilities given by [Seibert, 2005].

$$\frac{\mu}{\rho} = \frac{\tau}{\rho} + \frac{\sigma_{coh}}{\rho} + \frac{\sigma_c}{\rho} + \frac{\kappa}{\rho} \qquad 3.14$$

3.3.3 Energy transfer coefficient

When a photon interacts with electrons in a material, part of all of its energy is converted into the kinetic energy of the electrons. If some photon energy is given to the electron, the photon itself is scattered with reduced energy. The scatter photon may interact again with partial or complete transfer of energy to the electrons. Thus the photon may undergo multiple interactions in which the energy lost by the photon is converted into the kinetic energy of the electrons. Consider a photon beam traversing a material, the fraction of the photon energy transferred into kinetic energy of charged particle per unit thickness of absorber is given by the energy transfer coefficient , μ_{tr} , and is related to μ as follows

$$\mu_{tr} = \frac{\overline{E}_{tr}}{h\upsilon}\mu \qquad 3.15$$

Where $\overline{E}_{tr}$ is the average energy transfer into kinetic energy of charged particles per interaction. [Khan, 2003].

3.3.4 Energy absorption coefficient

Electrons set in motion by the photons lose their energy by elastic collision with atomic electrons of the material. Some electrons will lose energy by Bremsstrahlung depending on the material of the target. The energy absorption coefficient, μ_{en}, is defined as the product of the energy transfer coefficient and (1-g) where g is the fraction of the energy of secondary charged particles that is lost to Bremsstrahlung in the material.

$$\mu_{en} = \mu_{tr} (1 - g) \quad 3.16$$

For interaction involving soft tissues or other low Z material in which electrons lose energy by ionizing collisions, the Bremsstrahlung component is negligible. Thus $\mu_{en} = \mu_{tr}$. [Khan, 2003].

3.4 Kerma and absorbed dose

Chemical and biological changes in the tissue exposed to ionizing radiation are caused by the deposition of energy from the radiation into the tissue. This has been explained in detail in chapter 1. The deposition of energy is described by kerma and absorbed dose. The SI unit for kerma and absorbed dose is the gray (Gy), defined as 1 Joule/kg of irradiated medium.

The centigray (cGy) is $\frac{1}{100}$ gray or 1 rad.

$$1Gy = 100cGy = 100rads$$

Absorbed dose is the energy absorbed per unit mass in the volume element. [Hendee and Ibbott, 1996] and kerma is the kinetic energy released in a medium. [Dowsett *et al*, 1998]. The kerma is greater than the absorbed dose when energy is irradiated from the volume of element as Bremsstrahlung or characteristic radiation. [Hendee and Ibbott, 1996].

3.5 X-ray beam quality

Quality is an indication of X-ray beam's penetrating ability. For a given material the penetrating ability of an X-ray beam depends on the energy of the photons. For X-ray beam that contains a spectrum of photon energies, the penetration is different for each energy. The overall penetration generally corresponds to the penetration of photon energy between the minimum and maximum energies of the spectrum. [Sprawls, 1995].

3.5.1 Measurement of the beam quality

The measurement of beam quality is called the half value layer. [Panichello, 1998] and is the factor that describes the penetrating ability of specific radiation and the penetration through specific objects. HVL is the thickness of material penetrated by one half of the original intensity of the radiation and is in units of mm or cm. Increasing the penetrating ability of a radiation increases its HVL.

The HVL is given by

$$HVL = \frac{0.693}{\mu} \qquad 3.17$$

This shows that HVL is inversely proportional to the attenuation coefficient. The number, 0.693 is the exponent value that gives a penetration of 0.5 [Sprawls, 1995]:

$$(e^{-0.693} = 0.5). \qquad 3.18$$

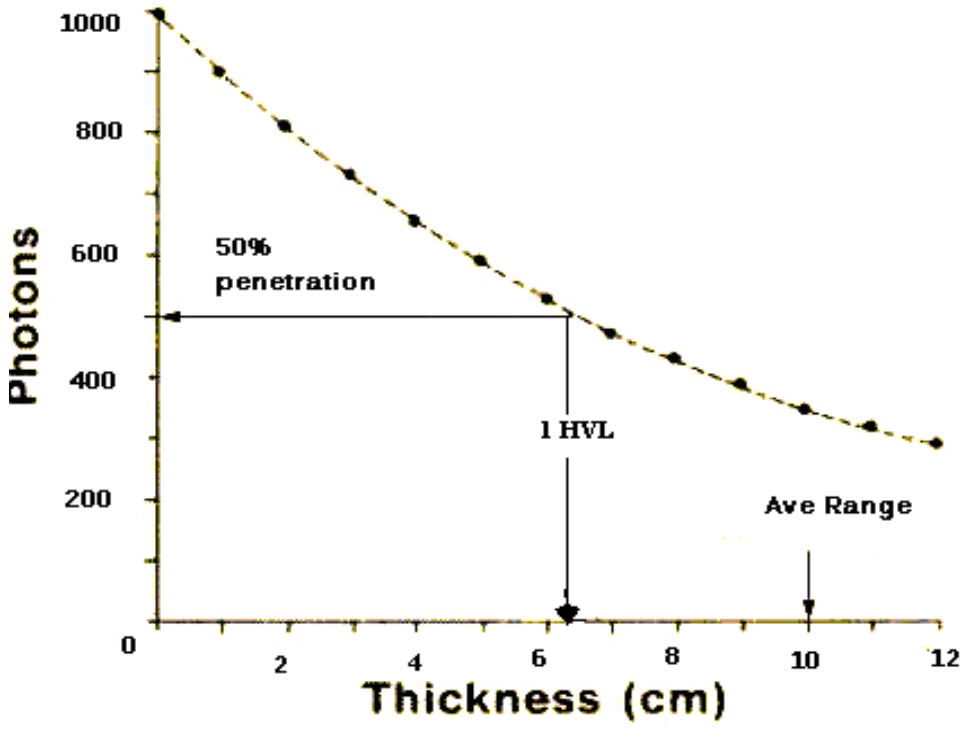

Figure 3.6: Penetration range of individual photons. [Sprawls, 1995].

Beam hardening is the process in which the quality, or energy, of an X-ray beam is increased by the removing lower energy X-ray photons with appropriate filtration. A "hard" X-ray beam is produced by a high kV and a thick filter, a "soft" beam by a low kV and a thin filter. kV and filtration affect the HVL or effective energy. [Farr, 1997].

3.6 Factors affecting the X-ray beam quantity and quality

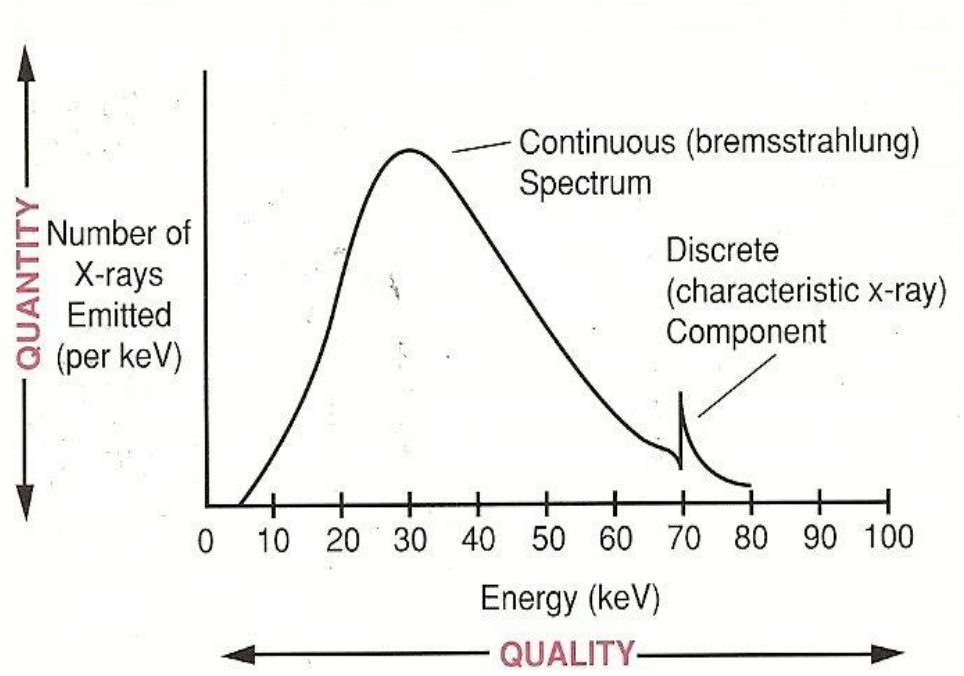

Figure 3.7: The general form and shape of the discrete and continuous X-ray spectra. [Thompson *et al*, 1994].

Figure 3.7 shows the general X-ray spectrum, the peak for the characteristic spectrum or discrete spectrum is sometimes denoted by a straight line as in Figure 3.11.

3.6.1 The effect of mA on the X-ray beam

X-ray beam per unit time (intensity) is directly proportional to the mA through the tube. If the X-ray beam current increases, the intensity will increase too.

$$I \propto mA \qquad 3.19$$

The effect on the X-ray beam of altering the mA is shown in Figure 3.8

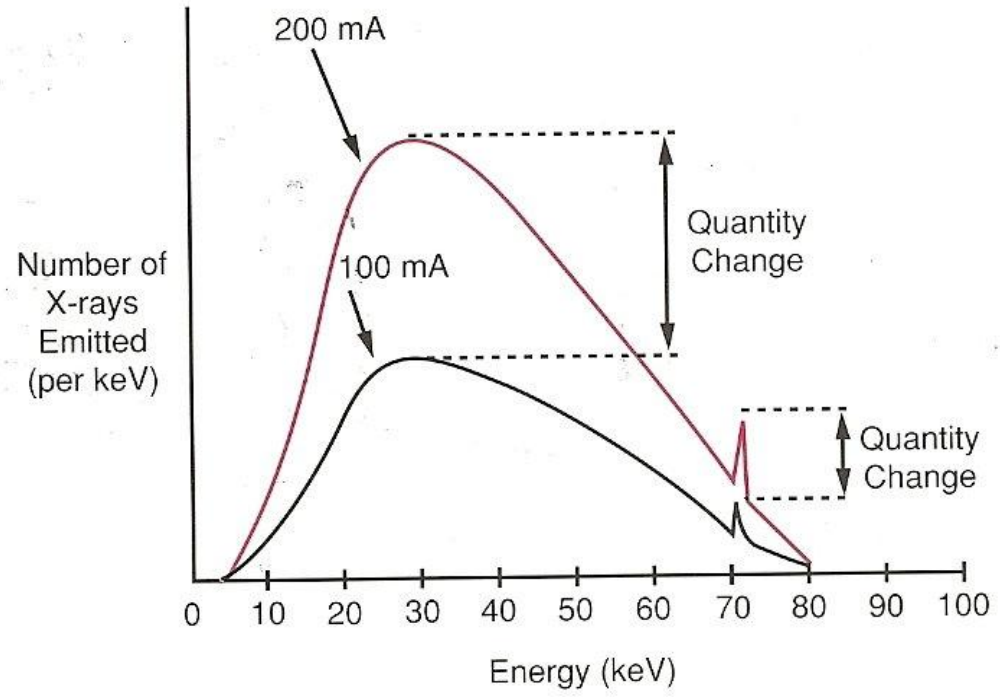

Figure 3.8: The effect of mA on the X-ray spectrum. [Thompson *et al*, 1994].

The area under the graph for 100 mA is half of the area under the graph of 200 mA. The maximum photon energy and the minimum photon energy are the same in each case. There is no shift of the amplitude on the photon energy axis, indicating that mA does not affect the beam energy. [Graham, 1996].

3.6.2 The effect of kVp on the X-ray beam

The kVp across the X-ray tube influences the force of attraction experienced by an electron released by the filament as it moves towards the anode. Thus, if the kVp is increased, then the kinetic energy of the electron at the point when it starts to interact with the target will be increased. The efficiency of X-ray production by Bremsstrahlung is proportional to E^2 and so this improved efficiency means that

$$I \propto kVp^2 \qquad 3.20$$

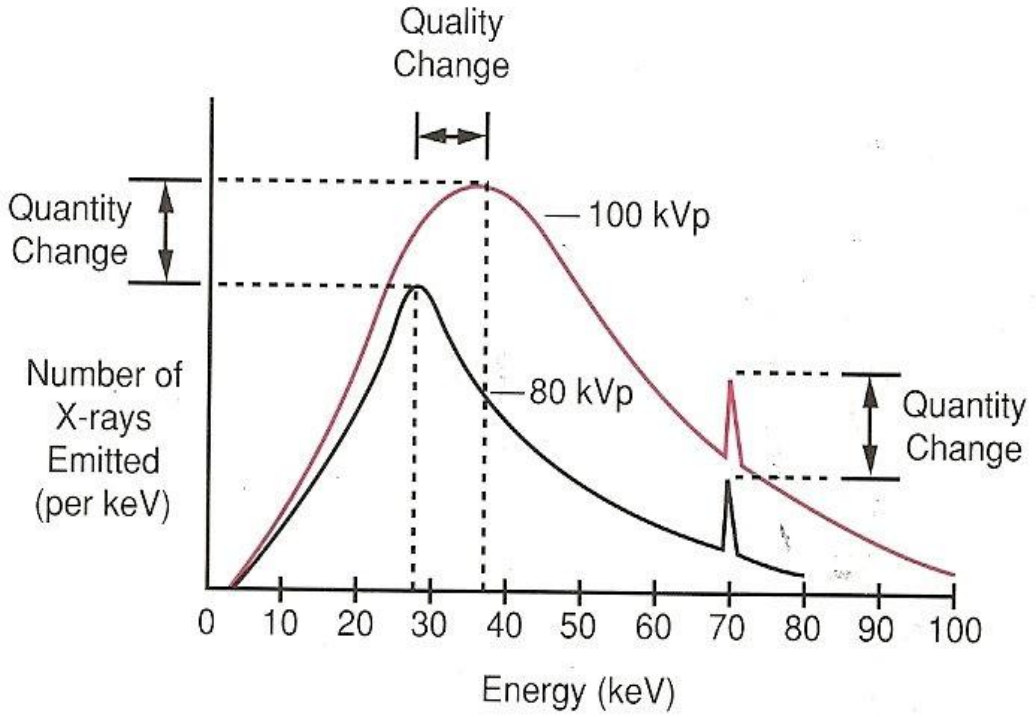

Figure 3.9: The effect of kVp on the X-ray spectrum. [Thompson *et al*, 1994].

Figure 3.9 shows that the selected kVp for an exposure affects both the quality and quantity of the X-ray beam, the discrete spectrum remains at the same position on the energy axis while the amplitude of the continuous spectrum shifts to the higher energy region. The continuous spectrum increases in amplitude for high kVp techniques. [Graham, 1996].

3.6.3 The effect of the target material on the X-ray beam

The atomic number of the target material has an effect on the X-ray beam. The higher the atomic number of the target material the more positive the nucleus of the target atom and so the more it attracts the electrons from the filament which pass close to it. Thus the production of X-ray by the Bremsstrahlung process is more efficient and the intensity of the beam is increased. The maximum and the minimum photon energies in the beam are not affected by the target material. The target material also affects the characteristic radiation produced. The energies of the characteristic radiations from tungsten and a molybdenum target are shown in Table 3.2. [Graham, 1996].

Table 3.2: Comparison of characteristic radiation energies produced from a tungsten target and a molybdenum target. [Graham, 1996].

	Energy of k_α characteristic radiation.	Energy of l_α characteristic radiation.
Tungsten	59.32 KeV	8.39 KeV
Molybdenum	17.48 KeV	2.22 KeV

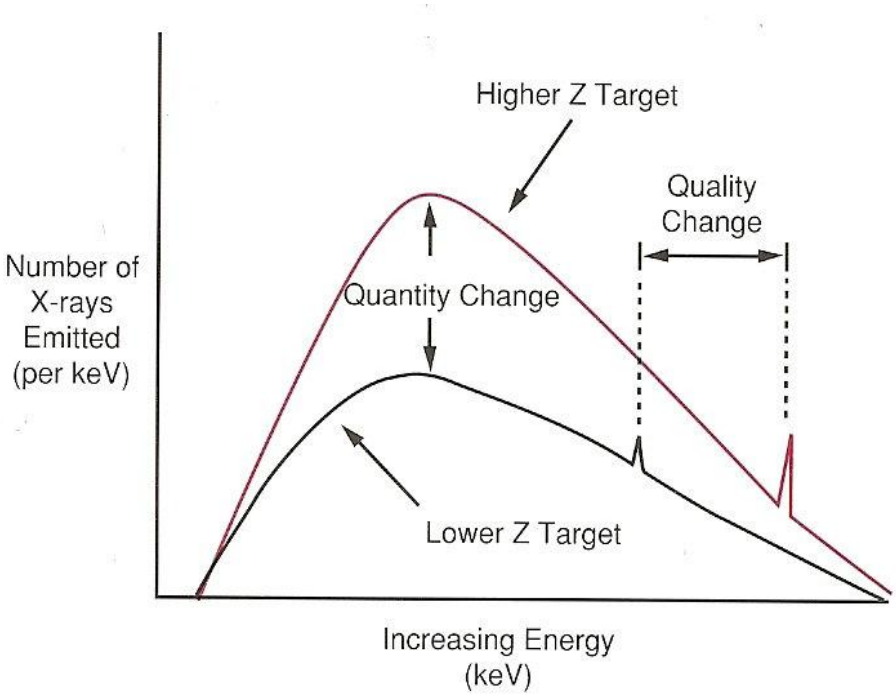

Figure 3.10: The effect of the target material on the X-ray spectrum. [Thompson *et al*, 1994].

From Figure 3.10, in the Bremsstrahlung spectrum, the changes occurs in amplitude (quantity) but not in the energy (quality) and in characteristic spectrum, there is only a shift in energy.

3.6.4 The effect of wave rectification on the X-ray beam

The high-tension rectification of the X-ray generator affects the spectrum of radiation produced at the target of the X-ray tube, because of the changing energy of the electron beam striking the target each half cycle. Consider full-wave rectification with no capacitor smoothing as produced by the two-pulse generator.

The potential across the tube varies from zero to the maximum kVp each half-cycle and the energy of the electron striking the target varies from zero to a keV with numerical value equal to that of the kVp. The time-averaged spectrum for full-wave rectification is shown in Figure 3.11(a). Consider the constant potential applied to the X-ray tube during the entire exposure. This will be the same as if voltage B is applied for the whole exposure so the spectrum for voltage B is labelled in Figure 3.11(b) as the spectrum from a constant potential unit.

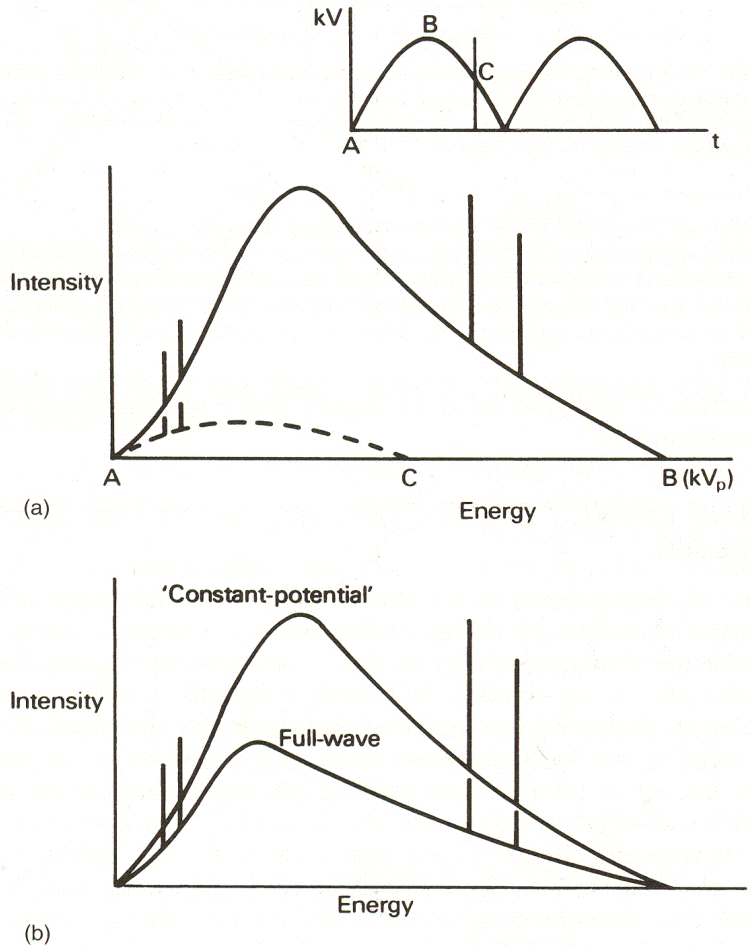

Figure 3.11: The effect of rectification on the X-ray spectrum. [Graham, 1996].

3.6.5 The effect of filtration on the X-ray beam

Filtration is the process of removing unwanted low energy radiation from the X-ray beam. This low energy radiation is removed by placing thin sheets of aluminium in the path of the beam at the point close as possible to the X-ray tube, usually at the

collimators, since they increase the dose to patient and do not contribute to the image in general radiography. When the filter is placed close to the tube effectively blurs out any imperfections in the filter. The aluminium "filters" the beams by removing low energy X-ray photons from the beam as shown as graph C in Figure 3.12. [Panichello, 1998].

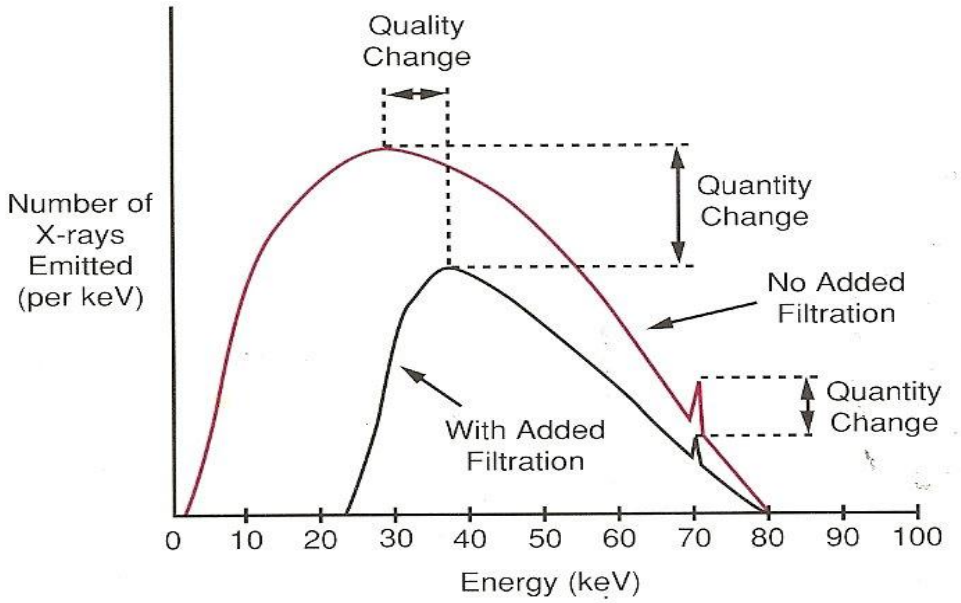

Figure 3.12: The effect of filtration on the X-ray spectrum. [Thompson *et al*, 1994].

Figure 3.12 shows an increase in filtration changes the shape and position of the continuous spectrum but the discrete spectrum is not affected. For a higher filtration, there is a reduction in the intensity of the beam and an increase in the beam energy (the amplitude of the continuous spectrum shifts to the right on the energy axis).

Inherent filtration is the filtration resulting from the absorption of X-rays as they pass through the X-ray tube and its housing. The materials responsible for inherent filtration are the glass envelope, closing the anode and the cathode and insulating oil surrounding the tube housing. The inherent filtration of diagnostic X-ray tubes is expressed in mm of aluminium equivalent i.e. the inherent filtration is equivalent to the filtration of the beam achieved by the stated number of millimetres of aluminium. The inherent filtration of most diagnostic X-ray tubes is between 0.5 mm and 1.0 mm of aluminium equivalent. The total filtration in the beam is the sum of the inherent filtration and the additional filtration. This total filtration is between 1.5 mm and

2.5 mm depending upon the maximum kVp at which the tube is design to operate. [Graham, 1996].

3.6.5.1 Wedge filter

Wedge filters are used in diagnostic radiology to adjust variations in patient thickness, thus achieving a beam that promotes a more uniform film density after it exit the patient. Less radiation is absorbed by the thinner part of the filter so more is available to penetrate the thicker part of the patient.

3.6.5.2 K-edge filter

K-edge filters use high-Z material to take advantage of K absorption edge effects, especially when used with high-speed intensifying screens and high capacity X-ray tubes. The purpose of K-edge filters is to produce an X-ray beam that has a high number of photons in the specific energy range that will be most useful in diagnostic imaging. Table 3.3 lists K-edge absorption energies for several elements that can be used to take advantage of the K-edge effect. [Martin, 2006].

Table 3.3: Atomic number and K-edges important to heavy metal filters. [Martin, 2006].

Element	Symbol	Atomic number	K-edge (KeV)
Aluminium	Al	13	1.6
Molybdenum	Mo	42	20
Gadolinium	Gd	64	50.2
Holmium	Ho	67	55.6
Erbium	Er	68	57.5
Ytterbium	Yb	70	61.3
Tungsten	W	74	69.5
Iodine	I	53	33.17
Barium	Ba	56	37.45

3.7 Interaction of X-rays with matter

There are two basic types of energy transfer that may occur when X-rays interact with matter:

- Ionization, in which the incoming radiation causes the removal of an electron from an atom or molecule leaving the material with a net positive charge.
- Excitation, in which some of the X-ray's energy is transferred to the target material leaving it in an excited (or more energetic) state.

The important processes that occur when X-rays interact with matter are:

- The Compton effect and
- Pair production and photodisintegration
- The photoelectric effect
- Coherent scatter [Connolly, 2007].

3.7.1 Compton Effect

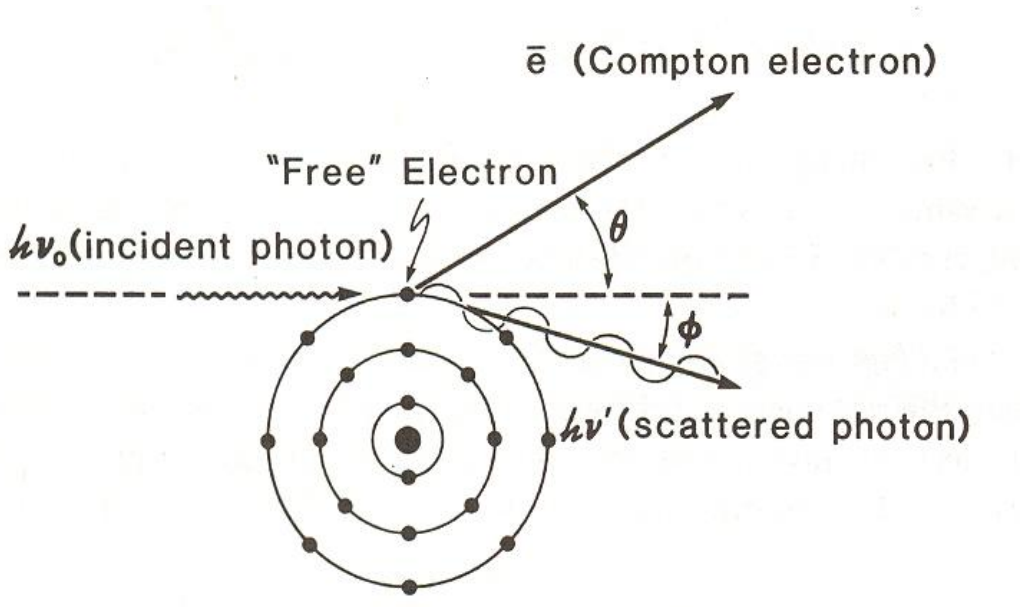

Figure 3.13: Illustrating Compton interaction. [Khan, 2003].

The Compton Effect involves the interaction of an incident X-ray with an atom. An electron is ejected from the atom with some kinetic energy, some of the incident photons energy is given to the Compton electron and its atom, but a significant fraction of it leaves the site of the interaction altogether, in a form of a newly created, lower-energy "scatter" photon.

The scattered X-ray and the high velocity Compton electron both appear at the exact instant of the collision. [Wolbarst, 1993]. By applying the conservation of momentum, one can derive the following relationships:

$$\mathrm{E} = h\upsilon_0 \frac{\alpha(1-\cos\phi)}{1+\alpha(1-\cos\phi)} \qquad 3.21$$

$$h\upsilon' = h\upsilon_0 \frac{1}{1+\alpha(1-\cos\phi)} \qquad 3.22$$

If the photon makes a direct hit with the electron, the electron will travel forward ($\theta = 0$) degrees and the scatter photon travel backward ($\phi = 180$ degrees) from the collision. Substituting $\cos\phi = \cos 180 = -1$ in equation 3.21 and 3.22, then the electron will have the maximum energy E_{Max} given by

$$E_{Max} = h\upsilon_0 \frac{2\alpha}{1+\alpha} \qquad 3.23$$

and the scatter photon will have a minimum energy [Khan, 2003]

$$h\upsilon'_{\min} = h\upsilon \frac{1}{1+2\alpha} \qquad 3.24$$

The Compton interaction coefficient σ consists of two components:

$$\sigma = \sigma_a + \sigma_s \qquad 3.25$$

Where σ is the total Compton interaction coefficient, σ_a is the Compton absorption coefficient for photon energy lost by collisions with electrons, and σ_s is the loss of energy due to the scattering of photons out of the beam. [Martin, 2006]. The Compton interaction coefficient is proportional to $\frac{1}{E}$. [Farr, 1997].

3.7.2 Pair production and photodisintegration

X-ray photons with energy greater than 1.02 MeV may interact with a nucleus to form an electron-positron pair. The interaction produces a pair of particles, an electron and positively charged positron. These particles have the same mass, each equivalent to rest mass energy of 0.511MeV. The positron is eventually captured by an electron and annihilation of the two particles occurs. [Sprawls, 1995]

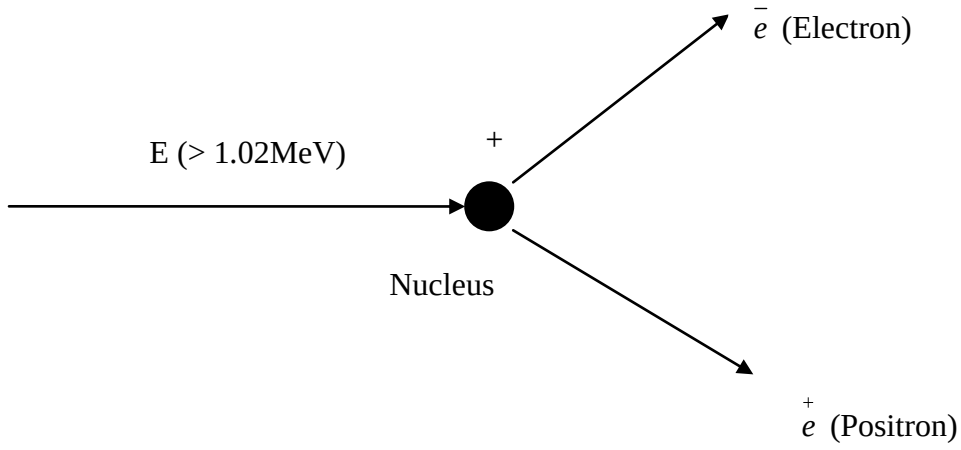

Figure 3.14: Illustration of pair production. [Graham, 1996].

Near the end of the range, the slowly moving positron interacts with one of the free electron in its vicinity to give rise to two annihilation photons, each having 0.51MeV energy. These photons are ejected in opposite direction because momentum is conserved [Khan, 2003] as shown in Figure 3.14.

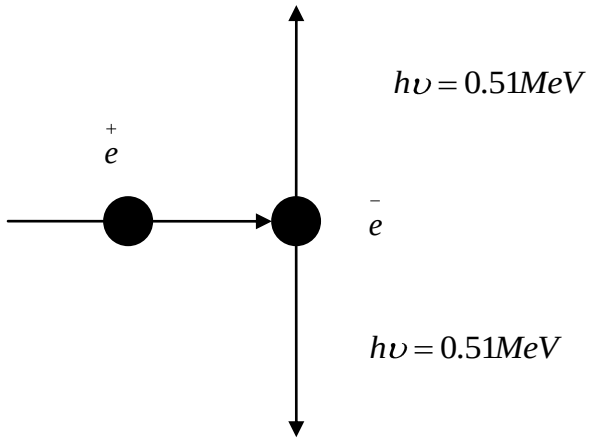

Figure 3.15: Illustration of the production of annihilation radiation. [Khan, 2003]

The pair production interaction coefficient κ is proportional to the square of the atomic number Z for photons with energy greater than $2 \times 0.511 MeV$ (the energy required to form an electron-positron pair) and has the following relationship:

$$\kappa \cong \text{Constant} \times Z^2 (E - 1.022)^n \qquad 3.26$$

Where E is the photon energy in MeV. [Martin, 2006]. Photodisintegration interactions occur when photons have enough energy to eject a nuclear particle when they are absorbed by a nucleus and can be used to measure the energy of a photon in a high-energy X-ray beam. [Hendee and Ibbott, 1996].

3.7.3 Photoelectric effect

The photoelectric effect is an interaction where a low energy photon collides with a bound orbital electron and ejects it from the atom. An ejected electron (photoelectron) has the energy equal to that of the incident electron, $h\upsilon$, minus the binding energy of the electron in its orbit ($h\upsilon - E_B$). A vacancy is created in the electron shell and a characteristic X-ray is emitted as an electron from the outer orbital shell (L or M shell electron) falls in to fill the vacancy. The kinetic energy of the ejected electron is absorbed in the medium when photoelectric absorption occurs.

The characteristic X-rays produced are absorbed in the medium typically by another photoelectric interaction or by the ejection of Auger electrons as shown in Figure 3.16.

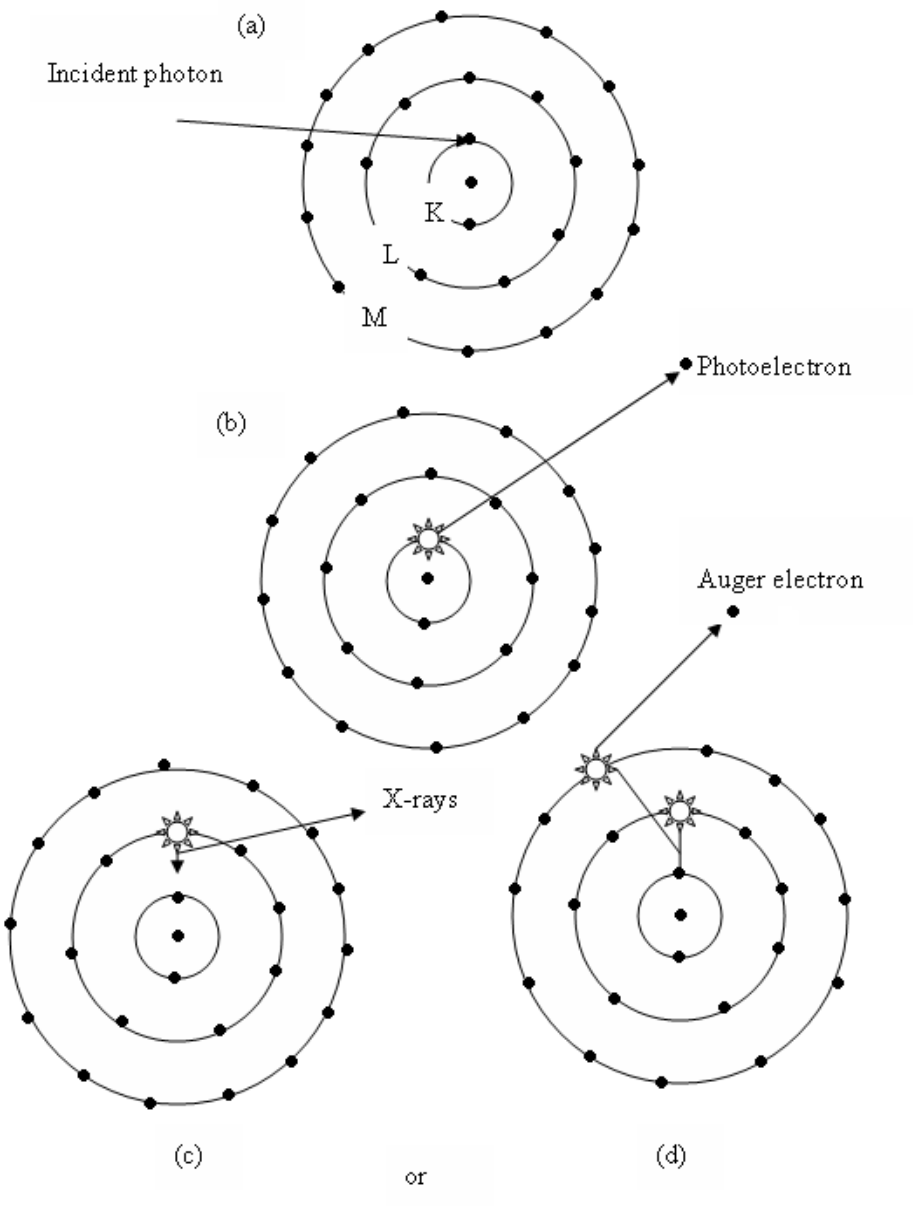

Figure 3.16: Photoelectric absorption. [Connolly, 2007].

Photoelectric absorber coefficient, τ , is a function of the atomic number Z of the absorbing material and the energy of the radiation as follows [Martin, 2006]:

$$\tau \cong \text{Constant} \times \frac{Z^3}{E^3} \qquad 3.27$$

3.7.4 Coherent scatter

When the energy of the incoming X-ray photon is less than the binding energy of an orbital electron, the Thompson interaction may occur. The orbital electron absorbs the entire photon, but this additional energy is not sufficient to eject the electron from its orbit. Instead, the electron is raised to a heightened state of energy for just a fraction of a second, after which it re-emits the photon with its original energy. This secondary photon, even though it is unchanged in energy from the original, is changed in direction and may be considered as scattered. However, coherent scattering accounts for only one percent of all scatter produced in the patient. These photons have very low energy and are less likely to reach the X-ray film.

When a free electron is irradiated with electromagnetic radiation, according to Dyson [1993] the differential cross-section for the scattering into a solid angle $d\omega$ is given by

$$d\sigma = \frac{\left\langle \mathrm{E}_s^2 \right\rangle}{\left\langle \mathrm{E}_i^2 \right\rangle} r^2 d\omega \qquad 3.28$$

Where E_s is the scattered field strength at a distance r and E_i is the incident electric field strength. From classical electrodynamics which states that the field strength E_s at a distance r from an accelerated charge e is given by

$$\mathrm{E}_s = \frac{1}{4\pi\varepsilon_0} \frac{ae}{rc^2} \cos\theta \qquad 3.29$$

Where a is the acceleration of the electron and θ is the angle shown in Figure 3.17. Since $a = \frac{\mathrm{E}_i e}{m}$ equation 3.29 becomes

$$\mathrm{E}_s = \frac{1}{4\pi\varepsilon_0} \frac{e^2}{mrc^2} \cdot \mathrm{E}_i \cos\theta \qquad 3.30$$

From equation 3.33 $$\frac{E_s}{E_i} = \frac{1}{4\pi\varepsilon_0}\frac{e^2}{mrc^2}\cos\theta \qquad 3.31$$

The differential cross-section becomes (from equation 3. 34)

$$d\sigma = \frac{1}{(4\pi\varepsilon_0)^2}\left(\frac{e^2}{mc^2}\right)^2 \cos^2\theta \cdot d\omega$$

$$= r_e^2 \cos^2\theta d\omega \qquad 3.32$$

Where r_e is the electron radius. If polarization of the incident radiation is perpendicular to the plane of Figure 3.17 all the rays scattered in a plane of the diagram is perpendicular to the acceleration of the electron $\cos\theta$ will be replaced by 1. For unpolarized radiation, the average value is used which is $\frac{1}{2}(1+\cos^2\theta)$.

Hence $$d\sigma = \frac{1}{2}r_e^2(1+\cos^2\theta)d\omega \qquad 3.33$$

And integrating over all values of θ, the total cross section becomes

$$\sigma = \frac{1}{2}r_e^2\int_0^{\pi} 2\pi\sin\theta(1+\cos^2\theta)d\theta = \frac{8}{3}\pi r_e^2 = 0.66\times10^{-28}m^2 \qquad 3.34$$

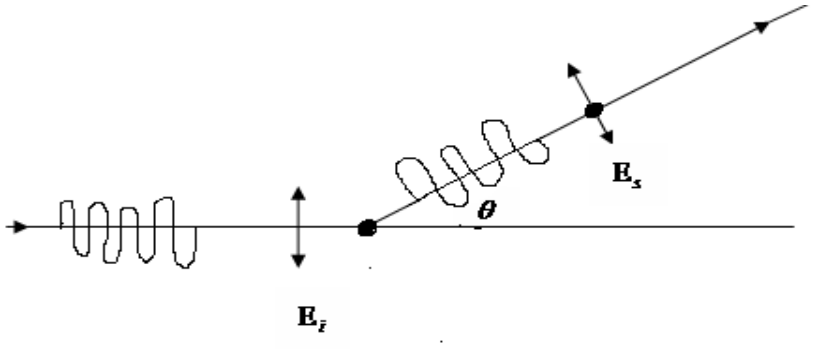

Figure 3.17: Thomson scattering. [Dyson, 1993].

Which process dominates is dependent on the mass absorption characteristics of the target (directly proportional to the atomic weight, Z) and the energy of the X-rays, shown in Figure 3.18. [Connolly, 2007].

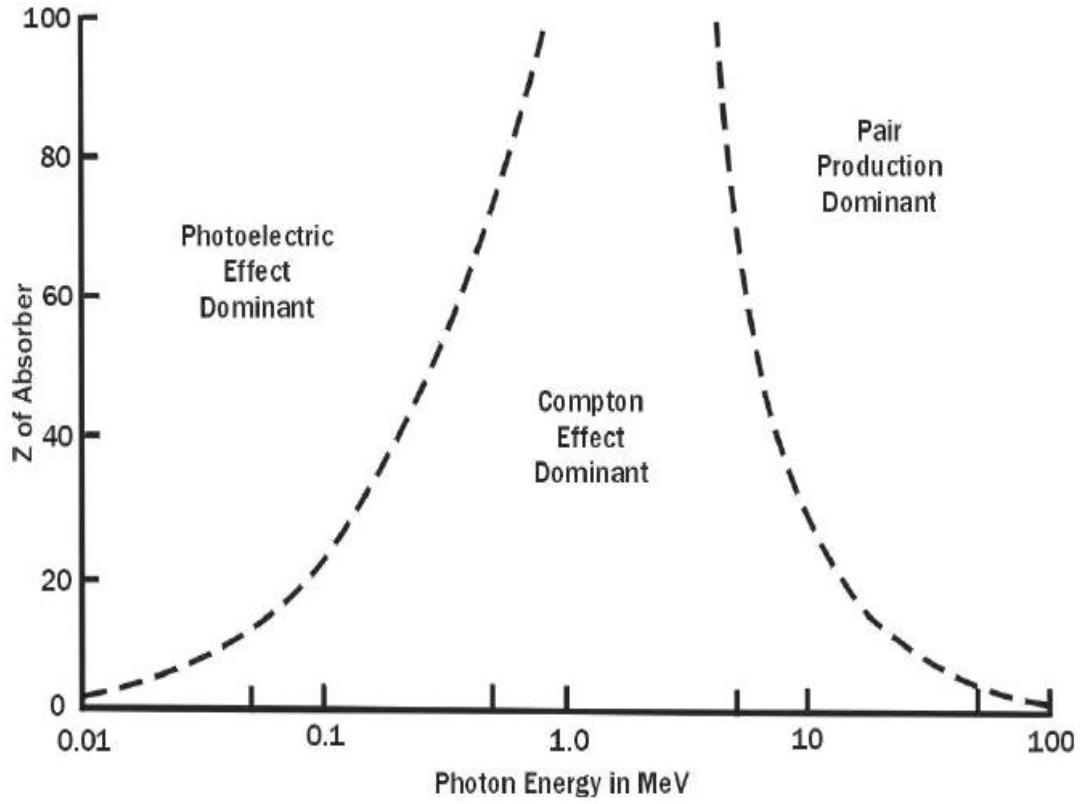

Figure 3.18: Importance of photoelectric absorption, Compton scattering and pair production. [Connolly, 2007]

The relative importance of photoelectric, Compton, and pair production interactions in different media is depicted in Figure 3.18. The photoelectric component τ increases with increasing atomic number of the absorber and the photoelectric effect dominates in heavy elements, at low photon energies. The photoelectric component also increases abruptly at energies corresponding to the orbital electron binding energies of the absorber element. The Compton-scatter component σ decreases slowly with increasing photon energy E and with increasing absorber atomic number Z. The pair production component κ is zero for energies less than the threshold energy of 1.02 MeV for this interaction, and then it increases logarithmically with increasing photon energy and with increasing atomic number of the absorber. Pair production is the

dominating effect at higher photon energies in absorbers of high atomic number. [Cherry *et al*, 2003].

Table 3.4: Contribution of each of the attenuation processes to absorption and scatter. [Graham, 1996].

Processes	Contribution to absorption coefficient	Contribution to scatter
Coherent scattering	No contribution to absorption coefficient as no energy is absorbed permanently by the medium	Makes a small contribution to the total scatter in medical radiography
Photoelectric absorption	Usually the energy of the photon is completely absorbed and so this process makes contribution to the total absorption coefficient	No scattering of the photon occurs as part of the photoelectric process
Compton scattering	Some of the energy of the photon is transferred to the medium during the scattering process and so contributes to the absorption coefficient	This is the major source of scatter in medical radiography
Pair production	Depending on the energy of the photon, this process produces partial or complete absorption	This process produces no scattering of the primary beam photons.

Chapter 4

QUALITY ASSURANCE OF EXPOSURE FACTORS

4.1 Introduction

The quality assurance programme for the diagnostic X-ray units is aimed to ensure that the image produced is consistently of high quality giving maximum diagnostic information with minimum radiation exposure to the patient at minimal cost. This will include quality control of the correctness and consistency of the various radiological parameters like: tube potential, tube current, time of exposure, half value layer, radiation output, field size, beam alignment and centering etc.

4.2 Exposure kilovotage and timer

The exposure time and peak kilovoltage (kVp) set on the X-ray generator must be accurate and repeatable to obtain properly exposed radiographs each time an exposure is made. The accuracy of the kilovoltage set on the control panel can have dramatic effect on the overall quality of the finished radiograph. A variation in the kilovoltage reading will result in a greater change on the radiograph than an equal variation in source film distance, exposure time, or tube current setting. [McLemore, 1981]

The X-ray generator must have an accurate and reproducible timer and kV for different settings. The accuracy of timer should be determined for a range of exposure times from the shortest to about 1 second. The resulting time should correspond to the actual exposure time within $\pm 5\%$. The normal range of kV is from 50 to 140 kV, the resulting accuracy of the measured value should be within $\pm 5\%$. [Code of Federal Regulations, U.S. Government printing office, Washington].

4.3 Half value layer

Before the half value layer can be measured, the kilovoltage levels produced by the machine must be known to be accurate. The quality of the X-ray beam is measured by placing increasing thickness of aluminium in the beam and measuring the decreasing intensity with the dosimeter. The thickness of aluminium that reduces the intensity to half is the half value layer (HVL). The HVL also indicates the relative quantity of soft radiation that increases patient dose without playing any part in image formation. HVL has an important influence on patient dose and image contrast. [Dowsett *et al*, 1998]. Table 4.1 gives the minimum values of the selected kV.

Table 4.1: Minimum values of HVL versus kV. [Dowsett *et al*, 1998].

kVp	Minimum HVL (mm)
30	0.3
50	1.2
70	1.5
80	2.5
100	2.8
120	3.2

The half value layer was calculated by logarithmic interpolation using the following formula

$$\mathrm{HVL} = \frac{t_b \ln[2\mathrm{E}_a / \mathrm{E}_o] - t_a \ln[2\mathrm{E}_b / \mathrm{E}_o]}{\ln[\mathrm{E}_a / \mathrm{E}_b]} \qquad 4.1$$

E_o is the direct exposure without added aluminium, E_a is the exposure greater than $\frac{\mathrm{E}_0}{2}$, t_a is the aluminium thickness of E_a, E_b is the exposure less than $\frac{\mathrm{E}_0}{2}$, t_b is the aluminium thickness of E_b. The graph of exposure (mR) versus added aluminium was plotted and the half value layers were indicated on the graphs.

4.4 Output linearity

Output linearity is the linearity of exposure (mAs) with radiation output (mR) and kilovoltage. Radiation output varies with kVp, mA and exposure timer; for a fixed kVp the radiation dose output (mR) should vary linearly with exposure (mAs). mR/mAs are measured in air and should show a linear relationship across the full range of exposure settings. The limiting value of mR/mAs should be less than or equal to 0.1 (≤ 0.1).

$$\left|X_1 - X_2\right| / \left(X_1 + X_2\right) \leq 0.1 \qquad 4.2$$

Where X_1 is the averaged value of mR/mAs of the first mA station and X_2 is the averaged value of mR/mAs of the second mA station.

4.5 Reproducibility of exposure

Reproducibility is a test that can document a problem with erratic or inconsistent exposures. Exposure reproducibility is called coefficient of variance (COV) and is calculated by dividing the standard deviation (σ) by the average value.

The coefficient of variance was calculated using the following equation:

$$COV = \frac{\sigma}{y} = \frac{1}{y}\left[\frac{\sum_{n-1}^{N}\left(y_n - \bar{y}\right)^2}{N-1}\right]^{\frac{1}{2}} \leq 0.05 \qquad 4.3$$

where σ is the standard deviation of the observation, $\bar{y}$ is the mean value of the observations, N is the total number of observations sampled. The coefficient of variance needs to be less than or equal to 0.05 as shown in equation 4.3.

4.6 Beam alignment and centering

One of the most common equipment problems is the misalignment of the light and X-ray field. This can be the results of shifts in the relative position of the light bulb filament, shifts in mirror position or shifts of collimator position on the tube head. [McLemore, 1981].

The set up of the beam alignment was 100 cm focus-surface-distance, 15 X 15 cm^2 field size , 60 kV and 25 mAs. For beam centering (Figure 4.1), if the images of two balls overlap, the centering are better than 1% and central ray is perpendicular to within 0.5°. If the images of the top ball intercept the first circle, the beam is centered to within 2% and the central ray is within 1.4° from perpendicular. If the image of the top ball intercepts the second circle, misalignment is 4% and should be corrected.

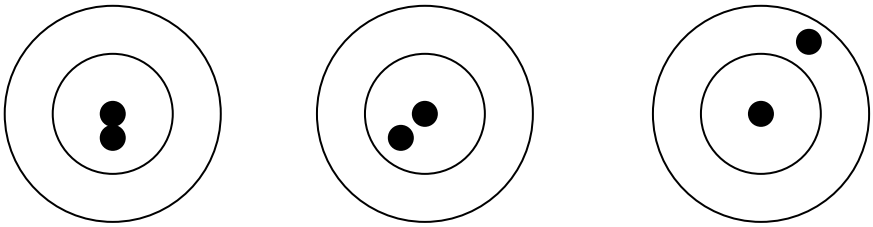

Figure 4.1: X-ray beam alignment tool. [McLemore, 1981].

The limiting value: The light beam diaphragm should be within 1 cm of the setting at a focus-film distance of 1 m. Further more the X-ray beam should not be misaligned by more than 2%.

Collimation of the X-ray beam is an important factor in optimization. Good collimation minimizes the dose to the patient and improves image quality because the amount of scatter radiation will increase if a larger volume of tissue is irradiated. [Martin, 2007].

It is important to check that the illuminated area of a light beam delineator coincides with the area irradiated by the X-ray beam. From Figure 4.2, the paper clips around the corners of the illuminated area should coincides with the irradiated area or should not be more than 2% misaligned for source to image distance of 1 m.

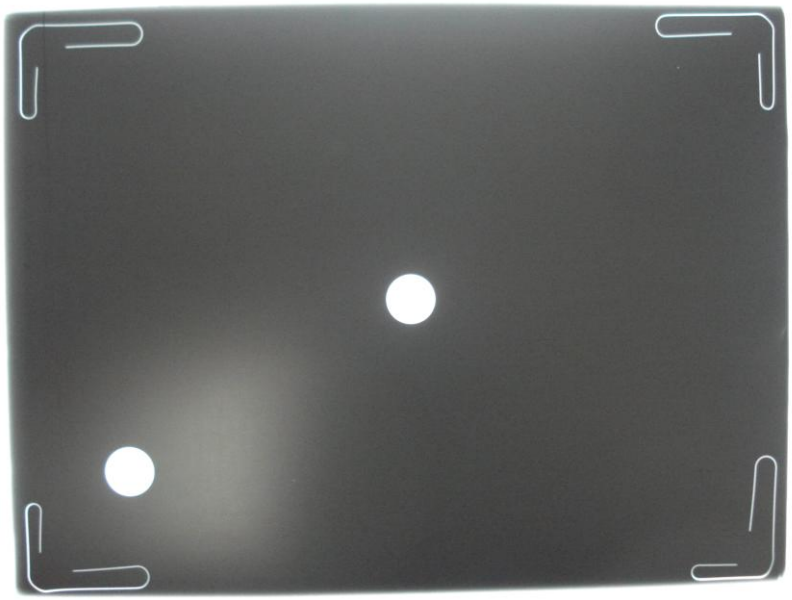

Figure 4.2: Radiograph of X-ray beam alignment obtained with the test cassette, paper clips and coins.

Chapter 5

MEASURING EQUIPMENT

5.1 Introduction

This chapter explains the behaviour, characteristics and the function of the material used to do quality assurance and to estimate the entrance surface dose. The equipment used was a full function meter for quality assurance and the thermoluminescence dosimetry and the Rando phantom for entrance surface dose measurements. The full function meter consists of the meter and ion chamber.

5.2 Full function meter

The full function meter RMI 242 is a complete X-ray beam quality assessment system for radiographic, fluoroscopic and mammographic X-ray units. In a single radiographic exposure the full function meter provides measurements for kilovoltage peak and effective, exposure and time duration in milliseconds and pulses.

5.2.1 Meter

The full function meter has three modes namely ‘A’ for radiographic, ‘B’ for mammography and ‘C’ for fluoroscopic. The RMI 242 incorporates a unique quad-cell detector with filter switching for kilovoltage measurements and ion chamber for exposure, exposure rate, exposure duration and relative mA/mAs linearity. The quad-cell detector with filter switching allows the meter to be used for a wide range of energies. It also provides accurate kilovoltage measurements independent of rotation and minor tilting effects. The Full Function Meter can be used to perform the following tests: kVp accuracy, exposure duration accuracy, relative linearity of mA/mAs linearity, mA/mR output and half value layer.

5.2.2 Ion chamber

The ion chamber has a volume of 22 cc so that signals will be large enough to have the precision needed for valid half value layer measurements. The chamber has a thin window where the radiation enters and this window is fragile, so it should be taken care of. The electrometer circuits resets several seconds after exposure but the digital storage of the value is reset at the start of the next exposure. The maximum value of exposure is 2500 mR with an overrange indicator above that value. [Gammex RMI, Full Function Meter RMI 242 User's Guide, 1995].

5.3 Thermoluminescence Dosimetry (TLD)

5.3.1 Theory of Thermoluminescent Dosimetry

The chemical and physical theory of TLD is not known, but simple models have been proposed to explain the phenomenon qualitatively.

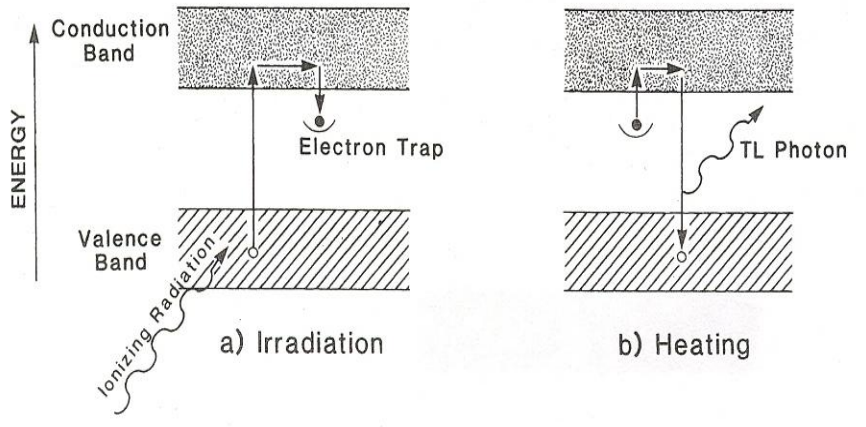

Figure 5.1: A simplified energy-level diagram to illustrate the thermoluminescence process. [Khan, 2003]

Figure 5.1 shows energy–level diagram of an inorganic crystal exhibiting TL by ionizing radiation. In an individual atom, electrons occupy discrete energy levels. In a crystal lattice, electronic energy levels are perturbed by mutual interactions between atoms and gives rise to energy bands: where electrons are allowed and where there are forbidden bands. The presence of impurities in the crystal creates energy traps in the

forbidden region, providing metastable states for the electrons. When the material is irradiated, some of the electrons in the valence band (ground state) receive sufficient energy to be raised to the conduction band. The vacancy thus created in the valence band is called a positive hole. The electron and the hole move independently through their respective bands until they recombine (electron returning to the ground state) or until they fall into a trap (metastable state).

If there is an instantaneous emission of light owing to these transitions, the phenomenon is called fluorescence. If an electron in the trap requires energy to get out of the trap and fall to the valence band, the emission of light in this case is called phosphorescence. If the phosphorescence at room temperature is very slow, but can be speeded up significantly with a moderate amount of heating (~300°C), the phenomenon is called thermoluminescence. A plot of thermoluminescence against temperature is called a glow curve. [Khan, 2003].

5.3.2 Glow Curve of LiF

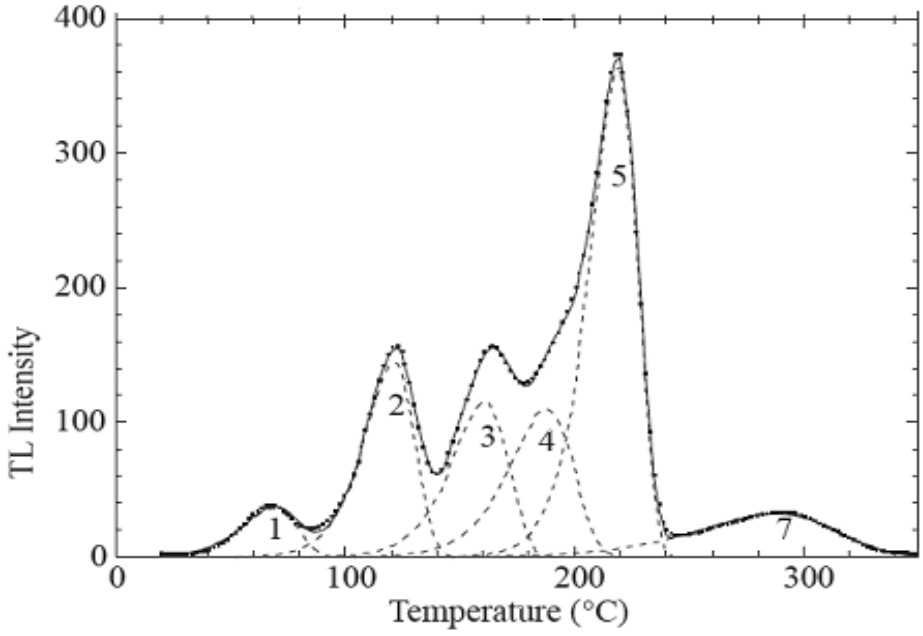

Figure 5.2: Glow curve of TLD-100 after an annealing at 400ºC for 1 hour followed by rapid cooling. [Yazici, 2002].

Linear heating of LiF allows the individual peaks of the glow curve to be discerned visually. If a mathematical function that describes the shape of the individual peaks that make up the curve is fitted to the experimental data, then the characteristics of the individual peaks can be quantified; this is the basis of glow curve deconvolution. It is assumed that the first order kinetic behaviour is given by

$$I = -dn/dt = s.n.\exp(-E/KT) \qquad 5.1$$

Where I is the TL intensity, n is the concentration of electrons in the trapped state, s is the frequency factor, k is the Boltzmann's constant, E is the activation energy in eV and T is the temperature in Kelvin. For a linear heating rate, B, TL intensity as a function of temperature, T, is given by:

$$I = s.n.\exp(-E/KT) \times \exp[-(s/B)\int \exp(-E/KT)dT] \qquad 5.2$$

This equation is difficult to implement on a computer as the second exponential term renders the equation unsolved by analytical means. For this reason, an approximation to equation 5.2 can be used:

$$I(T) = I_m \exp\left(1+\left(T-T_m\right)E/KT^2\right) - \exp[(T-T_m)E/KT^2] \qquad 5.3$$

I_m is the intensity and T_m is the temperature at peak maximum. Equation 5.3 indicates the individual glow peak, so to model the entire glow curve each of the individual glow peaks must be summed as:

$$I_{m,i}\exp\left(1+\left(T-T_{m,i}\right)E/KT_{m,i}^2\right) - \exp\left(\left(T-T_{m,i}\right)E/KT_{m,i}^2\right) \qquad 5.4$$

Where i is the i^{th} peak of the glow curve. The fitting of Equation 5.4 to the experimental data is accomplished by systematically altering the values of some or all of the variable parameters ($I_{m,i}$, $T_{m,I}$ and E_i) and assessing the statistical similarity between the theoretical and empirical glow curves at each instance to determine the optimum values. [Burke and Sutton, 1997].

5.3.3 Sensitivity

Sensitivity is defined as the ratio of absorbed dose and TL response (expressed as the area under the glow curve over a given temperature region or the peak height). [Ranogajec-Konor, 2002]. The sensitivity depends upon the TL readout system used in the measurement, along with the optical filters, the heating rate and the method of measurement of the TL signal (usually glow curve area between two chosen temperatures, or the height of a particular TL peak). To overcome uncertainties associated with the absolute measurement of sensitivity one normally defines a relative sensitivity by comparing the TL signal from the material of interest with the TL signal from LiF TLD-100. Thus TLD-100 has a sensitivity of 1; a sensitivity of S(D) is defined as

$$S(D) = \frac{F(D)_{material}}{F(D)_{TLD-100}} \qquad 5.5$$

Because of different degrees of supralinearity possessed by TLD material at different doses, compared to TLD-100, sensitivity is itself a function of dose. [McKeever *et al*, 1995].

5.3.4 Dose Response

McKeever *et al* [1995] defined the dose response as the functional dependence of the intensity of the measured TL signal upon the absorbed dose. The respond of a TLD material is linear and sublinear as the dose increased. The normalised dose response function $f(D)$ is given by

$$f(D) = \frac{F(D)/D}{F(D_1)/D_1} \qquad 5.6$$

Where $F(D)$ is the dose response at a dose D, and D_1 is a low dose at which the dose response is linear. In very favourable situations the dose function $f(D)$ will be linear over a broad dose range. At high doses, in practically all cases, superlinearity starts. At very high doses $f(D)$ may even decrease. [Ranogajec-Konor, 2002]

5.3.5 Energy Response

The energy response is the variation of the TL output, for a fixed dose, as a function of the energy of the absorbed radiation. This variation stems from the dependence of the material's absorption coefficient on radiation energy and for photon irradiation is defined in terms of the mass energy absorption coefficient μ_{en}/ρ of the material. The photon energy response $S_E(E)$ is defined thus:

$$S_E(E) = \frac{(\mu_{en}/\rho)_m}{(\mu_{en}/\rho)_{ref}} \qquad 5.7$$

Where m, refers to the TLD material and ref, refer to a reference material (normally air). Energy loss can take place by pair production, Compton scattering or the photoelectric effect. Which process dominates does not only depend on the energy of the incident photon but also on the critical material parameter, the effective atomic number Z_{eff}. The photoelectric component of the mass absorption coefficient varies approximately as Z_{eff}^3; the Compton component is proportional to Z_{eff}/M (M is the molar mass of the TLD material); and the pair production component varies as Z_{eff}^2.

The photoelectric interaction is dominant as the energy increases. Pair production is only important at high energies ($E >$ several MeV). The exact energy ranges for which these effects predominate are governed by Z_{eff}. For materials with low effective atomic numbers, the Compton Effect is the dominant energy loss mechanism for energies between ~25 keV to ~10 keV. [McKeever *et al*, 1995].

5.3.6 Accuracy of TLD's

The accuracy of the TLD is subject to uncertainty arising from a variety of sources including

- TLD calibration
- TLD signal fade

- Variations in TLD reader performance
- Nonlinear response of TLD to dose variation
- TLD response dependency on the beam energy [Seeram and Brennan, 2006]

5.3.7 Annealing Process

The reliable re-use of TLD materials often requires the use of strict thermal annealing procedures. Thermal annealing consists of pre-irradiation annealing (i.e. given temperature for a given period). The purpose of pre irradiation annealing is to re-establish the thermodynamic defect equilibrium which existed in the material before irradiation and readout. This is achieved by reversing the thermally driven diffusion reactions which sometimes occur during the TL process. These reactions may themselves be catalysed by the trapping of non-equilibrium charge at the defects during irradiation.

The TL sensitivity of a given peak is affected by the presence of deep, thermally disconnected, competing traps so it will be necessary to reset the occupancy of these more stable centres, if they exist, by high temperature annealing. The right equilibrium state must be achieved each time if the material is to be reliably re-used. The annealing protocols which have been established are believed to achieve these aims. [McKeever *et al*, 1995]

5.3.8 Handling of TL Dosimeter

Whatever material is used in a TLD system, great care should be taken when handling the TL detectors to avoid scratches or contamination of the chip. Therefore all TL material should be handled with vacuum tweezers. Trays made from ceramics or pyrex glass have been commercially available to avoid contamination of the chip (or rod) surface. Contamination should be carefully avoided because it reduces the light emitted from the chip. [Metcalfe *et al*, 1997]. Before used on a patient or phantom, TLD's are contained within a plastic sachet to protect the device from grease or dirt and light. [Seeram and Brennan, 2006].

5.3.9 Reading Process

The TLD Reader allows onboard evaluation of the dosimeters at the end of the exposure period. It consists of a power supply, photomultiplier tube, microprocessor controller, and data command and display. When the TLD is inserted into the reader, the glow curve and historical data about the TLD are retrieved. Current is supplied to the TLD, heating the crystal. As the crystal glows, the photons are counted by the photomultiplier tube and recorded by the reader processor as a glow curve. This glow curve is compared with the characteristic glow curve of the crystal and the controller provides a total dose measurement, by integrating the difference. [Apathy, 2002]. In Harshaw TLD's reader, the data is transferred to the personal computer (PC) and stored.

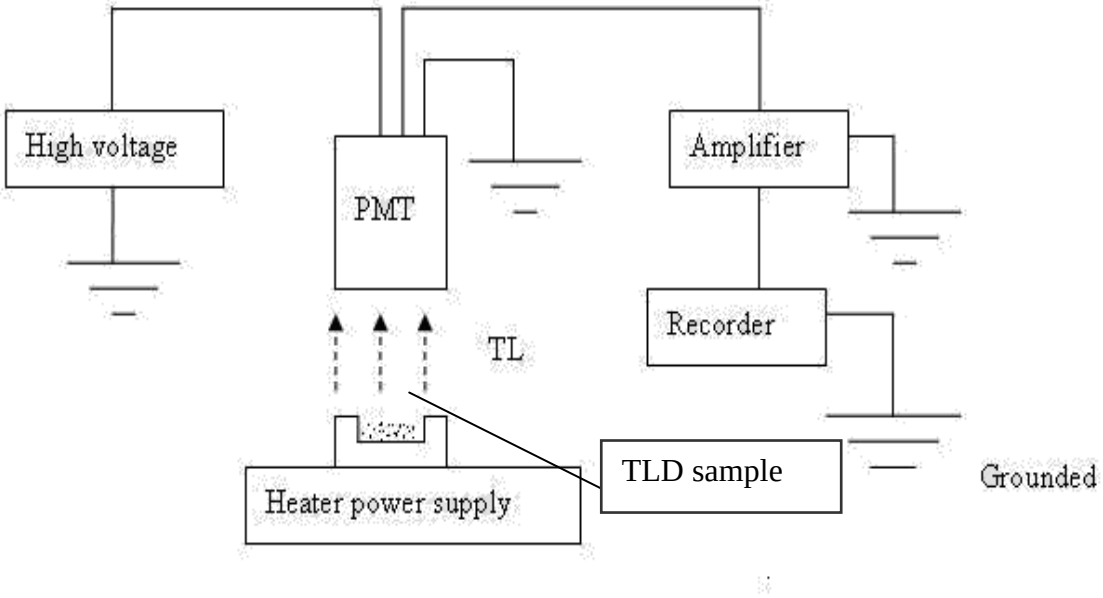

Figure5.3: Schematic diagram showing apparatus for measuring thermoluminescence. [Khan, 2003].

5.3.10 Materials for TLD's LiF

Lithium fluoride doped with magnesium (Mg) and titanium (Ti) is the most popular TL material used for dosimetry (TLD) today. Its popularity arises from its near tissue equivalence and its adequate sensitivity for personal dosimetry applications. [Ramos-Bernal *et al*, 2002; Yazici, 2002].

LiF has almost negligible fading at room temperature and it has low a atomic number, which does not differ much from that of air or tissue. The minimum sensitivity of LiF is about 10^{-2} rads (100 μGy) and the signals remains linearly related to dose up to about 10^3 rads (10Gy). [Knoll, 1989].

5.3.11 Advantages of TLD's

- Response is linear with dose over a wide range.
- Sensitivity is almost energy independent.
- Adequate sensitivity is achieved in a very small volume.
- Almost tissue equivalent.
- Usable over a wide range of radiation quantities.
- They are small, cheap, do not require an electronic power supply and can be used in a large dose range. [Ranogajec-Konor, 2002].

5.3.12 Disadvantages of TLD's

- They must be calibrated against standard radiation sources.
- Careful annealing is required after read-out to ensure that the TLD material returns to the same condition with reheat to the number of available traps otherwise the sensitivity and hence calibration factor of the TLD may change.
- It requires a complex series of pre-irradiation. Thermal anneals are used to assure acceptable reproducibility of the TL dose response curve, such as 400ºC for 1 h and 80°C for 24 h. [Ramos-Bernal *et al*, 2002].
- The stability of the TL signal of the LiF during storage is complex. Thus, it becomes important to assess the trapped charge within the material to predict any kind of fading.

5.3.13 Uses of TLD's

Clinical dosimetry

- TLD are fused into chips or rods of very small dimension. They may be placed in the body cavities to explore dose patterns produced by radiation.
- Useful to explore the dose in regions where the dose varies rapidly.
- TLD capabilities help to calculate dose in complex situations experimentally.

Personnel dosimetry

- Radiation monitoring and is rapidly replacing the use of film.
- Offers greater precision than film.

Dose Calibration Service

- Used to compare the procedure from one centre to another.
- TLD samples can be mailed to a group or centre and the user in each requested to irradiate the sample to a specified dose.

Physicists use this technique to:

- Measure the personnel dose.
- Calibrate high energy machines.
- Determine the dose in small inaccessible places in the body.

5.4 Phantom

When measuring the dose delivered to patient, the latter is often substituted by a phantom of the same general size and shape as the relevant part of the body and made of tissue-equivalent material. This material matches tissue as regards density and effective atomic number. It therefore absorbs and scatters an X-ray beam, whatever its

energy, in the same manner and to the same extent as the same volume of tissue. [Farr, 1997].

5.4.1 The Rando phantom

Figure 5.4: The Rando phantom [The Phantom Laboratory, 2009].

There are two Rando models: The Rando woman represents a 163 cm tall and 54 kg female figure and the Rando male represents a 175 cm tall and 73.5 kg male figure. Neither have arms or legs. Both phantoms are constructed with a natural human skeleton which is cast inside soft tissue-simulation material. Lungs are molded to fit the contour of the natural rib cage. The air space of the head, neck and stem bronchi are duplicated. The phantom is sliced at 2.5 cm intervals for the intersection film. Hole grid patterns can be drilled into the sliced section to enable the intersection of dosimeters.

5.4.2 Tissue-simulating material

Two tissue-simulations used to construct the Rando phantom are: the Rando soft tissue material and the Rando lung material. Both of these are designed to have the same absorption as human tissue at the normal radiotherapy exposure levels.

5.4.3 Soft tissue

The Rando phantom's soft tissue has an effective atomic number and mass density which simulates muscle tissue with randomly distributed fats. Small air bubbles may be evident in an image of the Rando phantom. These happen during the moulding process and are small enough that they should not have significant effect on studies.

5.4.4 Lungs

Rando lung material has the same effective atomic number as the soft tissue material with a density which simulates in the median respiratory state. The moulded lungs are hand-shaped and fitted to naturally fill the rib cage and natural human skeletons are used in the phantom.

5.4.5 Assembly

Each phantom section has registered pins mounted within it. These pins assist in the proper alignment of the phantom sections. An assembly unit is supplied with the phantom. It holds the entire phantom or a small set section together at one time. [The Phantom Laboratory, 2009].

Figure 5.5: The Rando phantom sections. [The Phantom Laboratory, 2009].

5.5 Some of the detectors that can be used to measure radiations

5.5.1 Geiger müller counter

The Geiger müller counter is a special type of ionization chamber which can detect individual ionizing particles and photons. The operation principle of Geiger müller is as follows, the incoming radiation produces ion pairs by direct ionization and through secondary for electrons (delta rays) created in the ionizations process. These ion pairs are then multiplied by avalanches process that in turn triggers further avalanches through the emission of ultraviolet radiation. This process is terminated when a sufficient number of positive ions collected around the anode, effectively reducing the electric field experienced by the electrons owning to charge build up at the anode. [Cherry *et al*, 2003].

5.5.2 Ionization chamber

Most gas-filled detectors belong to a class of detectors called ionization detectors. The detectors respond to radiation by means of ionization-induced electric current. To measure the charge, the ions are separated before they can recombine by applying a polarizing voltage between the outer thimble wall and a thin central electrode. The positive ions are attracted to the negative electrode and the negative ions (electron to the positive electrode. Ionization current I flows, proportional to the dose rate of the radiation and the mass of air in the chamber. The charge can be collected and the air kerma indicated on a meter or digital read out. [Farr, 1997].

5.5.3 Semiconductor detectors

Semiconductor detectors are essentially solid-state analogs of gas-filled ionization chamber. Because the solid detectors materials used in semiconductor detectors are 2000 to 5000 times denser than gas, they have more efficient detectors for X-rays. Semiconductor are poor electrical conductors; however when they are ionised by an ionizing radiation event, the electric charge applied voltage, as it is with gas-filled detectors. This principle cannot be applied using a conducting material for the detector because the conducting materials would conduct a large amount of current even without ionization event. The most commonly used semiconductor detector materials are silicon (Si) and germanium (Ge). [Cherry *et al*, 2003].

Chapter 6

METHODOLOGY

6.1 Introduction

This chapter describes the method used for quality assurance test and the method used to estimate the entrance surface dose test using a phantom and TLD's while illustrating the equipment used.

6.2 Quality assurance procedure

Quality assurance was done using a Full Function Meter RMI 242 (Gammex RMI)

The ion chamber was connected to the meter before turning it on. Focus to surface distance was set to 1m and the light field was collimated to 15cm$\times$15cm. Radiographic mode was selected ('A') and the rear panel was switched to integral.

6.2.1 Accuracy of kV and timer

The desired kVp and exposure timer were selected on the X-ray units and the exposure was made. The function buttons on the front of the meter was used to display the values for kVp, time/pulse, dose/dose rate and rel mA/mAs and was recorded. This was done five times with the same exposure setting and the average was calculated. This was repeated with the various exposure settings. The values obtained from the meter were compared with the set values on the X-ray units and the % difference were calculated using this equation

$$\frac{|\text{Actual value} - \text{Measured value}|}{\text{Actual value}} \times 100 \qquad 6.1$$

The exposure (mR) obtained while measuring the accuracy of timer and kV were used to calculate the coefficient of variance. COV was calculated using equation 4.3.

6.2.2 Half value layer measurement

The kVp, time, and mAs or mA was set on the X-ray units and the exposure was made. The exposure (mR) obtained from the full function meter was recorded. A 0.5 mm sheet of aluminium was taped to the collimator and the exposure was made and the value was recorded. A aluminium sheets were added to the collimator in 0.5 mm thickness until the total thickness of about 5 mm was achieved and the exposure (mR) were recorded while adding the aluminium sheets. The exposure value that was half the value of the initial value (without aluminium sheet) is the half value layer. The halve value layer was calculated by logarithmic interpolation using equation 4.1.

6.2.3 Linearity of mA and mAs

The procedure was the same as that one of measuring the accuracy of timer and kV but here the exposure was repeated three times for the same exposure settings. mR/mAs was calculated for each set of exposure and the average it was calculated. The linearity between mA stations was calculated using equation 4.2. [Gammex RMI, Full Function Meter RMI 242 User's Guide, 1995]

6.2.4 Beam alignment and centering

For beam centering, the template was placed on the film cassette and the beam alignment tool was located carefully over the central target area on the template. The light diaphragms were opened until the inner square was covered completely. The tube focal spot was positioned 1 m above the template. The exposure was made. For beam alignment, the field size was selected and paper clips were placed on the corners of the field size on the cassette. One coin was placed in one of the corners to identify the orientation of the tube and one at the center. The exposure factors were selected on the X-ray units. Exposure was made with the appropriate machine settings and films were processed in the dark room.

6.3 Cleaning TLD's

Forty TLD's were placed in a small clean beaker filled with alcohol to cover the TLD's. The ultrasound cleaner was plugged in, switched on and the timer was set to run for five minutes. The TLD's were then rinsed with distilled water using the ultrasound cleaner by setting the timer to run for three minutes. TLD's were left over night to dry.

Figure 6.1: Ultrasound cleaner

6.4 Annealing TLD's

TLD's were annealed in the oven for one hour at 400ºC followed by four hours at 100ºC using a Thermolyne heater. The dried TLD's were placed on the oven tray and put in the oven and the oven was switched on. The oven automatically began the heating cycle and was left overnight to complete the heating cycle and cool down. The TLD's were then placed in the TLD's holder and numbered.

Figure 6.2: Annealing oven

6.5 Calibrating TLD's

The TLD's were calibrated using Pitman 623 dosimeter irradiator. Before the TLD's were calibrated, the number of revolutions was calculated which were needed to irradiate the TLD's with a dose of 1 rad or 0.01Sv using the decay equation given by:

$$N_t = N_o e^{-\lambda t} \qquad 6.2$$

Where N_o is the initial (i.e. the number of revolutions used by the previous user in the irradiator) number of revolutions. The dosimeter irradiator has a radioactive source of Sr-90 which has a half life of 28.5 years.

The half life given by:

$$T_{\frac{1}{2}} = \frac{\ln 2}{\lambda} \qquad 6.3$$

Then $$\lambda = \frac{\ln 2}{T_{\frac{1}{2}}} \qquad 6.4$$

$$= \frac{0.693}{28.5 years} = 0.0243\ years^{-1}$$

From equation 6.2 t is the time elapsed from the previous number of revolutions. This is calculated by using the previous date the irradiator was used minus the present day. To ensure that the number of revolution used by the previous user was correct, the number of revolution was also calculated using the date of measurement found in the irradiator. The number of years, months or days elapsed found will be t in equation 6.2. The number of revolutions was calculated using equation 6.2.

Figure 6.3: Dosimeter irradiator.

The dosimeter irradiator only accommodates 29 TLD's at a time, so from the 40 TLD's the first 29 were selected and placed in and irradiated in the order as numbered. The number of revolutions calculated was punched on the irradiator to expose these TLD's to 1 rad. The rest of the TLD's were also irradiated to 1 rad using

the same number of revolutions. The TLD's used for chest examinations were irradiated to 0.125 rad.

6.6 Reading out the TLD's

The program used to read the TLD's was DXT software from Harshaw.

6.6.1 Opening response file

Before any reading could be made, a response file was opened as all TLD data is stored in the response file.

The response file was selected from the main menu and then the option "Open" was selected from the file pull-down menu. The file selection Dialogue Box was displayed, from the filename field, which read 'TLD', Dumela was typed and saved, the filename read as "C:\TLDATA\DUMELA.TLD". The selection Dialog Box disappeared from view and the message box was cleared from the screen by pressing enter.

6.6.2 Setting a time temperature profile

Time temperature profile defines a new time temperature profile (TTP). A TTP is the temperature to which the TL element is heated as a function of time.

From the main menu, TTP was selected from the Parameter pull-down menu; on the profile field option "A" was entered. From the title field "Medical Physics" and the date was entered. Instrument ID is a display field which shows the Reader for which TTP is intended. This instrument ID field on the acquisition setup Parameters should match this ID, or the TTP would not be recognised.

The fields identified as roi1, roi2, roi3 and roi4 are the region of interest (ROI) fields that divide the 200 data channels of a glow curve into four sub ranges. The region of

interest defines the specific temperature intervals for which charge may be collected. The following ROI values were typed:

roi1:”1”, ‘50’

roi2: “51”, ‘100’

roi3:”101”, ‘150’

roi4:”151”,’200’

After entering the last ROI value, the calibration region field was selected and it determined the range of channels of the glow curve for which an integral value was reported. From Pre-heat Temp field, the pre-heat time field was set to 10ºC/seconds, the acquired temperature was set to 300ºC and the acquired time field at 33.33 sec. The anneal Temp Field was set at 300ºC and the anneal Time field at 0sec. The TTP setting dialog looked like the one in Figure 6.4.

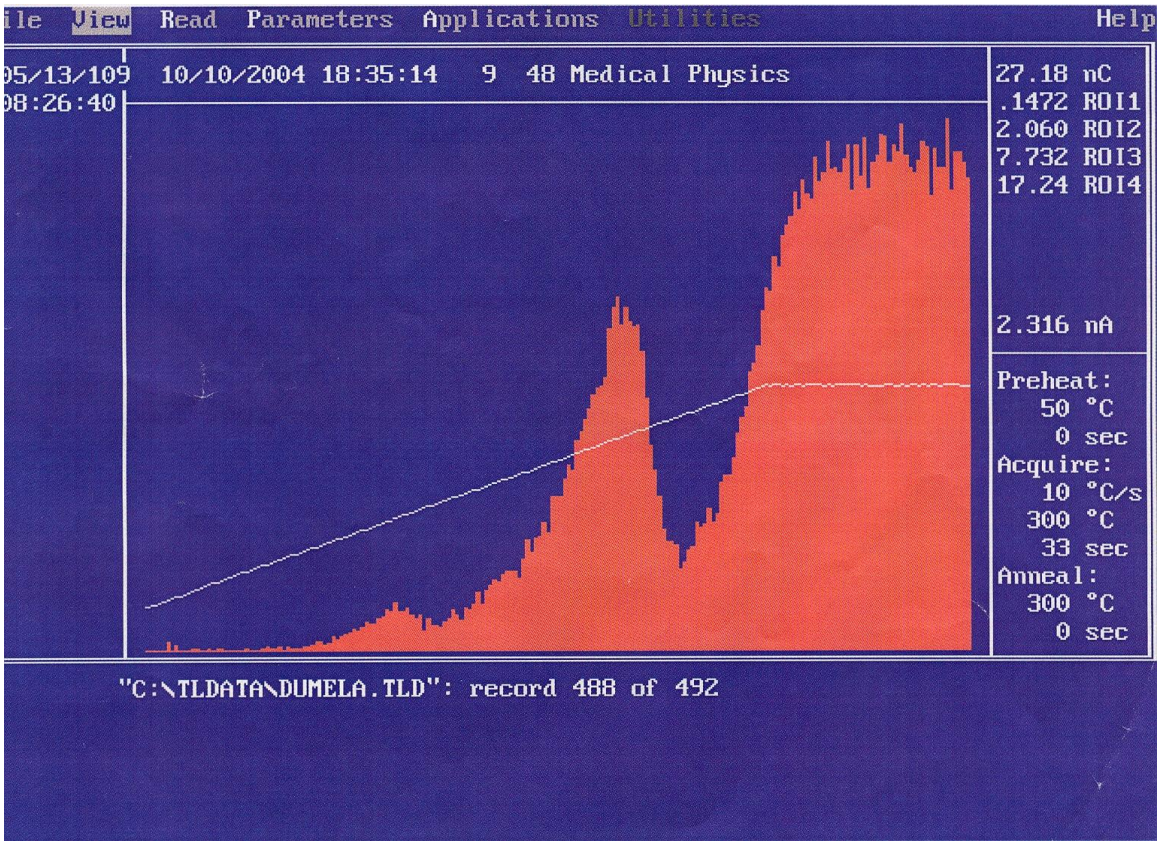

Figure 6.4: The glow curve after TLD has been read.

6.6.3 Reading TL materials

The following procedure was used to read a set of TL samples.

(a)

(b)

Figure 6.5: (a) Overview of the Harshaw 3500 TLD reader. (b) The open planchet where TLD chip is placed.

The reader was turned on and warmed up for 30 minutes to bring the PMT temperature down to its operating level. On the controlling PC, TLD shell was

selected and the response file opened. The desired acquisition parameters were defined and the TTP with the desired parameter was confirmed if it was available. The reading from the main menu was selected and brought a pull-down menu into view with the selection Go. Go was selected from the acquired menu to initiate the TL reading. This started the reading process from the top of the chipset file.

The PMT Noise and the Test light readings were required. The PMT Noise was read by pulling the drawer open until the drawer status on the screen displayed "between" and enter was pressed to initiate the PMT Noise reading. The reading was plotted on the screen as the reading was performed and the curve on the computer was displayed. The results appearing on the right side of the screen was recorded automatically. To read the Test light, the drawer was pulled all the way out and the Drawer status read "Opened". This was the position for the Test light reading, and the read button was pressed on the front of the instrument. All the subsequent readings were started by the pressing the READ button on the instrument.

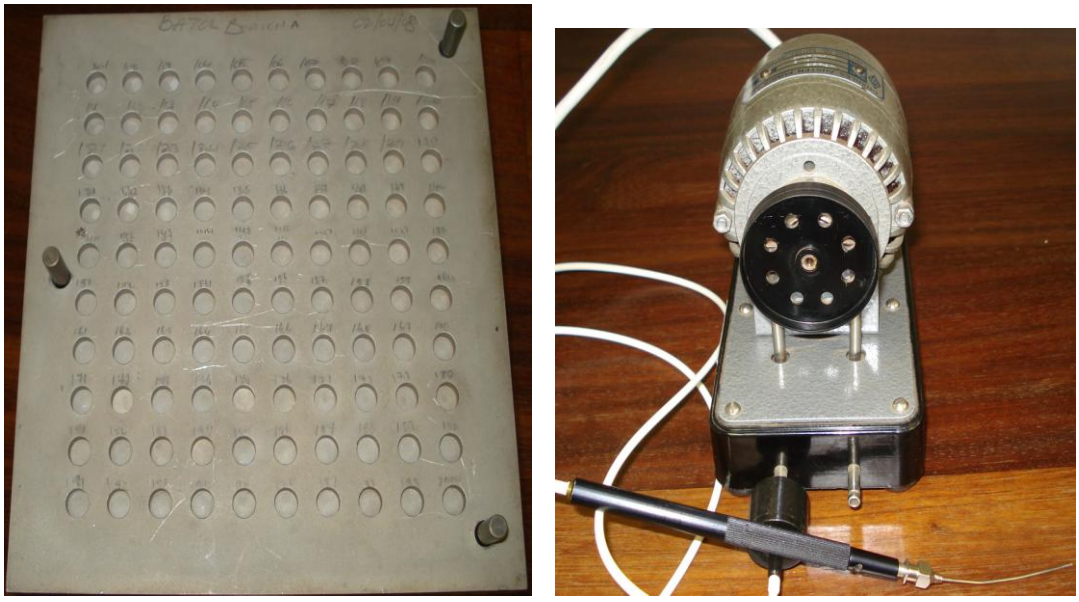

Figure 6.6: The TLD's in the numbered tray and the suction tweezer.

The instrument accommodates only one TLD at a time. The TLD was placed in the planchet and the sample drawer was closed and the Read button was pressed to start the TL data acquisition.

The glow curve was plotted on the screen as it is acquired, and when the cycle was completed, the curve on the computer screen was replotted to full scale and the numerical results (charge integral $\langle Q \rangle$) appeared on the right side of the screen was recorded since the TLD reader was connected to a computer). When the reading was stabilized and the main menu reappeared, the reading was recorded in the book with TLD position and number but these readings were also stored in the computer. The drawer was pulled out to remove the TLD and place it in the tray in its original position. The next TLD was read and so on. [Radiation Measurement Products Model 3500 TLD Reader User's Manual, 1993].

When all the TLD's were read, the average charge integral (reading) $\overline{Q}_c$ was calculated by adding up all the charge integral readings dividing by the number of observations. The reader calibration factor (RCF) was calculated using the equation:

$$RCF = \frac{\overline{Q}_c}{D} \qquad 6.5$$

Where D is the actual exposure (1 rad) given to the TLD's.

6.7 Calculating the element correction coefficient

It is important to calculate individual Element Correction Coefficients since not all TLD's are manufactured with the same thermoluminescent efficiency (TLE). TLE is defined as the emitted thermoluminescent light intensity per unit of absorbed dose. ECC_j for each TLD was calculated using the formula:

$$ECC_J = \frac{RCF \times L}{q_j} \qquad 6.6$$

Where j is the number of the TLD, L is equal to 1 rad and q_j is its reading. RCF was calculated using spread a sheet.

6.8 Covering TLD's

Figure 6.7: The TLD covered with plastic cover, wrapped by masking tape with its unique number.

Before TLD's were used in light or X-rays, each TLD was placed in a clean plastic cover using a suction tweezer to avoid contamination and touching it by hand before use. The plastic cover was wrapped in masking tape. The package has a unique number that corresponds to the TLD position.

6.9 Measuring the entrance surface dose (ESD)

The survey took place with 5 X-ray machines (Shimadzu, Philips, Toshiba and two Digital diagnost). The following ten examinations were taken into consideration: skull (AP and LAT), chest (PA and LAT), lumber spine (PA and LAT), pelvis (AP), abdomen (AP) and cervical spine (AP and LAT). Not all of the listed examinations were assessed in each X-ray unit. To eliminate the problem of globally defining the "standard-sized patient", a phantom was used in this study. [Seeram *et al*, 2006].

The radiation dose was measured for each examination with thermoluminescent lithium fluoride (LiF) (TLD-100 Harshaw) and was 3.16 X 3.16 X 0.9 mm^3 in dimension.

The dosimeters were placed in the centre of the X-ray beam on the surface of the patient. The clinically used focus-film distance (FFD) was set and recorded, the focus-to-surface distance was measured taking into account the position of the focal spot inside the X-ray tube and the field size was recorded. The same field size was used for each examination in all the X-ray units used. The tissue/phantom was positioned in the X-ray field in the standard way as shown in Figure 6.8. Three TLD's were mounted on the tape and placed in the centre of the X-ray beam on the surface of the phantom external to the organ being imaged.

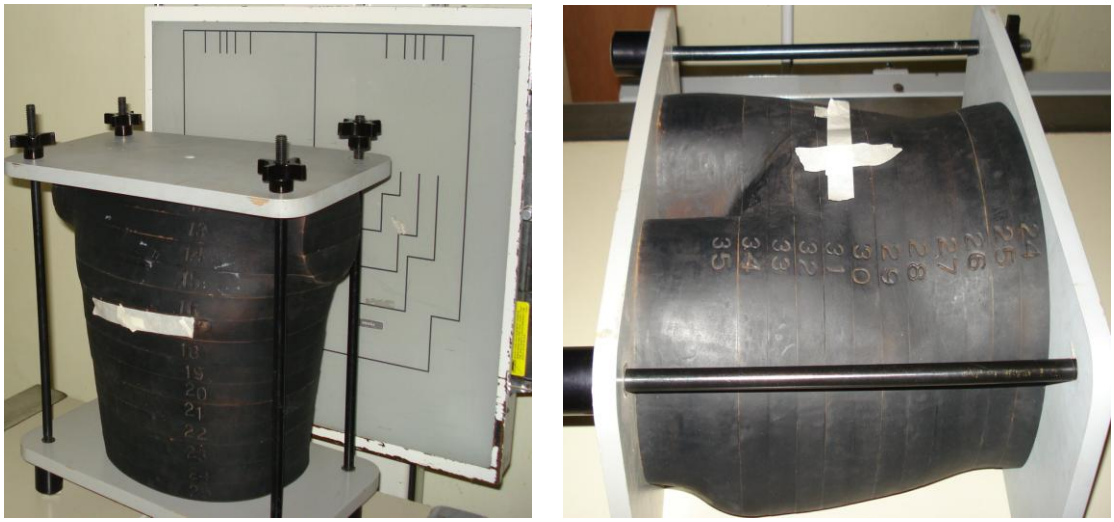

Figure 6.8: The Rando phantom with the TLD's taped on it.

The X-ray generator was set to a desirable technique for an average person (technique factors used were displayed on the technique chart), kV and mAs values were recorded and the cassette was placed into the bucky tray then removed and taken to the developer to process the film. Due to the small size of the TLD's, the imaging process was not affected and therefore there is no loss of diagnostic information on X-ray images. For digital machines, the image was shown on the screen and was printed to check if any diagnostic information was lost for a particular technique.

The exposure switch was used to initiate and terminate X-ray production, this control automatically terminated the exposure after a preset time, product of current and time, or exposure has elapsed. The phantom was exposed and the film was developed. This was repeated three times for each examination. The backscattered radiation was

included in the recording. The TLD's were read out from the Harshaw 3500 TLD reader. The method of how to read the TLD is explained in section 6.6.3.

6.10 Calculating exposure dose

The dose for each TLD exposed to radiation was calculated using the following formula:

$$D = \frac{Q_j \times ECC_j}{RCF} \qquad 6.7$$

Where Q_j is the charge integral for each of the TLD's exposed to radiation. The dose was reported in Appendix 2 as D and was in Rad. The doses were converted into mGy and were considered as entrance surface dose in mGy. 1 rad= 0.01Sv= 10 mSv = 10mGy.

The mean dose (ESD) of three TLD's was calculated for each exposure and the mean ESD's per X-ray unit were calculated from the individual ESD's measured on the phantom of the examination considered. With this procedure the final estimate of ESD for the examination considered is independent of the number of ESD's measured for each X-ray unit. Subsequently the read-out TLD's were annealed again to ensure that the TLD material returns to the same condition with response to the number of available traps, otherwise the sensitivity and the calibration factor of the TLD might have changed. These TLD's can be used for another examination.

The standards deviations were calculated from the entrance surface dose for each examinations of each X-ray unit.

Chapter 7

RESULTS AND DISCUSSION

7.1 Introduction

This chapter is divided into two sections: the first section consisting of the results for the quality assurance and the second section discussing the entrance surface dose.

7.2 Quality assurance test

Before the study was commenced, quality assurance was done on the X-ray machines used. The following quality assurance was done: timer reproducibility, to ensure that the timer will give consistent and reproducible results; half value layer, to assess the X-ray beam quality and determine the adequacy of filtration; relative mA and mAs linearity, to determine that the mA or mAs stations are linear, relative to the first exposure throughout the range of mA and mAs stations; timer and kVp accuracy, to determine that the machine is producing the time and kVp selected on the control panel; reproducibility of the output (coefficient of variance), to determine that the exposure is consistent from exposure to exposure with the same kV, mA, time and focus-surface distance and beam alignment, to ensure alignment of the X-ray field with the light field and bucky tray.

The X-ray units used for this study were:

- Shimadzu CID 150L-R11
- Philips digital diagnost (1)
- Philips digital diagnost (2)
- Toshiba finescope 8000 (Fluoroscopic unit)
- Shimadzu chest digital (Chest unit)

7.2.1 Accuracy of timer and kV

The percentage accuracy between the set values and the measured values of the kilovoltage (kV) and exposure timer are given in Table 7.1. The original values can be found in Appendix 1A.

Table 7.1: Percentage accuracy of kilovoltage and exposure timer

X-ray unit	% accuracy	
	Kilovoltage	Exposure timer
Shimadzu CID	<5.98	<4.8
Philips digital diagnost (1)	<3.6	<4.2
Philips digital diagnost (2)	<1.9	<2.04
Fluoroscopic unit	<7.46	--
Chest unit	<3.8	<0.26

-- The values are not available

7.2.2 Half value layer

Table 7.2 shows the half value layer of each X-ray unit measured by a full function meter (FFM) and sheets of mm of aluminium. The measurements of each X-ray unit were drawn on the graphs of output (mR) versus added aluminium (mm) and the half value layers were indicated on the graphs. (Appendix 1B)

Table 7.2: Half value layer

X-ray unit	kV set	HVL (mmAl)
Shimadzu CID	80	2.4
Phiips digital diagnost (1)	81	3.2
Phiips digital diagnost (2)	81	3.2
Fluoroscopic unit	90	4.02
Chest unit	90	3.04

7.2.3 Reproducibility of output (mR)

Table 7.3 shows the coefficient of variance (COV) of each X-ray unit for different kV and mAs set. The coefficient of variance was calculated using equation 4.3.

Table 7.3: Coefficient of variance of the output (mR)

X-ray unit	kV set	mAs set				COV			
Shimadzu CID	60	25	50	80		0.007	0.002	0.008	
	90	16	32	50	63	0.003	0.002	0.002	0.003
	110	12	25	40	50	0.003	0.002	0.001	0.001
Philips digital diagnost (1)	60	80	200	320	400	0.001	0.00	0.001	0.001
	80	80	160	200	250	0.001	0.001	0.000	0.000
Philips digital diagnost (2)	50	80	200	320	400	0.000	0.002	0.002	0.001
	80	80	160	200	250	0.000	0.002	0.001	0.000
	110	10	20	32	40	0.006	0.000	0.001	0.001
Fluoroscopic unit	70	5	16	20	25	0.014	0.005	0.007	0.004
	90	5	16	20	25	0.009	0.003	0.006	0.007
	120	11				0.005			
Chest unit	70	50	100	160	180	0.009	0.002	0.009	0.008
	90	50	80	125	140	0.006	0.002	0.002	0.003
	125	63	80	100		0.003	0.002	0.001	

The column for mAs set and COV have four cells, the first cell of mAs set corresponds with the first cell of COV and so on. The coefficient of variance calculated are all less than 0.05 for all the kV and mAs considered and they comply with the requirement that they should be less than 0.05, as indicated in equation 4.3.

7.2.4 Linearity of mA and mAs stations

Table 7.4 shows the linearity of mA and mAs. The linearity between mA stations was calculated using equation 4.2.

Table 7.4: Linearity of mA and mAs stations

X-ray unit	kV set	Between mAs stations		
		10-25	25-32	32-40
		Linearity		
Shimadzu CID	60	0.011	0.010	0.015
	70	0.021	0.008	0.002
	80	0.019	0.011	0.002
	90	0.014	0.009	0.004
	100	0.005	0.017	
	110	0.005	0.003	0.014
Philips digital diagnost (1)	60	0.000	0.007	0.003
	70	0.003	0.005	0.002
	81	0.000	0.001	0.001
	90	0.001	0.003	0.001
	102	0.001	0.002	0.001
Philips digital diagnost (2)	50	0.013	0.005	0.005
	60	0.027	0.015	0.002
	70	0.004	0.001	0.001
	80	0.006	0.001	0.001
	90	0.001	0.000	0.003
	100	0.004	0.003	0.003
	110	0.002	0.003	0.006
Chest unit	70	0.000	0.006	0.006
	90	0.006	0.004	0.004
	110	0.007	0.011	0.001
	125	0.022	0.014	0.002
		Between mAs	Stations	
		5-16	16-20	20-25
Fluoroscopic Unit	70	0.003	0.034	0.002
	90	0.018	0.019	0.004

The column ‘between mAs stations’ has three cells and their values for linearity also have three cells, thus the first cell of ‘between mAs stations’ corresponds with the first column of linearity and so on. The output of the different kV set and mAs was found to be less than 0.1 for all the X-ray units considered, which complies with the requirement.

7.2.5 Beam alignment and centering

Table 7.5: Beam alignment

X-ray units	%	
	Cathode (-)	Anode (+)
Shimadzu CID	0.3	0.5
Philips digital diagnost (1)	0.5	0.0
Philips digital diagnost (2)	0.5	0.4
Fluoroscopic unit	0.6	0.4
Chest unit	0.3	0.2

All the X-ray units showed a good alignment of the light and X-ray field since they comply with the requirement of $\pm 2\%$ and for beam centering, all the images (balls) were located in the inner circle which is acceptable. (Appendix 1D).

7.3 Entrance surface dose test

In order to facilitate measurements and optimization of patient dose, the national Radiological Protection Board (NRPB) introduced the national protocol for patient dose measurement in 1992. The national protocol recommended that entrance surface dose (ESD) be directly measured on a sample of patients or experiments with phantom using thermoluminescent dosimeters (TLD's). [Obed *et al*, 2007].

Determination of patient dose or entrance surface dose and their comparison with diagnostic reference levels are an important part of the optimization process in diagnostic radiology. The ESD's were measured at the centre of the X-ray beam and in compliance with ALARA (As Low As Reasonably Achievable); all the measurements were made with no patients in position. The Rando phantom was used to measure ESD including backscatter radiation.

Table 7.6: The mean ESD (mGy) for each machine and examination considered and the standard deviations.

Examination	Shimadzu CID	Philips digital diagnost (1)	Philips digital diagnost (2)	Fluoroscopic unit	Chest unit
Cervical spine (AP)	2.72 ± 0.20	3.53 ± 0.26	2.82 ± 0.16	--	--
Cervical spine (LAT)	3.31 ± 0.34	3.54 ± 0.26	3.11 ± 0.22	--	--
Skull (AP)	3.96 ± 0.28	3.81 ± 0.37	2.80 ± 0.34	--	--
Skull (LAT)	2.90 ± 0.26	2.30 ± 0.18	2.63 ± 0.17	--	--
Abdomen (AP)	4.93 ± 0.39	4.56 ± 0.33	3.78 ± 0.31	3.49 ± 0.40	--
Pelvis (AP)	4.61 ± 0.31	4.11 ± 0.30	3.79 ± 0.33	3.58 ± 0.31	--
Lumber spine (AP)	5.40 ± 0.31	5.00 ± 0.24	4.76 ± 0.39	3.74 ± 0.36	--
Lumber spine (LAT)	9.54 ± 0.61	8.26 ± 0.52	9.13 ± 0.67	7.48 ± 0.52	--
Chest (PA)	0.67 ±0.12	0.75 ± 0.13	0.72 ± 0.13	0.69 ± 0.11	0.82 ± 0.27
Chest (LAT)	0.82 ± 0.29	0.90 ± 0.34	1.12 ± 0.36	1.15 ± 0.45	1.11 ± 0.33

-- The values are not available

The values after ± sign is the standard deviation, which is the uncertainty of the measuring equipment calculated from entrance surface dose obtained from the nine TLD's of each examination for each X-ray unit. The mean entrance surface dose of each examination for each X-ray unit was different (Table 7.6) due to a number of factors among which is the performance of equipment, type of X-ray generator, the effect of age on the machine and radiographic techniques used or the age of X-ray equipment. The mean entrance surface dose values for each X-ray unit were below the ESD published internationally except for chest (PA). Measured doses for this examination were higher than the ESD published internationally for all 5 X-ray units.

The Shimadzu CID machine showed a high ESD value for pelvis (AP), lumber spine (AP and LAT), skull (AP and LAT) and abdomen (AP); the Philips digital diagnost (1) machine showed a high ESD value for cervical spine (AP and LAT) and abdomen (AP); the chest unit, showed a high ESD value for chest (PA) and fluoroscopic unit showed the high value of chest (LAT). Most of the mean ESD values obtained from the fluoroscopic unit were less than the values from all the X-ray units considered.

It is known that ESD is proportional to the tube current, the length of the exposure, the square distance of the peak voltage and the distance between X-ray source and patient.

Changing several factors at the same time (kVp, mAs, FFD) may lower the quality of the radiograph, therefore FFD for all X-rays units were kept constant at 180 cm for chest (PA and LAT) and 110 cm for the rest of the examinations considered in the study as shown in Table 7.9.

High kVp is normally used with low mAs. The mean, maximum, minimum and maximum/minimum of the entrance surface doses for each examination are reported in Table 7.7. Maximum/minimum ratio of ESD for individual examination ranged from 1.43 for cervical spine (LAT) to 6.75 for chest (PA).

Table 7.7: Distribution of mean entrance surface dose values (mGy), minimum, maximum and maximum to minimum ratios across 5 X-ray units for each of the ten examinations.

Examination	Min.	Mean	Max.	Max./Min.
Cervical spine (AP)	2.40	2.99	3.86	1.61
Cervical spine (LAT)	2.72	3.23	3.89	1.43
Skull (AP)	2.35	3.50	4.50	1.91
Skull (LAT)	1.98	2.60	3.20	1.62
Abdomen (AP)	2.97	4.18	5.46	1.84
Pelvis (AP)	3.23	3.96	5.07	1.57
Lumber spine (AP)	3.15	4.72	6.11	1.94
Lumber spine (LAT)	6.68	8.56	10.23	1.53
Chest (PA)	0.16	0.72	1.08	6.75
Chest (LAT)	0.55	1.02	2.30	4.51

Min., minimum

Max., maximum

The chest X-ray is one of the lowest radiation exposure medical examinations performed today.

Figure 7.1-7.10, shows the histogram of the frequency distributions of ESD for each projection with the mean values indicated. Figure 7.11 shows the histogram of the mean entrance surface dose (mGy) for each examination and the standard deviations of the mean indicated by the error bars.

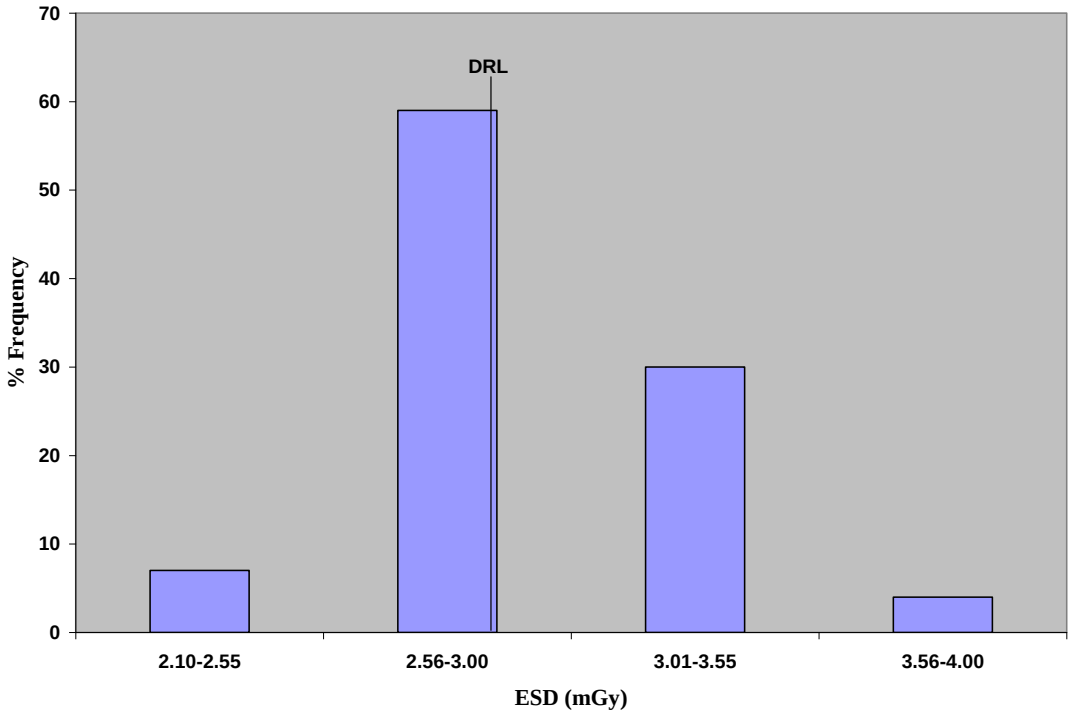

Figure 7.1: Histogram of ESD distributions of cervical spine (AP) and the solid line on the histogram indicates the diagnostic reference levels.

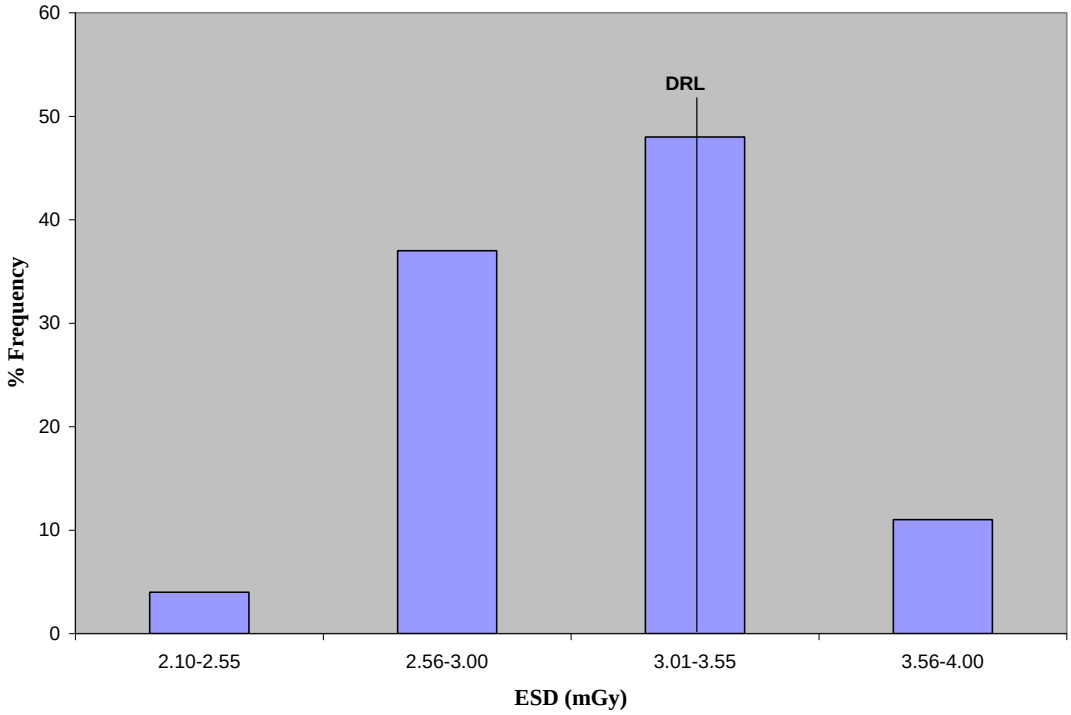

Figure 7.2: Histogram of ESD distributions of cervical spine (LAT) and the solid line on the histogram indicates the diagnostic reference levels.

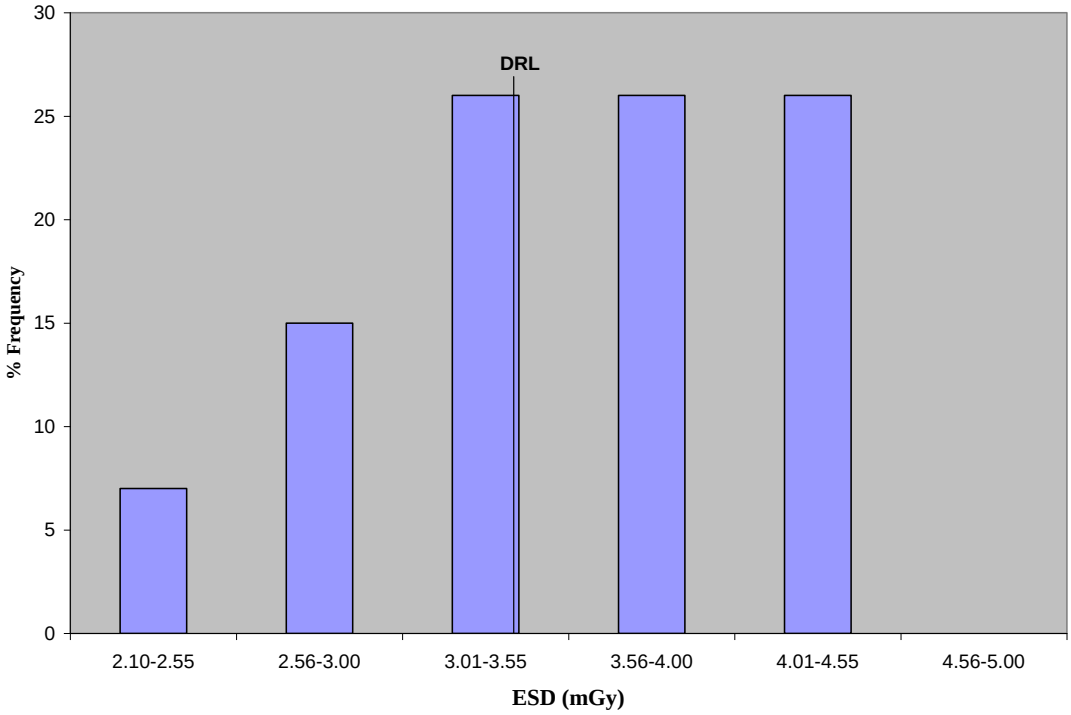

Figure 7.3: Histogram of ESD distributions of skull (AP) and the solid line on the histogram indicates the diagnostic reference level.

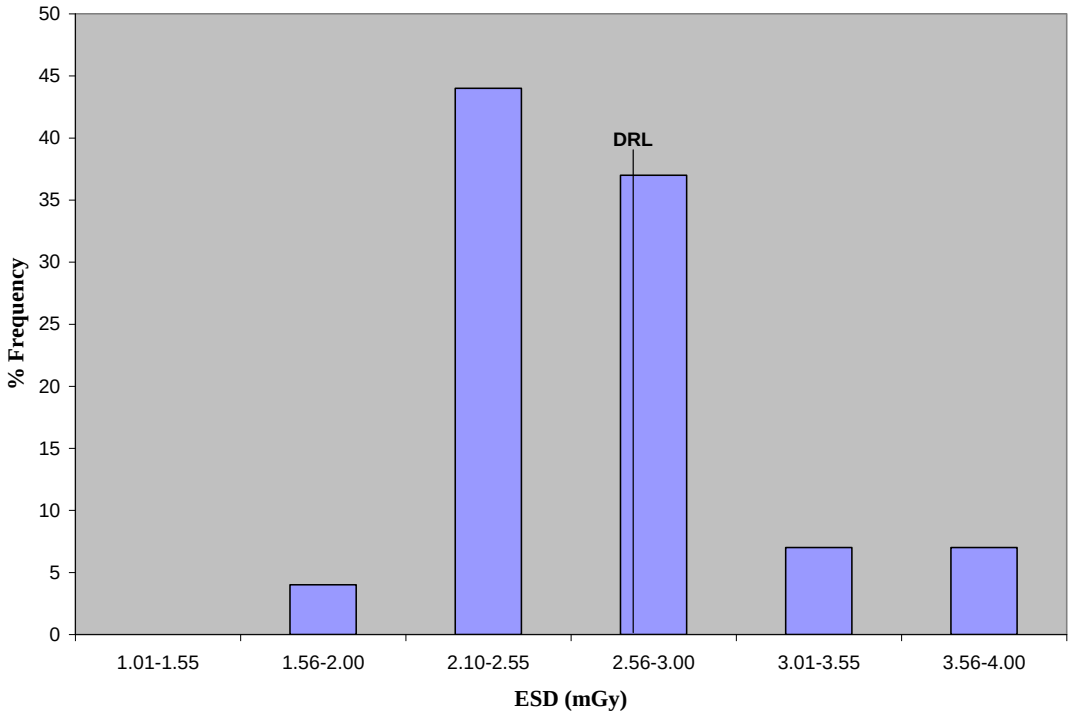

Figure 7.4: Histogram of ESD distributions of skull (LAT) and the solid line on the histogram indicates the diagnostic reference level.

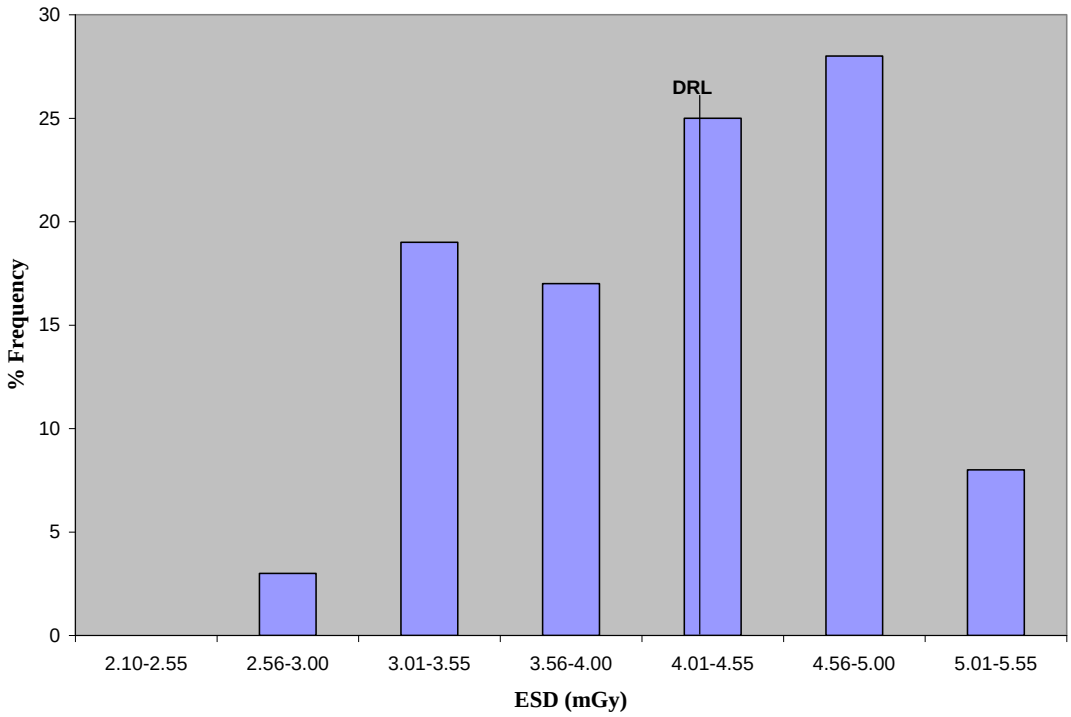

Figure 7.5: Histogram of ESD distributions of abdomen (AP) and the solid line on the histogram indicates the diagnostic reference level.

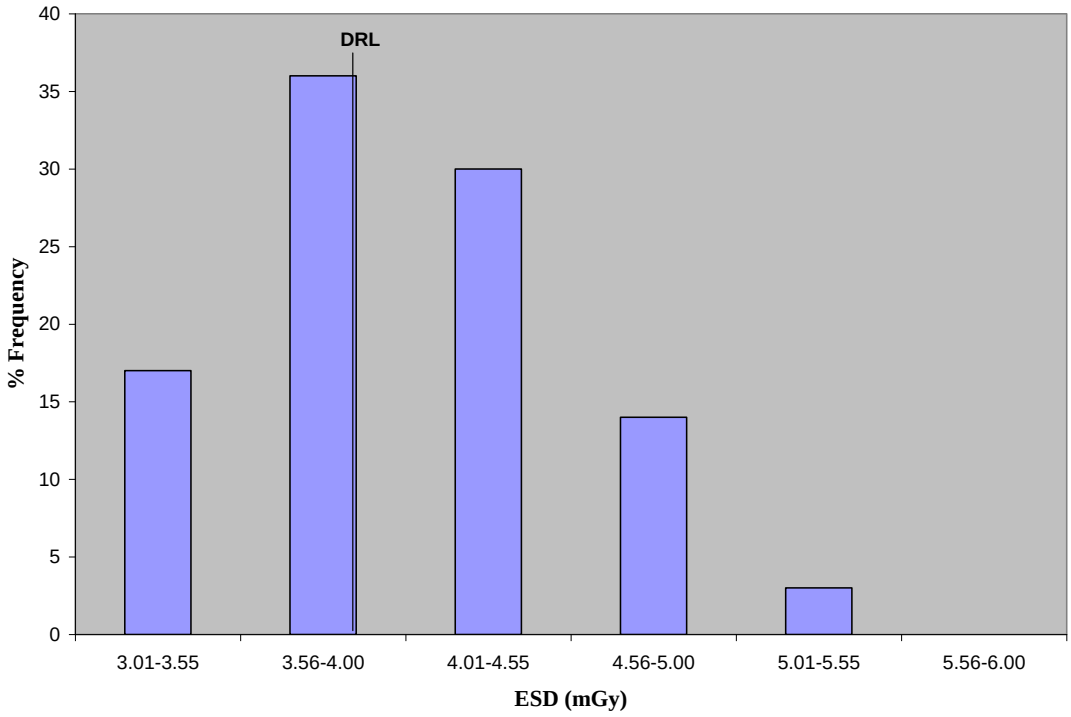

Figure 7.6: Histogram of ESD distributions of pelvis (AP) and the solid line on the histogram indicates the diagnostic reference level.

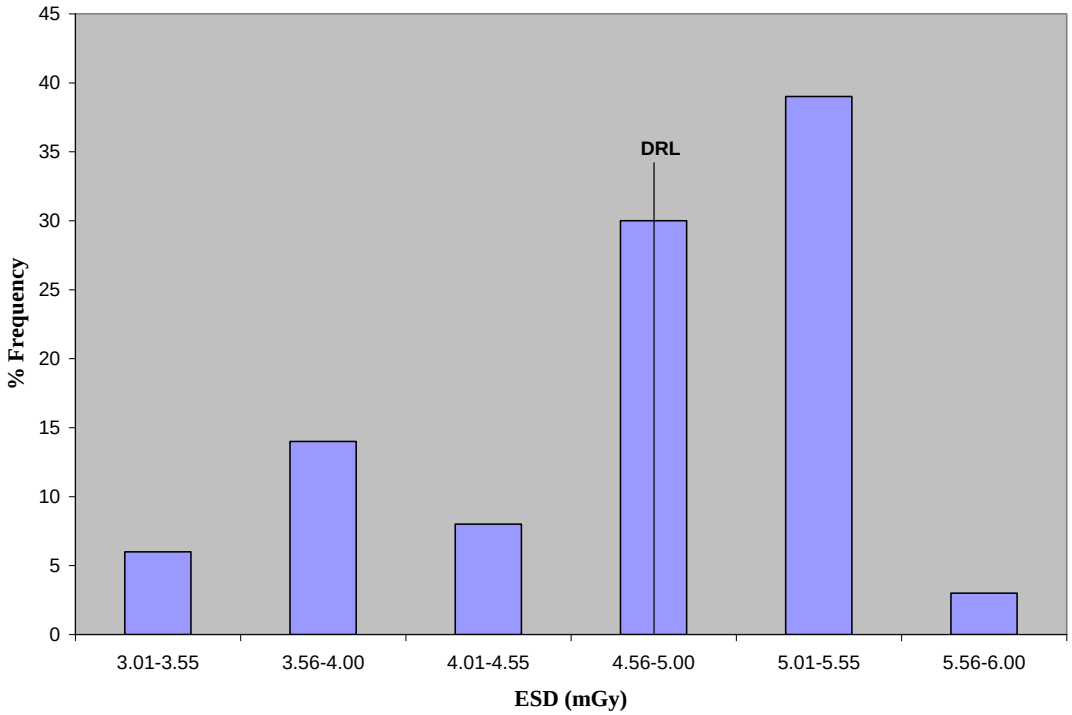

Figure 7.7: Histogram of ESD distributions of lumber spine (AP) and the solid line on the histogram indicates the diagnostic reference level.

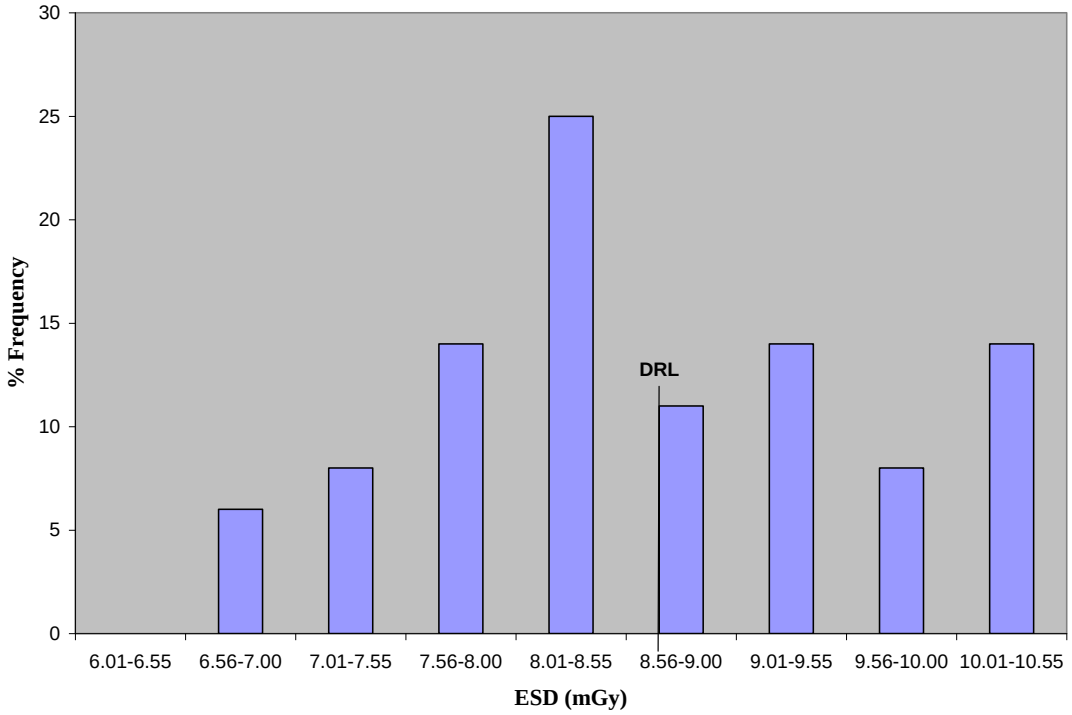

Figure 7.8: Histogram of ESD distributions of lumber spine (LAT) and the solid line on the histogram indicates the diagnostic reference level.

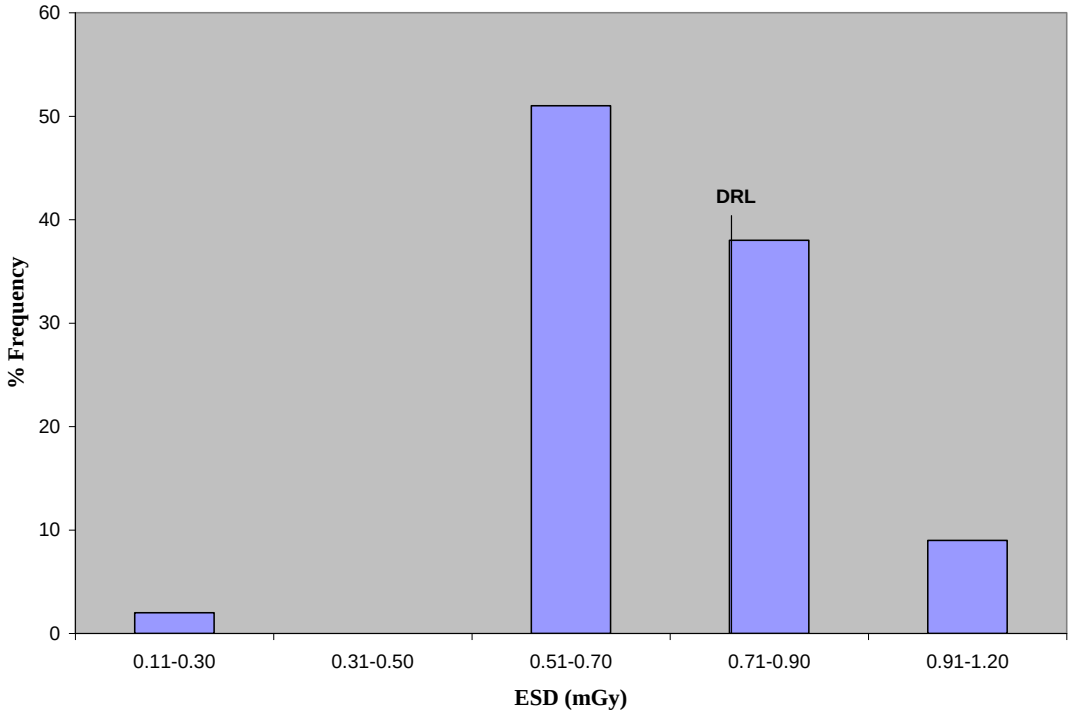

Figure 7.9: Histogram of ESD distributions of chest (PA) and the solid line on the histogram indicates the diagnostic reference level.

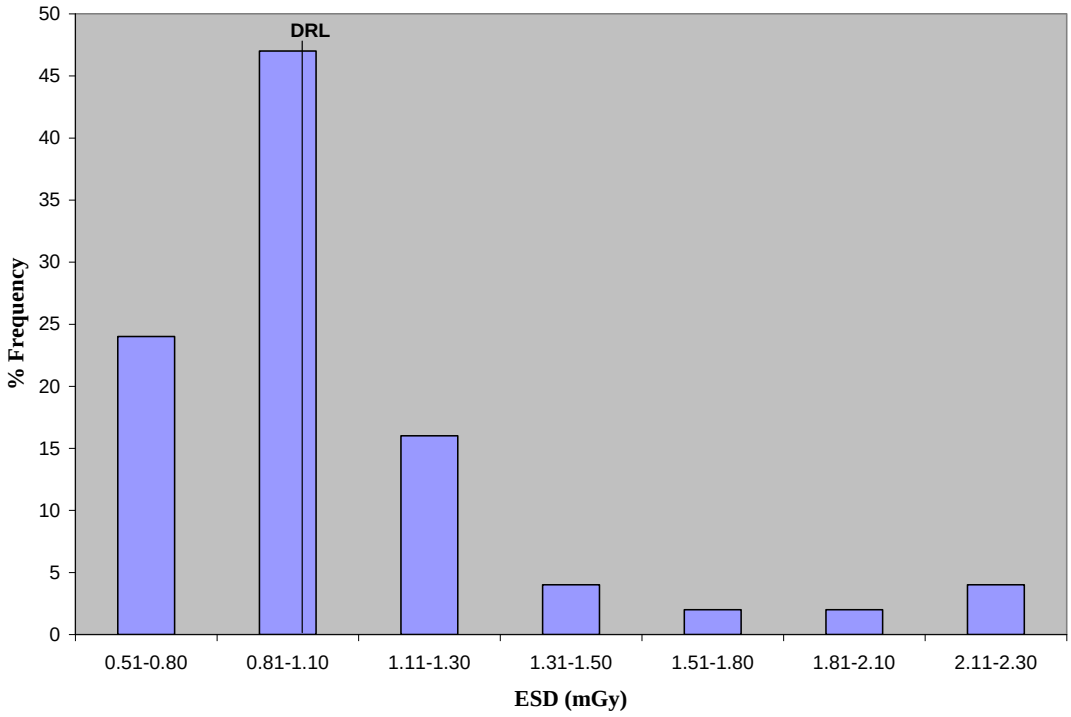

Figure 7.10: Histogram of ESD distributions of chest (LAT) and the solid line on the histogram indicates the diagnostic reference level.

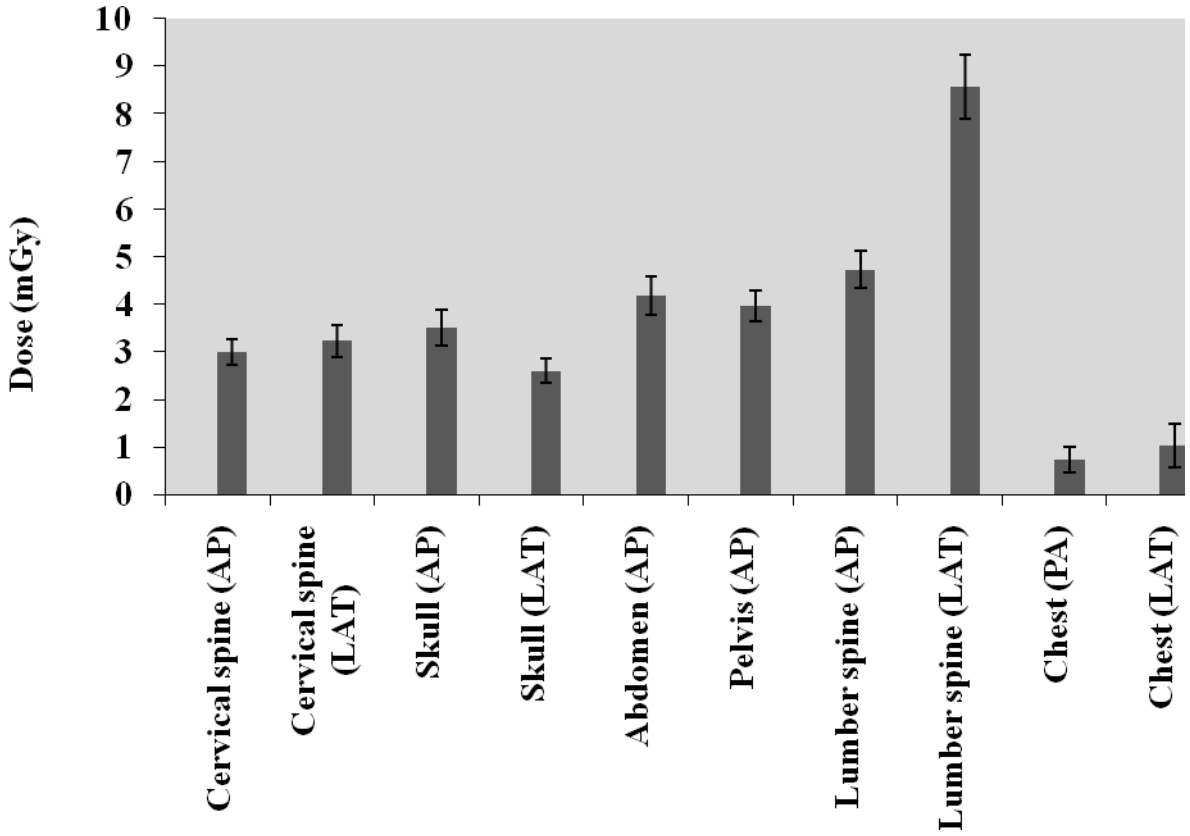

Figure 7.11: Histogram of mean ESD and the error bars of the examination considered.

In Figure 7.11 the error bars indicated the standard deviations (the accuracy associated with the measuring equipment, the standard deviations were found to be ± 0.26 mGy of cervical spine (AP), ± 0.34 mGy of cervical spine (LAT), ± 0.37 mGy of skull (AP), ± 0.26 mGy of skull (LAT), ± 0.40 mGy of abdomen (AP), ± 0.33 mGy of pelvis (AP), ± 0.39 mGy of lumber spine (AP), 0.67 mGy of lumber spine (LAT), 0.27 mGy of chest (PA) and 0.45 mGy of chest (LAT). These standard deviations are the maximum standard deviations for each examination from all the machines. (See Table 7.6)

Table 7.8 gives the comparison of ESD with international established diagnostic reference levels (mGy). The NRPB, UK IPSM (1992), IAEA (BSS) (1996), EC (1996a) (1999a) and EC (1996a) (1999a) have established DRL values (Table 7.8) of entrance surface doses for some routine radiological examination.

Table 7.8: Comparison of the ESD (mGy) with international established diagnostic reference levels (mGy). [Osibote *et al*, 2007]

Examination	The Dr George Mukhari hospital, mean ESD	UK IPSM (1992)	IAEA (BSS) (1996)	EC (1996a) (1999a)	NRPB (1999) (2000)
Cervical spine (AP)	2.99	--	--	--	--
Cervical spine (LAT)	3.23	--	--	--	--
Skull (AP)	3.50	5	5	5	5
Skull (LAT)	2.60	3	3	3	3
Abdomen (AP)	4.18	10	10	--	10
Pelvis (AP)	3.96	10	10	10	10
Lumber spine (AP)	4.72	10	10	10	10
Lumber spine (LAT)	8.56	30	30	30	30
Chest (PA)	0.72	0.3	0.4	0.3	0.3
Chest (LAT)	1.02	1.5	1.5	1.5	1.5

-- The values are not available

AP, anteroposterior; PA, posteranterior; LAT, lateral

UK IPSM, Institute of Physics in Medicine, United Kingdom (1992)

IAEA (BSS), International Atomic Energy Agency (1996)

EC, European Commission (1996a and 1999a)

NRPB, National Radiological Protection Board, United Kingdom (1999 and 2000)

The mean ESD of the measured doses are much lower than most reference levels established internationally except for the chest (PA) examination. This may be caused by the use of high kV and lower tube current on the chest (PA/LAT) examination and the fact that the chest has a considerable amount of soft tissue namely: heart, lungs and etc. As far as the image quality of standard patients obtained is concerned, all the diagnostic requirements prescribed by European guidelines were fulfilled. The above DRL values represent the entrance surface dose at the point of intersection of the beam axis with the surface of the phantom. At present there are no published DRL's

in South Africa, thus the values obtained are compared with the international published values.

Table 7.9 shows the distribution of kV, FFD (cm) and FSD (cm) in comparison with the EC recommendations.

Table 7.9: The distribution of kV and FSD and comparison with EC recommendations. [Osibote *et al*, 2007]

Examination	kV		FSD (cm) and FFD (cm)		
	The Dr George Mukhari hospital	EC	The Dr George Mukhari hospital (FSD)	The Dr George Mukhari hospital (FFD)	EC (FFD)
Cervical spine (AP)	64-66	--	88-96	110	--
Cervical spine (LAT)	66	--	84-85	110	--
Skull (AP)	60-77	70-85	88	110	100-150
Skull (LAT)	60-73	--	81-83	110	--
Abdomen (AP)	64-81	--	83-86	110	--
Pelvis (AP)	66-84	--	83-87	110	--
Lumber spine (AP)	66-90	75-90	82-89	110	100-150
Lumber spine (LAT)	70-90	80-95	73-80	110	100-150
Chest (PA)	84-125	125	149-157	180	140-200
Chest (LAT)	90-125	125	141-156	180	140-200

-- The values are not available

EC, European Commission

The technical factors used in this study were either too low or within the ranges recommended by the EC. This study presented maximum values of 125 kV and FFD of 180 cm for chest (PA/LAT); these values correspond to the EC recommended mean values (Table 7.9). All the FFD (cm) values were within the ranges recommended by EC.

Chapter 8

CONCLUSION

The objective of the study was to determine the diagnostic reference levels by assessing the dose received by a patient in radiographic exposure comparing different X-ray techniques to estimate the entrance surface dose for different examinations. The outcome of this study was to optimize patient protection during diagnostic procedures at the Dr George Mukhari hospital.

The diagnostic reference levels for patients have been analysed in terms of entrance surface dose (ESD). Entrance surface doses of patients undergoing cervical spine (AP and LAT), skull (AP and LAT), abdomen (AP), pelvis (AP), lumber spine (AP and LAT) and chest (PA and LAT) have been monitored by the use of the Rando phantom and TLD's. It is concluded that the TLD method is best for evaluating ESD although it requires more time and effort.

The determination of patient dose (ESD) and the comparison with the international DRL's is an important factor in the optimization process in diagnostic radiology and it is of special concern for the patient's protection.

The individual ESD values obtained were generally lower than the ESD values that have been reported in the literature. However, the ESD values of Shimadzu CID machine were high in most of the examinations considered; this shows that there is a need for changing the techniques at the Shimadzu CID machine. Increasing the tube potential at Shimadzu CID machine will further reduce the ESD without the loss of image quality, pointing to the importance of quality assurance. The ESD value of the chest (PA) from the chest unit was higher than that of other ESD values measured in other X-ray units. Again a lower ESD for this chest unit can be obtained by increasing the tube potential.

The overall results obtained from all 5 X-ray units were compared with the international published DRL's since there is no published national DRL's in South Africa and were below the DRL's published internationally except in the case of chest (PA). The results obtained could be useful for future patient dose measurements in the diagnostic radiology department at the Dr George Mukhari hospital. Although the results obtained were below the one in the literature, the quality assurance on the X-ray units need to be done regularly to further ensure the protection of patients.

The baseline of diagnostic reference levels for the George Mukhari hospital has been established. The fact that most of the values are within international norms gives us confidence that we are on the right track but are not the grounds for compliancy.

REFERENCE

Andreassi, M.G. (2004). The Biological Effects of Diagnostic Cardiac Imaging on Chronically Exposed Physicians: The Importance of being Non-ionized, *Cardiovascular ultrasound.* 2:25.

Apathy, I. (2002). Dose Measurements in Space by the Hungarian Pile TLD System, *Radiation Measurements*. 35(5): 381-39.

Bourguighan, M.H. (2009). Application of Diagnostic Reference Levels in Medical Practice. Refresher course 7 medical. http://w3.tue.nl/fileadmin/sbd/Documenten/IRPA_refresher_courses/DiagnosticReferenceLevelsMedical_RC-7.pdf viewed on 15/06/2009

Burke, K. and Sutton, D. (1997). Optimization and Deconvolution of Lithium Fluoride TLD-100 in Diagnostic radiology, *The British Journal of Radiology*. 70(1779): 261-271.

Bushing, S.C. (1997). Radiologic Science for Technologists Physics, Biology and Protection 6th ed, Mosby-year book. ISBN 0-8151-1579-2.

Capps III, C.J. (2006). Medical, Scientific and Commercial Uses of Roentegens X-rays Today, *Journal of Business and Economics Research*. 4(1).

Carroll, Q.B. (2003). Funchs's radiographic Exposure and Quality Control, 7th ed, Charles C.Thomas publisher. ISBN 039073732.

Cherry, S.R.; Sorenson, J.A. and Phelps, M.E. (2003). Physics in Nuclear Medicine, 3rd ed, Saunders. ISBN 0-7216-8341-X.

Chougule, A. (2005). Reference Doses in Radiological Imaging, *Pol J Med Phys Eng.* 11(2):1425-4689.

Code of Federal Regulations, U.S. Government printing office, Washington, 1020.31(a) (4), page 567.

Compagnone, G.; Pagan, L. and Bergamini, C. (2005). Local Diagnostic Reference Levels in Standard X-ray Examination, *Radiation Protection Dosimetry*. 113(1):54-63.

Compagnone, G; Pagan, L and Bergamini, C. (2005). Comparison of Six Phantoms for Entrance Skin Dose Evaluation in 11 Standard X-ray Examinations, *Journal of Applied Clinical Medical Physics*. 6 (1).

Connolly, J.R. (2007). Interaction of X-ray with Matter and Radiation Safety, for EPS400-002, Introduction to X-ray Powder Diffraction.

Cousins, C. and Sharp, C. (2004). Medical Interventional Procedures-Reducing the Radiation Risks. *Clinical radiology*. 59(6):468-478.

Curry III, T.S.; Dowdey, J.E. and Murry, R.C. (1990). Christensen's Physics of Diagnostic Radiology 4th ed, Lea & Febiger. ISBN 0-8121-1310-1.

Dendy, P.P. and Heaton, B. (1987). Physics for Radiologist, Blackwell scientific publication. ISBN 0-632-01351-6.

Dendy, P.P. and Heaton, B. (1999). Physics for Diagnostic Radiology, 2nd ed, institute of Physics Publishing. ISBN 0-7503-0591-6.

Dowsett, D.J.; Keerry, P.A. and Johnston, R.E. (1998). The Physics of Diagnostic Imaging, 1st ed, Chapman & Hall Medical. ISBN 0-412-460602.

Dyson, N. (1993). Radiation Physics with Application in Medicine and Biology, 2nd ed, Ellis Horwood. ISBN 0-13-741108-6.

Eggermont, G.; de Saint-Georges, L. and Vanmarke, H. (2006). The Health Effects of Low-dose Ionization Radiation. New Epidemiological Results and Perspectives, *HESA News Letter*. 29.

Farr, R.F. (1997). Physics for Medical Imaging. Harcourt publishers limited. ISBN 0-7020-17701.

Freitas, M. B.; and Yoshimura, E. M. (2009). Diagnostic Reference Levels for the most Frequent Radiological Examinations Carried out in Brazil, *REV Panam Salud Publica*. 25(2): 95-104.

Frigran, S. (1999). European Commission, Radiation protection 109: Guidance on Diagnostic Reference Levels (DRL's) for Medical Exposures.

Furlow, B. (2004). Biological Effects of Diagnostic Imaging. *Radiologic Technology*. 75(5): 355-63.

Gammex RMI, Full function meter RMI 242 user's guide (1995). Quality Control in Diagnosti Radiography, Gammex RMI. CM Nuclear System, CK 86104075/23, Johannesburg, P.O Box 46235, Orange Grove, 2119.

Graham, D.T. (1996). Principles of Radiological Physics. ISBN 0-443-04816-9.

Gray, J.E.; Archer, R,B.; Butler, P.F.; Hobbs, B.B.; Mettler, F.A.; Pizzutiello, R.J.; Schueler, B.A.; Strauss, K.J.; Suleiman, B.A. and Yaffe, M.J. (2005). Reference Values for Diagnostic Radiology: Application and Impact, *Radiology*. 235:354-358.

Hall, E.J. and Graccia, A.J. (2006). Radiobiology for the Radiologist. 6th ed, Williams and Wilkins. ISBN 0-7817-4151-3.

Hendee, W.R and Ibbott, G.S. (1996). Radiation Therapy Physics, Mosby. ISBN 0-8016-8099-9.

Hendee, W.R. and Ritenour, R. (1992). Medical Imaging Physics, 3rd ed, Mosby. ISBN 0-151-4241-2.

ICRP Draft. (2001). Diagnostic Reference Levels in Medical Imaging. Draft (5 February 2001) ICRP Committee 3. www.ICRP.org/News and Drafts.

Kelsey, C.A. (1985). Essentials of Radiology Physics, Warren H. Green, INC. ISBN 87527-354-8.

Khan, F.M. (2003). The Physics of Radiation Therapy 3rd ed, Lippincott Williams & Wilkins. ISBN 0-7817-3065-1.

King, S.; Pitcher, E.M. and Smail, M.A. (2002). Optimizing Medical Radiation Exposures for Uroradiological Procedures, with Special Emphasis on the Paediatric Imaging, *BJU International*. 89:510-516.

Knoll, G.F. (1989). Radiation Defection and Measurements 2nd ed, New York. Wiley & Sons. ISBN 047161761X.

Lin, J.; Chu, T.; Lin, S. and Liu, M. (2001). Skin Dose Measurement by Using Ultra-Thin TLDs, *Applied Radiation and Isotopes.* 55:383-391.

Love, G., Pillai, A. and Gibson, S. (2007). Entrance Skin Value Calculation for the Mini C-arm-Establishing a Diagnostic Reference Level for Wrist Fractures, *Injury Extra*. 38(4):136-137.

Mahesh, M. (2001). The AAPM/RSNA Physics Tutorial for Residents Fluoroscopy: Patient Radiation Exposure Issue. 21(4).

Martin, C.J. (2007). Optimization in General Radiography, *Biomedical imaging and intervention journal*. 2(18). www.biij.org/2007/2/e18.

Martin, C.J.; Sutton, D.G. and Sharp, P.F. (1999). Balancing Patient Dose and Image Quality, *Applied Radiation and Isotopes*. 50: 1-19.

Martin, J.E. (2006). Physics for Radiation Protection, 2nd ed, Wiley-VCH Verlag GmbH & Co.KGaA. ISBN 3-527-40611-5.

Matthews, K. and Brennan, P.C. (2008). The Application of Diagnostic Reference Levels: General Principle and an Irish Perspective, *Journal of Radiology*. 3(1).

McEntee, M.F.; Brennan, P.C.; Connor, G.O. (2004). The Effect of X-ray Tube Potential on Image Quality of PA Chest Radiographs when Using Digital Image Acquisition Devices, *Radiography*. 10: 287-292.

McKeever, S.W.S.; Moscovitch, M.; Townsend, P.D. (1995). Thermoluminescence Dosimetry Material: Properties and Uses, Nuclear Technology Publishing. ISBN 1-871965-19-1.

McLemore, J.J. (1981). Quality Assurance in Diagnostic Radiology, Year Book Medical Publishers, INC. ISBN 0-8151-5832-7.

Medical Council of Ireland. (2004). Diagnostic reference levels. Position paper. www.hse.ie/eng/about/who/diagnostic-refrence-levels.pdf.

Metcalfe, P.; Kron, T.; Hoban, P. (1997). The Physics of Radiotherapy X-rays from Linear Accelerators, Medical physics Publishing. ISBN 0-944838-76-6.

Mortazavi, S.S.J.; Ghiassi-Nejad, M.; Bakhshim,.; Jafari-Zadeh, M.; Kavousi, A.; Ahmadi, J. and Shareghi, A. (2004). Entrance Surface Dose Measurement on the Thyroid Gland in Orthopantomography. The Need for Optimization, *Iran. J. Radiant. Res*. 2(1): 1-7.

Nave, R (2009). X-rays. http://hyperphysics.phy-astr.gsu.edu/HBASE/quacon.html#quacon, viewed 20/07/2009.

Obed, R.I.; Ademola, A.K.; Adewony, K.A. and Okunade, O.A. (2007). Doses to Patients in Rountin X-ray Examinations of Chest, Skull, Abdomen and Pelvis in Nine Selected Hospital in Nigeria, *Research Journal in Medical Science*. 1(4): 209-214.

Osibote, O.A. and de Azeredo, A.C.P. (2008). Estimation of Adult Patient Doses for Common Diagnostic X-ray Examinations in Rio de Janeiro, Brazil, *Physica Medica*. 24: 21-28.

Panichello, J.J. (1998). X-ray Repair: A Comprehensive Guide to the Installation and Servicing of Radiographic Equipment, Charles C. Thomas publisher. ISBN 0-398-06815-1.

Pillai, A. and Jain, M. (2004). Dose Area Product Measurement in Orthopaedic Trauma. An Attempt at Establishing a Local Diagnostic Reference Level, *J.radi*. 02:002.

Radiation Measurement Products Model 3500 TLD Reader User's Manual. (1993). Release date July 30 1993, Saint-Gobain/Norton industrial ceramics corporation. publication number 3500-0-U-0779-005. 6801 Cochran Road, Ohio, U.S.A, 44139.

Ramos-Bernal, S.; Eruz, E.; Negrón-Mendoza, A. and Bustos, E. (2002). Irradiation Dose Determination below Room Temperature, *Radiation Physics and Chemistry*. 63:813-815.

Rampado, O. and Ropolo, R. (2004). A Method for a Real Time Estimation of Entrance Surface Dose Distribution in Interventional Neuroradiology, *American Association of Physicists in Medicine, Medical Physics*. 31(8).

Ranogajec-Konor, M. (2002). Thermoluminescence Dosimetry-Application in Enviromental Monitoring, *Radiation safety management*. 2(1): 2-16.

Reference Levels in Diagnostic X-rays. (2006). Patient Dose Measurements in Diagnostic Radiology. 1. http://www.doh.gov.za/department/radiation/codeofpractice/electronicproducts/ionising/patient.pdf.

Ruiz-cruces, R.; Ruiz, F.; Perez-martinez, M.; Lopez, J.; Tort Ausina, I. and Diez de los Rois, A. (2000). Patient Dose from Barium Procedures, *The British Journal of Radiology*. 73: 752-761.

Seeram, E and Brennan, P.C. (2006). Diagnostic Reference Levels in Radiology, *Radiological Technology*. 77:376-384.

Seeram, E. (1997). Radiation Protection, Lippin cott-Raven publishers. ISBN 0-397-55032-4.

Seibert, J.A; Boone, J.M. (2005). X-ray Imaging Physics for Nuclear Medicine Technology. Part 2: X-ray Interactions and Image Formation, *Journal of Nuclear Medicine*. 33(1).

Shrimpton, P.C.; Wall, B.F. and Hart, D. (1999). *Applied Radiation and Isotopes*. 50: 261-169.

Sprawls, P. (1995). Physical Principles of Medical Imaging, 2nd edition. ISBN 0-944838-54-5.

The Phantom Laboratory (2009). www.phantomlab.com viewed 15/07/2009.

Thompson, M.A.; Hattaway, M.P.; Hall, J.D. and Dowd, S.B. (1994). Principle of Imaging Science and Protection, W.B Saunders Company. ISBN 7216-3428-1.

Vano, E.; Fernandez, J.M.; Ten, J.I.; Gulbelalde, E.; Gonzalez, L. and Pedrosa, C.S.A. (2002). Real-time Measurement and Audit of Patient Undergoing Computed Radiography, *Radiology***.** 225(1):283.

Wolbarst, A.B. (1993). Physics of Radiology, Medical Physics Publishing. ISBN 0-8385-5769-4.

Workman, A.; Koter, J.; Shaw, A.: Fong, R.; Wall, B.; Bury, R.; Barlow, S.; Sutton, D.; Wiliams, J. and Ebdon-Jackson, S. (2009). Diagnostic Reference Levels: Working Partly Statement. http://www.e-radiography.net/regsetc/DRL-statement.htm viewed 2/4/2009.

Yazici, A. (2002). Defect Structure of Glow Peak 1 in LiF: Mg,Ti (TLD-100), *Turk.J.Phys*. 26: 473-481.

APPENDIX

Appendix 1

QUALITY ASSURANCE TEST

Appendix 1A

ACCURANCY OF TIMER AND kV

SHIMADZU CID

Set values			Average	Measured values	% error	
kV	mAs	sec	kV	Sec	kV	sec
60	25	0.10	61.20	0.09680	-2.000	3.200
	50	0.25	61.20	0.24660	-2.000	1.300
	80	0.40	61.20	0.39670	-2.000	0.800
70	20	0.10	71.96	0.09950	-0.500	2.800
	40	0.20	71.80	0.19960	-0.200	2.560
	63	0.40	72.00	0.39970	-0.075	2.857
	80	0.50	71.20	0.49690	-0.620	1.710
80	20	0.10	82.90	0.09960	-3.600	0.400
	32	0.20	82.90	0.19966	-3.600	0.170
	50	0.32	82.90	0.31970	-3.600	0.094
	63	0.40	82.90	0.39980	-3.600	0.060
90	16	0.10	91.20	0.09960	-1.300	0.400
	32	0.20	91.40	0.19962	-1.550	1.190
	50	0.40	93.50	0.39990	-3.880	0.025
	63	0.50	91.50	0.51353	-1.670	2.000
100	16	0.10	104.50	0.09960	-4.500	0.400
	25	0.20	104.90	0.19980	-4.900	0.100
	40	0.32	104.90	0.31980	-4.900	0.063
	50	0.40	105.00	0.39980	-5.000	0.050
110	12	0.10	116.00	0.10480	-5.450	4.800
	25	0.20	116.40	0.19980	-5.581	0.100
	40	0.40	116.58	0.40040	-5.980	0.010
	50	0.5	116.56	0.50010	-5.963	0.020

PHILIPS DIGITAL DIAGNOST (1)

Set values			Average	Measured values	% error	
kV	mAs	sec	kV	Sec	kV	Sec
60	80	0.0888	58.14	0.08666	3.100	2.409
	200	0.2220	58.28	0.22190	2.866	0.045
	320	0.3550	58.30	0.35536	2.833	0.101
	400	0.4440	58.32	0.44408	2.800	0.018
70	80	0.0888	68.30	0.08702	2.428	2.005
	200	0.2220	68.20	0.22122	2.571	0.351
	250	0.2770	68.20	0.27680	2.571	0.072
	320	0.4200	68.28	0.41956	2.457	0.105
80	80	0.0996	78.80	0.09880	1.500	0.803
	160	0.1990	78.80	0.19832	1.500	0.342
	200	0.2800	78.68	0.27860	1.650	0.500
	250	0.3680	78.60	0.36686	1.750	0.310
90	80	0.1110	87.04	0.11026	3.288	0.666
	125	0.1790	87.02	0.17146	3.311	4.200
	200	0.3180	86.76	0.31658	3.600	0.446
	250	0.4230	86.80	0.42180	3.555	0.284

PHILIPS DIGITAL DIAGNOST (2)

Set values			Average	Measured values	% error	
kV	mAs	Sec	kV	Sec	kV	Sec
50	80	0.0992	50.06	0.09718	-0.120	2.040
	160	0.1980	50.12	0.19884	-0.240	0.424
	250	0.3100	50.20	0.30974	-0.400	0.083
	400	0.4960	50.16	0.49620	-0.320	0.040
60	80	0.0888	59.20	0.08840	1.333	0.405
	160	0.1770	59.18	0.17818	1.366	0.666
	250	0.2770	59.20	0.27758	1.333	0.209
	400	0.4440	59.20	0.44440	1.333	0.090
70	80	0.0888	70.72	0.08870	-1.020	0.011
	160	0.1770	70.80	0.17790	-1.140	0.508
	250	0.2770	70.80	0.27750	-1.140	0.194
	400	0.4440	70.78	0.44180	-1.114	0.495
80	80	0.0984	81.52	0.09814	-1.900	0.264
	160	0.2090	81.44	0.20894	-1.800	0.029
	250	0.3620	81.38	0.36220	-1.725	0.055
	320	0.5020	81.30	0.50188	-1.625	0.024

CHEST UNIT

Set values			Average	Measured values	% error	
kV	mAs	Sec	kV	Sec	kV	Sec
70	50	0.10	69.84	0.09974	0.229	0.260
	100	0.20	69.80	0.19982	0.286	0.090
	160	0.32	69.80	0.31990	0.286	0.031
	180	0.45	69.90	0.45000	0.143	0.000
90	50	0.10	90.10	0.09968	0.111	0.320
	80	0.20	87.24	0.19980	3.067	0.100
	125	0.32	86.58	0.31982	3.800	0.056
	140	0.45	86.62	0.44992	3.756	0.018
110	40	0.10	106.74	0.09976	2.964	0.240
	63	0.20	106.90	0.19980	2.818	0.100
	100	0.32	106.78	0.31990	2.927	0.031
	125	0.50	106.92	0.50000	2.800	0.000
125	63	0.20	120.70	0.19982	2.440	0.090
	80	0.32	120.70	0.31992	2.440	0.025
	100	0.40	120.70	0.39980	2.440	0.050

FLUOROSCOPIC UNIT

Set values			Average	Measured values	% error	
kV	mA	sec	kV	Sec	kV	Sec
70	5	--	67.50	98.06	3.571	--
	16	--	68.00	96.90	2.857	--
	20	--	70.30	97.90	0.429	--
	25	--	68.68	98.62	1.886	--
80	5	--	77.98	98.00	2.525	--
	16	--	79.30	99.22	0.875	--
	20	--	76.70	98.48	4.125	--
	25	--	77.78	99.90	2.775	--
90	5	--	87.20	98.44	3.111	--
	16	--	88.68	98.72	1.467	--
	20	--	87.10	99.48	3.222	--
	25	--	86.42	93.22	3.978	--
100	15	--	96.10	67.22	3.900	--
110	11	--	103.16	52.80	6.200	--
120	11	--	111.04	52.33	7.466	--

Appendix 1B

HALF VALUE LAYER (HVL)

Equipment used: Full function meter (FFM) 242 MRI

SHIMADZU CID

Set up values: kV=80 mAs=20 ms=100 Field size=15x15cm^2 FSD=100cm

mmAl	mR
0.0	140
0.5	106
1.0	95
1.5	84
2.0	76
2.5	69
3.0	64
3.5	56

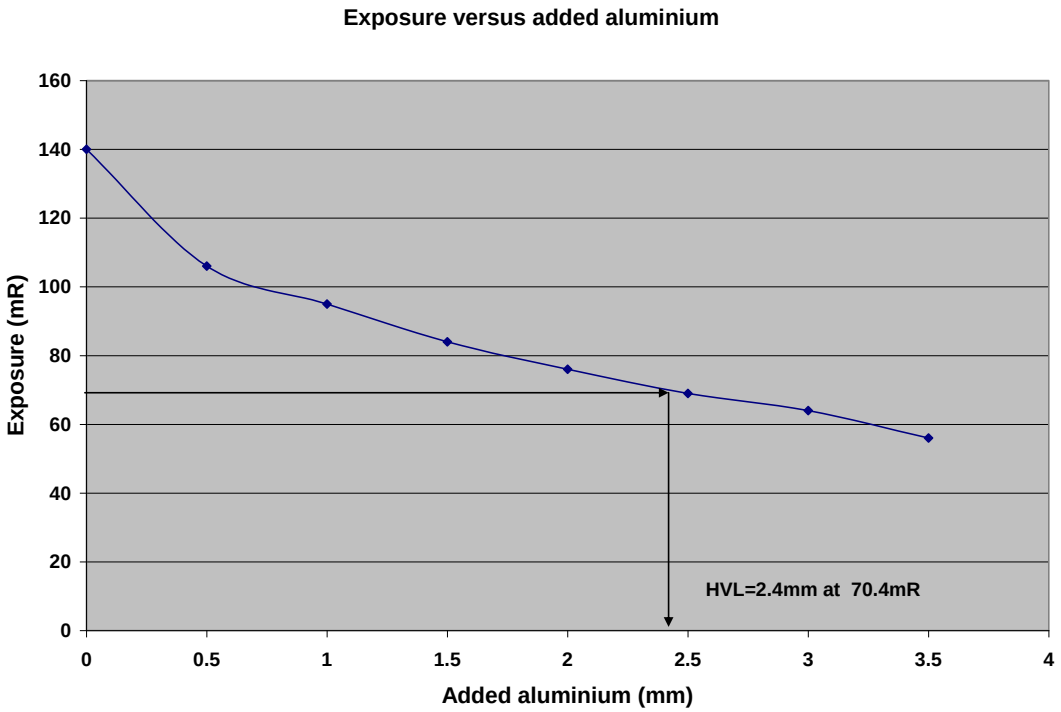

PHILIPS DIGITAL DIAGNOST (1)

Set up values: kV=81 mAs=50 ms=62.3 Field size= 15x15cm^2 FSD=100cm

mmAl	mR
0.0	338
0.5	279
1.0	261
1.5	237
2.0	212
2.5	194
3.0	176
3.5	161
4.0	149
4.5	138
5.0	128

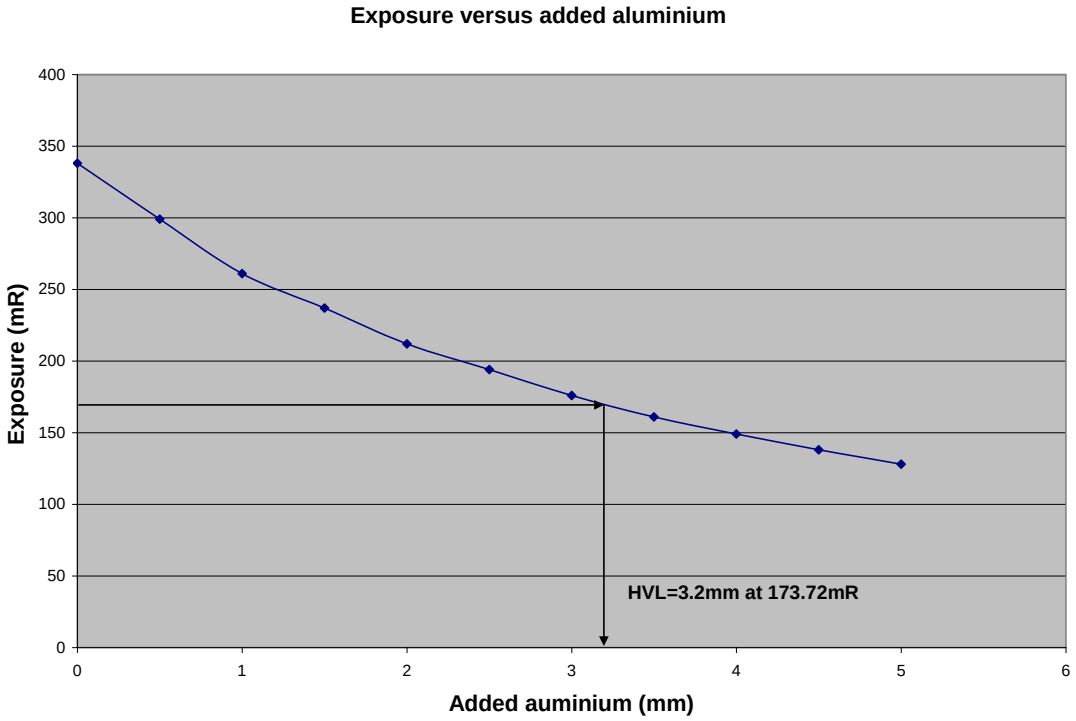

PHILIPS DIGITAL DIAGNOST (2)

Set up values: kV=81 mAs=50 ms=138 Field size= 15x15cm^2 FSD=100cm

mmAl	mR
0.0	305
0.5	267
1.0	235
1.5	212
2.0	191
2.5	173
3.0	158
3.5	144
4.0	123
4.5	114

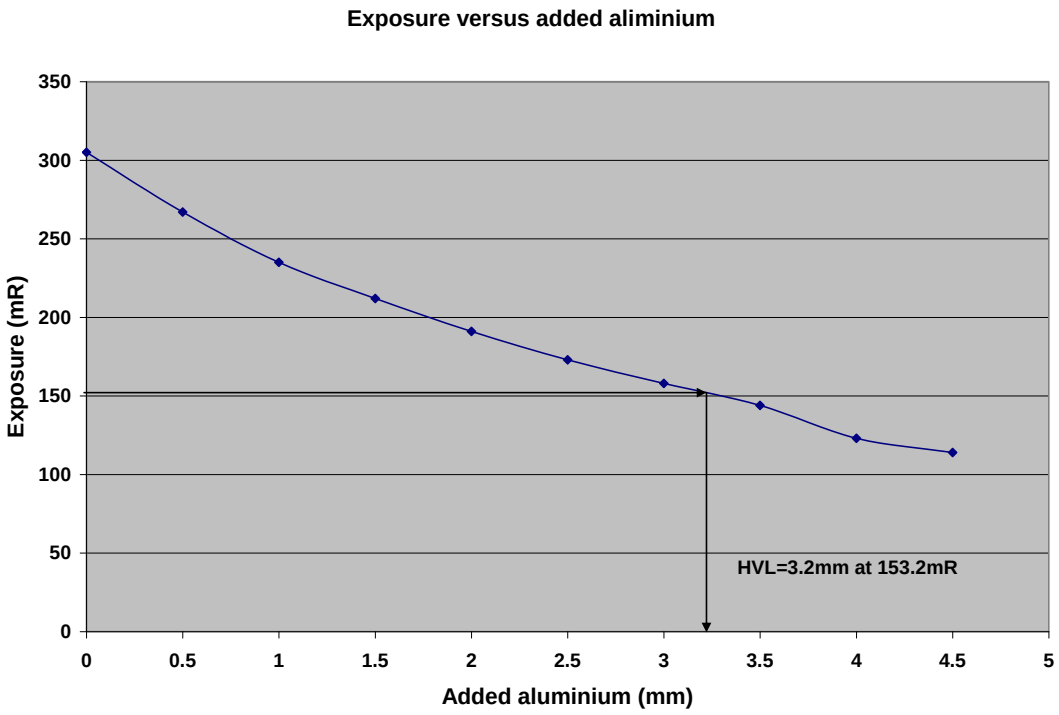

CHEST UNIT

Set up values: kV=90 mAs=50 ms=100 Field size= 15x15cm^2 FSD=100cm

mmAl	mR
0.0	301
0.5	273
1.0	242
1.5	226
2.0	207
2.5	188
3.0	177
3.5	163
4.0	151
4.5	139
5.0	131

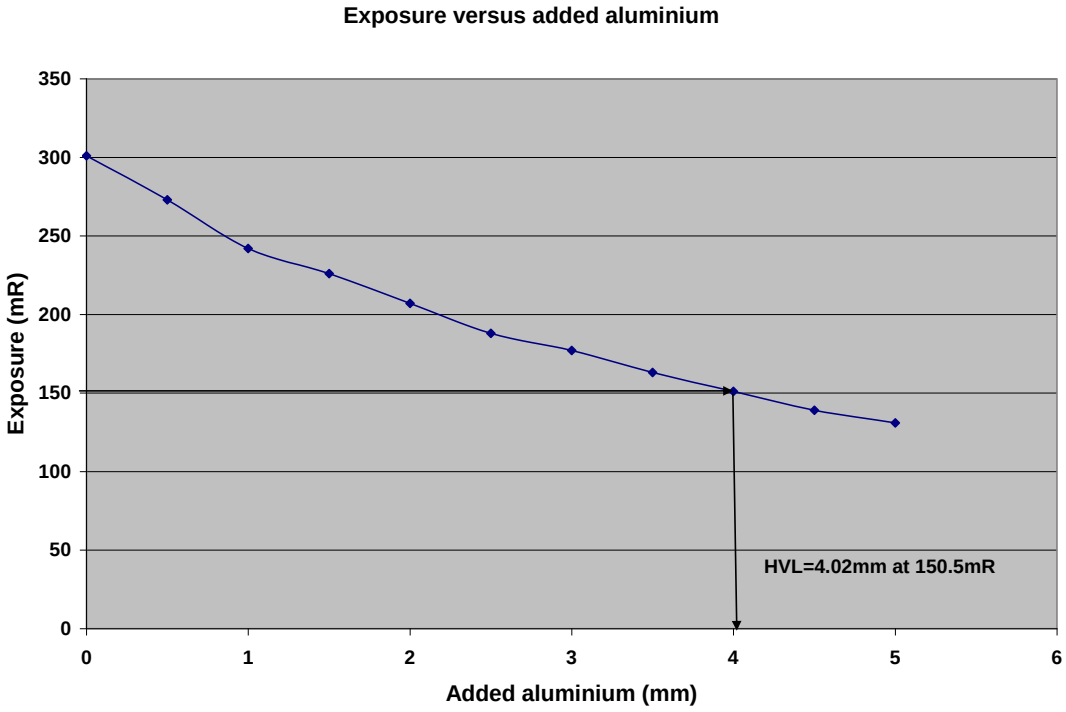

Fluoroscopic unit

Set up values: kV=90 mAs=25 ms=100 Field size= 15x15cm^2 FSD=100cm

mmAl	mR
0.0	258
0.5	229
1.0	197
1.5	183
2.0	162
2.5	141
3.0	128
3.5	114
4.0	103

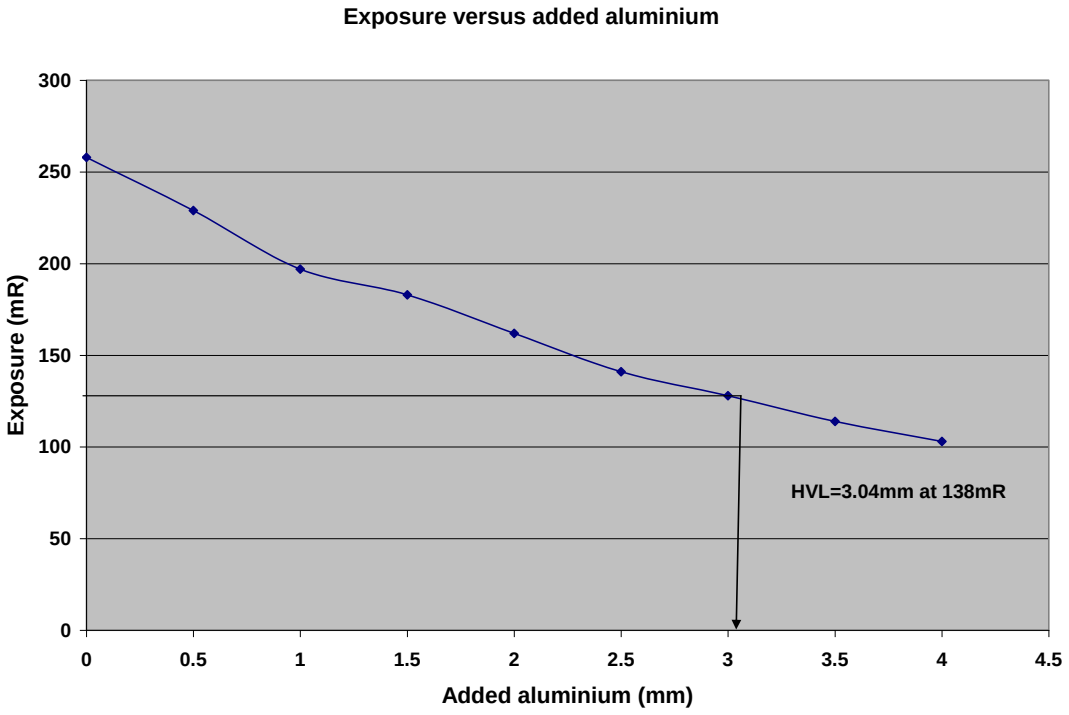

Appendix 1C

COEFFICIENT OF VARIENCE (COV)

SHIMADZU CID

Coefficient of variance (COV) ≤ 0.05 $\quad COV = \frac{\sigma}{y} = \frac{1}{y}\left[\frac{\sum_{n-1}^{N}(y_n - \bar{y})^2}{N-1}\right]^{\frac{1}{2}}$

FSD=100cm Field size=15x15cm^2

Set values (high kV)			Measured values			COV
kV	Sec	mAs	kV Eff	Sec	mR	
110	0.1	12	116.0	0.1048	202	0.003
			116.0	0.1048	202	
			116.0	0.1048	202	
			116.0	0.1049	201	
			116.0	0.1049	201	
	0.2	25	116.1	0.1998	319	0.002
			116.2	0.1998	318	
			116.1	0.1998	319	
			1161	0.1998	319	
			116.2	0.1998	318	
	0.4	40	116.5	0.4001	508	0.001
			116.6	0.4001	508	
			116.6	0.4001	508	
			116.6	0.4001	509	
			116.6	0.3998	508	
	0.5	50	116.5	0.5001	634	0.001
			116.5	0.5001	633	
			116.6	0.5001	634	
			116.6	0.5001	634	
			116.6	0.5001	632	

Set values (In between kV)			Measured values			COV
kV	Sec	mAs	kV Eff	Sec	mR	
90	0.1	16	91.2	0.0996	223	0.003
			91.2	0.0996	224	
			91.2	0.0995	224	
			91.2	0.0995	224	
			91.2	0.0996	225	
	0.2	32	91.4	0.1996	433	0.003
			91.4	0.1996	434	
			91.4	0.1996	435	
			91.4	0.1996	435	
			91.4	0.1997	436	
	0.4	50	93.5	0.3999	439	0.002
			93.5	0.3999	440	
			93.5	0.3999	441	
			93.5	0.3999	441	
			93.5	0.3999	441	
	0.5	63	91.5	0.5189	547	0.002
			91.5	0.5197	547	
			91.5	0.5896	495	
			91.5	0.5198	547	
			91.5	0.5197	550	

Set values (Low kV)			Measured values			COV
kV	Sec	mAs	kV Eff	Sec	mR	
60	0.10	25	61.2	0.9660	100	0.007
			61.2	0.9660	101	
			61.2	0.9690	100	
			61.2	0.9690	102	
			61.2	0.9720	101	
	0.25	50	61.2	0.2467	207	0.002
			61.2	0.2467	206	
			61.2	0.2466	206	
			61.2	0.2466	206	
			61.2	0.2466	206	
	0.40	80	61.2	0.3967	327	0.008
			61.2	0.3968	327	
			61.2	0.3968	312	
			61.2	0.3968	313	
			61.2	0.3967	313	

PHILIPS DIGITAL DIAGNOST (1)

Set values (In between kV)			Measured values			COV
kV	Sec	mAs	kV Eff	Sec	mR	
80	0.0996	80	78.7	0.0990	518	0.001
			78.7	0.0989	518	
			78.7	0.0986	519	
			78.7	0.0989	519	
			78.7	0.0990	519	
	0.1996	160	78.8	0.1984	1037	0.001
			78.8	0.1981	1037	
			78.8	0.1983	1037	
			78.8	0.1984	1038	
			78.8	0.1984	1038	
	0.2800	200	78.6	0.2786	1302	0.000
			78.7	0.2786	1303	
			78.7	0.2786	1303	
			78.7	0.2786	1303	
			78.7	0.2786	1303	
	0.3680	250	78.6	0.3669	1627	0.000
			78.6	0.3670	1628	
			78.6	0.3669	1627	
			78.6	0.3666	1627	
			78.6	0.3669	1627	

Set values (Low kV)			Measured values			COV
kV	Sec	mAs	kV Eff	Sec	mR	
60	0.088	80	58.1	0.0867	279	0.002
			58.1	0.0867	279	
			58.1	0.0860	279	
			58.2	0.0866	279	
			58.2	0.0867	278	
	0.222	200	58.2	0.2218	700	0.001
			58.3	0.2219	700	
			58.3	0.2219	700	
			58.3	0.2219	701	
			58.3	0.2220	702	
	0.355	320	58.3	0.3555	1124	0.001
			58.3	0.3554	1125	
			58.3	0.3554	1126	
			58.3	0.3553	1127	
			58.3	0.3552	1127	
	0.444	400	58.3	0.4441	1410	0.001
			58.3	0.4441	1410	
			58.3	0.4441	1412	
			58.4	0.4440	1413	
				0.4440	1413	

PHILIPS DIGITAL DIAGNOST (2)

Coefficient of variance (COV) ≤ 0.05 $\quad COV = \frac{\sigma}{y} = \frac{1}{y}\left[\frac{\sum_{n-1}^{N}(y_n - \bar{y})^2}{N-1}\right]^{\frac{1}{2}}$

FSD=100cm

Set values (High kV)			Measured values			COV
kV	Sec	mAs	kV Eff	Sec	mR	
110	0.0366	10	111.0	0.0358	115	0.006
			111.0	0.0358	114	
			111.9	0.0361	115	
			111.9	0.0356	116	
			111.9	0.0356	115	
	0.0733	20	111.1	0.0729	230	0.000
			111.1	0.0729	230	
			111.1	0.0730	230	
			111.2	0.0729	230	
			111.1	0.0730	230	
	0.1190	32	111.3	0.1200	367	0.001
			111.0	0.1200	368	
			111.2	0.1202	368	
			111.2	0.1201	368	
			111.3	0.1200	368	
	0.1530	40	111.4	0.1534	461	0.001
			111.4	0.1534	460	
			111.4	0.1534	461	
			111.4	0.1532	460	
			111.4	0.1535	460	

Set values (In between kV)			Measured values			COV
kV	Sec	mAs	kV Eff	Sec	mR	
80	0.0984	80	81.5	0.0981	493	0.000
			81.6	0.0982	493	
			81.5	0.0982	493	
			81.5	0.0982	493	
			81.5	0.0980	493	
	0.2090	160	81.4	0.2091	984	0.001
			81.4	0.2090	987	
			81.4	0.2088	987	
			81.5	0.2090	988	
			81.4	0.2088	987	
	0.3620	250	81.3	0.3620	1545	0.001
			81.4	0.3620	1546	
			81.4	0.3621	1546	
			81.4	0.3628	1546	
			81.4	0.3621	1548	
	0.5020	320	81.3	0.5019	1983	0.000
			81.3	0.5019	1984	
			81.3	0.5018	1983	
			81.3	0.5019	1983	
			81.3	0.5019	1983	

Set values (Low kV)			Measured values			COV
kV	Sec	mAs	kV Eff	Sec	mR	
50	0.0992	80	50.3	0.0972	158	0.000
			50.0	0.0973	158	
			50.0	0.0971	158	
			50.0	0.0971	158	
			50.0	0.0972	158	
	0.1980	160	50.2	0.1988	316	0.002
			50.2	0.1989	317	
			50.1	0.1988	316	
			50.1	0.1989	317	
			50.1	0.1988	316	
	0.3100	250	50.3	0.3097	493	0.002
			50.2	0.3097	493	
			50.1	0.3097	495	
			50.2	0.3098	495	
			50.2	0.3098	495	
	0.4960	400	50.3	0.4962	792	0.001
			50.1	0.4962	792	
			50.2	0.4962	791	
			50.1	0.4962	792	
			50.1	0.4962	792	

CHEST UNIT

Coefficient of variance (COV) ≤ 0.05 $\quad COV = \frac{\sigma}{y} = \frac{1}{y}\left[\frac{\sum_{n-1}^{N}(y_n - \bar{y})^2}{N-1}\right]^{\frac{1}{2}}$

FSD=100cm

Set values (High kV)			Measured values			COV
kV	Sec	mAs	kV Eff	Sec	mR	
125	0.2	63	121.3	0.1998	689	0.003
			121.3	0.1998	694	
			121.3	0.1998	691	
			121.3	0.1998	691	
			121.3	0.1998	691	
	0.32	80	120.7	0.3199	896	0.002
			120.7	0.3199	895	
			120.7	0.3199	900	
			120.7	0.3199	895	
			120.7	0.3199	895	
	0.4	100	120.7	0.3998	1225	0.001
			120.7	0.3998	1227	
			120.7	0.3998	1227	
			120.7	0.3998	1227	
			120.7	0.3998	1227	

Set values (In between kV)			Measured values			COV
kV	Sec	mAs	kV Eff	Sec	mR	
90	0.10	50	90.1	0.0996	306	0.006
			90.1	0.0997	311	
			90.1	0.0997	308	
			90.1	0.0997	310	
			90.1	0.0997	310	
	0.20	80	86.5	0.1998	462	0.002
			86.5	0.1998	461	
			86.5	0.1998	463	
			86.5	0.1998	461	
			86.5	0.1998	461	
	0.32	125	86.5	0.3199	747	0.001
			86.6	0.3198	745	
			86.6	0.3198	744	
			86.6	0.3198	745	
			86.6	0.3198	745	
	0.45	140	86.7	0.4499	826	0.003
			86.6	0.4500	826	
			86.6	0.4499	831	
			86.6	0.4499	826	
			86.6	0.4499	826	

Set values (Low kV)			Measured values			COV
kV	Sec	mAs	kV Eff	Sec	mR	
70	0.10	50	69.8	0.0998	179	0.009
			69.7	0.0998	180	
			69.9	0.0997	183	
			69.9	0.0997	181	
			69.9	0.0997	182	
	0.20	100	69.8	0.1999	362	0.002
			69.8	0.1998	360	
			69.8	0.1998	361	
			69.8	0.1998	360	
			69.8	0.199	361	
	0.32	160	69.8	0.3199	581	0.009
			69.8	0.3199	592	
			69.8	0.3199	593	
			69.8	0.3199	592	
			69.8	0.3199	593	
	0.45	180	69.8	0.4500	661	0.007
			69.9	0.4500	661	
			69.6	0.4500	650	
			69.6	0.4500	661	
			69.6	0.4500	661	

FLUOROSCOPIC UNIT

Coefficient of variance (COV) ≤ 0.05 $COV = \frac{\sigma}{y} = \frac{1}{y}\left[\frac{\sum_{n-1}^{N}(y_n - \bar{y})^2}{N-1}\right]^{\frac{1}{2}}$

FSD=100cm

Set values (High kV)			Measured values			COV
kV	Sec	mAs	kV Eff	Sec	mR	
120	--	11	111.2	52.5	136	0.005
			111.0	52.5	135	
			111.0	53.0	137	
			111.0	52.5	136	
			111.2	53.0	136	

Set values (In between kV)			Measured values			COV
kV	Sec	mAs	kV Eff	Sec	mR	
90	--	5	87.6	0.0990	50	0.009
			85.6	0.0990	51	
			85.6	0.0990	51	
			85.6	0.0990	51	
			85.6	0.0990	51	
	--	16	88.7	0.0985	169	0.003
			88.6	0.0985	169	
			88.7	0.0985	168	
			88.7	0.0984	168	
			88.7	0.0984	168	
	--	20	87.1	0.0984	200	0.006
			87.1	0.0984	202	
			87.1	0.0988	202	
			87.1	0.0988	203	
			87.1	0.0985	203	
	--	25	86.4	0.0997	251	0.007
			86.5	0.0997	255	
			86.4	0.0997	253	
			86.4	0.0997	253	

Set values (Low kV)			Measured values			COV
kV	Sec	mAs	kV Eff	sec	mR	
70	--	5	67.7	0.0961	32	0.014
			68.1	0.0962	31	
			68.0	0.0974	32	
			68.0	0.0974	32	
			68.0	0.0974	32	
	--	16	70.3	0.0979	111	0.005
			70.4	0.0979	111	
			70.2	0.0979	112	
			70.3	0.0979	112	
			70.3	0.0979	112	
	--	20	68.7	0.0995	132	0.007
			68.6	0.0984	130	
			68.7	0.0984	130	
			68.7	0.0984	130	
			68.7	0.0984	131	
	--	25	68.5	0.0981	161	0.003
			68.5	0.0979	160	
			68.5	0.0981	160	
			68.5	0.0981	161	
			68.5	0.0981	161	

Appendix 1D

LINEARITY OF mA AND mAs

Apparatus: Full function meter (RMI 242) and measuring tape

SHIMADZU CID

Set values: kV= 60

ms	mAs	mR	mR/mAs	X	$\lvert X_1 - X_2 \rvert / (X_1 + X_2) \leq 0.1$
34.6	10	33	3.30	3.30	
		34	3.40		0.010
		33	3.30		
96.5	25	84	3.36	3.37	
		85	3.40		0.010
		84	3.36		
121.4	32	105	3.28	3.30	
		107	3.34		0.015
		105	3.28		
156.5	40	135	3.38	3.40	
		136	3.40		0.000
		136	3.40		

Set values: kV= 70

ms	mAs	mR	mR/mAs	X	$\lvert X_1 - X_2 \rvert / (X_1 + X_2) \leq 0.1$
39.6	10	50	5.00	5.03	
39.6		50	5.00		0.021
39.6		51	5.10		
99.4	20	97	4.85	4.82	
99.4		96	4.80		0.008
99.4		96	4.80		
159.6	32	152	4.75	4.74	
159.6		152	4.75		0.002
159.6		151	4.72		
199.5	40	189	4.73	4.72	
199.5		189	4.73		
199.5		188	4.70		

Set values: kV= 80

ms	mAs	mR	mR/mAs	X	$\left\|X_1 - X_2\right\| / \left(X_1 + X_2\right) \leq 0.1$
49.6	10	64	6.40	6.40	
		63	6.30		0.019
		65	6.50		
99.6	20	124	6.20	6.15	
		123	6.15		0.011
		122	6.10		
199.6	32	193	6.03	6.02	
		192	6.00		0.001
		193	6.03		
249.7	40	240	6.00	6.00	
		240	6.00		
		241	6.03		

Set values: kV= 90

ms	mAs	mR	mR/mAs	X	$\left\|X_1 - X_2\right\| / \left(X_1 + X_2\right) \leq 0.1$
62.6	10	78	7.80	7.83	
		78	7.80		0.014
		79	7.90		
124.6	20	152	7.60	7.62	
		153	7.65		0.009
		152	7.60		
199.6	32	240	7.50	7.48	
		239	7.47		0.004
		240	7.50		
319.9	40	297	7.43	7.42	
		297	7.43		
		296	7.40		

Set values: kV= 100

ms	mAs	mR	mR/mAs	X	$\left\|X_1 - X_2\right\| / \left(X_1 + X_2\right) \leq 0.1$
99.6	10	98	9.80	9.77	
		97	9.70		0.001
		98	9.80		
159.7	20	196	9.80	9.78	
		195	9.75		0.017
		195	9.75		
249.8	32	302	9.44	9.45	
		303	9.47		
		303	9.47		

Set values: kV= 110

ms	mAs	mR	mR/mAs	X	$\left\|X_1 - X_2\right\| / \left(X_1 + X_2\right) \leq 0.1$
159.8	10	119	11.90	12.03	
		121	12.10		0.005
		121	12.10		
199.8	20	239	11.95	11.92	
		238	11.90		0.003
		238	11.90		
249.8	32	384	12.00	11.98	
		383	11.97		0.014
		384	12.00		
399.5	40	493	12.33	12.31	
		492	12.30		
		493	12.33		

PHILIPS DIGITAL DIAGNOST (1)

Set values: kV= 60

ms	mAs	mR	mR/mAs	X	$\left\|X_1 - X_2\right\| / \left(X_1 + X_2\right) \leq 0.1$
11.1	10	36	3.60	3.667	
		37	3.70		0.000
		37	3.70		
22.2	20	74	3.65	3.667	
		73	3.65		0.007
		73	3.65		
35.3	32	119	3.72	3.720	
		119	3.72		0.003
		119	3.72		
44.4	40	148	3.70	3.700	
		148	3.70		
		148	3.70		

Set values: kV= 70

ms	mAs	mR	mR/mAs	X	$\left\|X_1 - X_2\right\| / \left(X_1 + X_2\right) \leq 0.1$
11.1	10	50	5.00	5.000	
		50	5.00		0.003
		50	5.00		
22.2	20	100	5.00	5.033	
		101	5.05		0.005
		101	5.05		
35.3	32	163	5.09	5.083	
		163	5.09		0.002
		162	5.06		
44.4	40	204	5.10	5.100	
		204	5.10		
		204	5.10		

Set values: kV= 81

ms	mAs	mR	mR/mAs	X	$\left\|X_1 - X_2\right\| / \left(X_1 + X_2\right) \leq 0.1$
12.4	10	68	6.80	6.8	
		68	6.80		0.000
		68	6.80		
24.9	20	136	6.80	6.8	
		136	6.80		0.001
		136	6.80		
39.8	32	218	6.81	6.81	
		218	6.81		0.001
		218	6.81		
49.8	40	271	6.80	6.8	
		272	6.80		
		272	6.80		

Set values: kV= 90

ms	mAs	mR	mR/mAs	X	$\left\|X_1 - X_2\right\| / \left(X_1 + X_2\right) \leq 0.1$
13.8	10	83	8.30	8.266	
		83	8.30		0.001
		82	8.20		
27.6	20	166	8.30	8.283	
		167	8.25		0.003
		166	8.30		
44.3	32	267	8.34	8.333	
		267	8.34		
		266	8.31		0.000
55.3	40	333	8.33	8.325	
		333	8.33		
		333	8.33		

Set values: kV= 102

ms	mAs	mR	mR/mAs	X	$\left\|X_1 - X_2\right\| / \left(X_1 + X_2\right) \leq 0.1$
15.6	10	105.0	10.50	10.5333	
		106.0	10.60		0.001
		105.0	10.50		
31.3	20	211.0	10.55	10.5500	
		211.0	10.55		0.002
		211.0	10.55		
50.2	32	339.0	10.59	10.5830	
		338.0	10.56		0.001
		339.0	10.59		
61.7	40	422.4	10.56	10.5600	
		422.4	10.56		
		422.4	10.56		

PHILIPS DIGITAL DIAGNOST (2)

Set values: kV= 50

ms	mAs		mR/mAs	X	$\lvert X_1 - X_2 \rvert / (X_1 + X_2) \leq 0.1$
12.4	10	19	1.90	1.9000	
		19	1.90		0.012
		19	1.90		
24.8	20	39	1.95	1.9500	
		39	1.95		0.005
		39	1.95		
39.7	32	63	1.97	1.9687	
		63	1.97		0.005
		63	1.97		
49.6	40	78	1.95	1.9500	
		78	1.95		
		78	1.95		

Set values: kV=60

ms	mAs	mR	mR/mAs	X	$\lvert X_1 - X_2 \rvert / (X_1 + X_2) \leq 0.1$
11.1	10	30	3.00	3.0000	
		30	3.00		0.027
		30	3.00		
22.2	20	64	3.20	3.1666	
		63	3.15		0.015
		63	3.15		
35.3	32	98	3.06	3.0729	
		99	3.09		0.002
		98	3.06		
44.4	40	123	3.08	3.0583	
		122	3.05		
		122	3.05		

Set values: kV= 70

ms	mAs	mR	mR/mAs	X	$\lvert X_1 - X_2 \rvert / (X_1 + X_2) \leq 0.1$
11.1	10	42	4.20	4.2000	
		42	4.20		0.004
		42	4.20		
22.2	20	85	4.25	4.2330	
		84	4.20		0.001
		85	4.25		
35.3	32	136	4.25	4.2292	
		135	4.22		0.001
		135	4.22		
44.4	40	170	4.25	4.2330	
		169	4.23		
		169	4.23		

Set values: kV= 80

ms	mAs	mR	mR/mAs	X	$\left\|X_1 - X_2\right\| / \left(X_1 + X_2\right) \leq 0.1$
12.4	10	55	5.50	5.5000	
		55	5.50		0.006
		55	5.50		
24.6	20	111	5.55	5.5666	
		112	5.60		0.001
		111	5.55		
39.2	32	179	5.59	5.5729	
		178	5.56		0.001
		178	5.56		
49.2	40	223	5.58	5.55833	
		222	5.55		
		222	5.55		

Set values: kV= 90

ms	mAs	mR	mR/mAs	X	$\left\|X_1 - X_2\right\| / \left(X_1 + X_2\right) \leq 0.1$
13.8	10	87	8.70	8.6330	
		86	8.60		0.001
		86	8.60		
27.6	20	173	8.65	8.6500	
		173	8.65		0.000
		173	8.65		
44.3	32	277	8.66	8.6458	
		277	8.66		0.003
		276	8.63		
55.3	40	348	8.70	8.7000	
		348	8.70		
		348	8.70		

Set values: kV=100

ms	mAs	mR	mR/mAs	X	$\left\|X_1 - X_2\right\| / \left(X_1 + X_2\right) \leq 0.1$
15.3	10	106	10.60	10.6666	
		106	10.60		0.004
		107	10.70		
30.7	20	212	10.60	10.5833	
		211	10.55		0.003
		212	10.60		
49.2	32	341	10.66	10.6563	
		341	10.66		0.003
		341	10.66		
61.5	40	434	10.85	10.7250	
		426	10.65		
		427	10.68		

Set values: kV= 110

ms	mAs	mR	mR/mAs	X	$\lvert X_1 - X_2 \rvert / (X_1 + X_2) \leq 0.1$
16.9	10	127	12.70	12.7666	
		129	12.90		0.002
		127	12.70		
33.8	20	254	12.75	12.7167	
		255	12.70		0.003
		254	12.75		
54.1	32	409	12.78	12.78125	
		409	12.78		0.006
		409	12.78		
68.3	40	521	13.03	12.97417	
		511	12.78		
		521	13.03		

CHEST UNIT

Set values: kV=70

ms	mAs	mR	mR/mAs	X	$\lvert X_1 - X_2 \rvert / (X_1 + X_2) \leq 0.1$
20	10	12	1.20	1.2333	
		12	1.20		0.000
		13	1.30		
40	20	25	1.25	1.2333	
		24	1.20		0.006
		25	1.25		
63	32	38	1.19	1.2187	
		40	1.25		0.006
		39	1.22		
80	40	49	1.23	1.2333	
		49	1.25		
		50			

Set values: kV= 90

ms	mAs	mR	mR/mAs	X	$\lvert X_1 - X_2 \rvert / (X_1 + X_2) \leq 0.1$
20	10	28	2.80	2.7000	
		27	2.70		0.006
		26	2.60		
40	20	53	2.65	2.6666	
		53	2.65		0.004
		54	2.70		
63	32	83	2.59	2.6458	
		86	2.69		0.004
		85	2.66		
80	40	108	2.70	2.6666	
		106	2.65		
		106	2.65		

Set values: kV= 110

ms	mAs	mR	mR/mAs	X	$\left\|X_1 - X_2\right\| / \left(X_1 + X_2\right) \leq 0.1$
25	10	46	4.60	4.53	
		45	4.50		0.007
		45	4.50		
50	20	94	4.70	4.60	
		91	4.55		0.010
		91	4.55		
80	32	143	4.47	4.50	
		146	4.56		0.001
		143	4.47		
100	40	177	4.43	4.51	
		182	4.55		
		182	4.55		

Set values: kV= 125

ms	mAs	mR	mR/mAs	X	$\left\|X_1 - X_2\right\| / \left(X_1 + X_2\right) \leq 0.1$
32	10	65	6.50	6.50	
		66	6.60		0.022
		64	6.40		
63	20	123	6.15	6.22	
		124	6.20		0.014
		126	6.30		
100	32	194	6.06	6.04	
		194	6.06		0.002
		192	6.00		
125	40	241	6.03	6.02	
		242	6.05		
		239	5.98		

FLUOROSCOPIC UNIT

Set values: kV= 70

ms	mAs	mR	mR/mAs	X	$\left\|X_1 - X_2\right\| / \left(X_1 + X_2\right) \leq 0.1$
--	5	32	7.00	7.00	
--		32	7.00		0.003
--		32	7.00		
--	16	113	7.06	7.04	
--		112	7.00		0.034
--		113	7.06		
--	20	131	6.55	6.58	
--		132	6.60		0.002
--		132	6.60		
--	25	164	6.56	6.56	
--		164	6.56		
--		164	6.56		

Set values: kV= 90

ms	mAs	mR	mR/mAs	X	$\left\|X_1 - X_2\right\| / \left(X_1 + X_2\right) \leq 0.1$
--	5	50	10.00	10.13	
--		51	10.20		0.018
--		51	10.20		
--	16	167	10.44	10.50	
--		169	10.56		0.019
--		168	10.50		
--	20	201	10.05	10.10	
--		203	10.15		0.004
--		202	10.10		
--	25	255	10.20	10.19	
--		254	10.16		
--		255	10.20		

Appendix 1E

BEAM ALIGNMENT AND CENTERING

SHIMADZU CID

Set up values: kV=60 mAs=2 ms=4 FSD=100cm

Beam centring

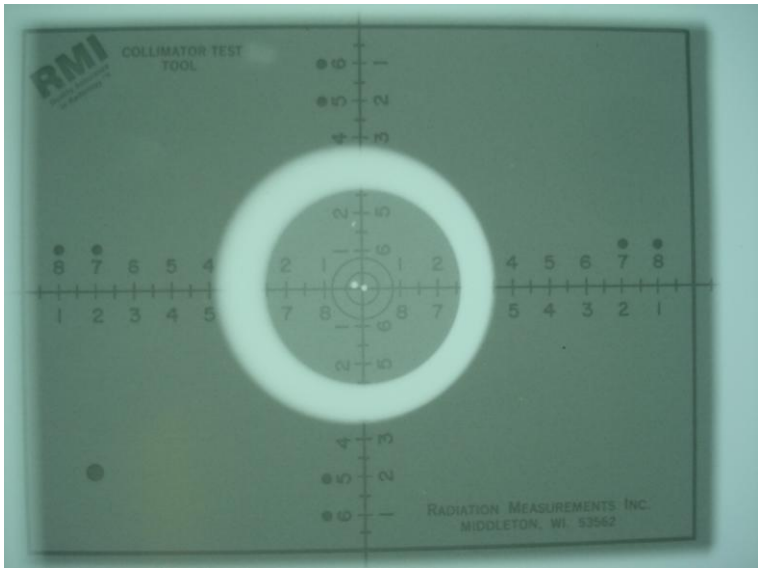

Beam alignment

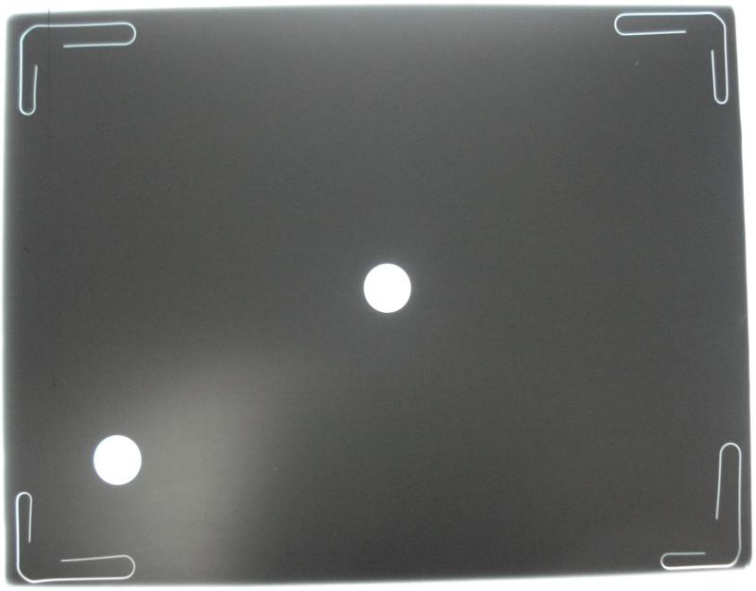

PHILIPS DIGITAL DIAGNOST (1)

Set up values: kV=60 mAs=2 ms=22.4 FSD=100cm

Beam centring

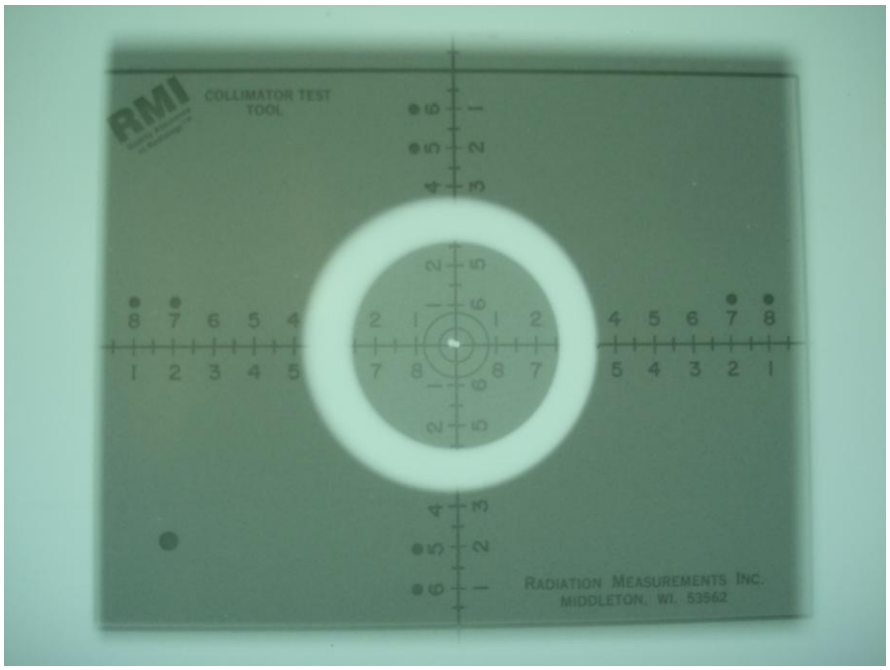

Beam alignment

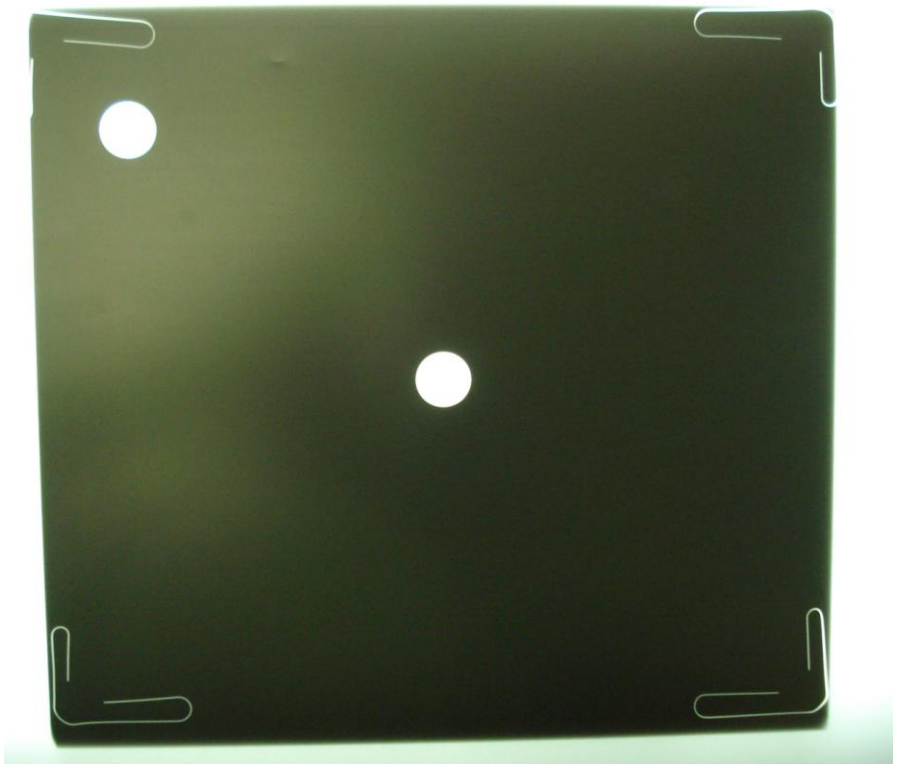

PHILIPS DIGITAL DIAGNOST (2)

Set up values: kV=60 mAs=2 ms=23.4 FSD=100cm

Beam centring

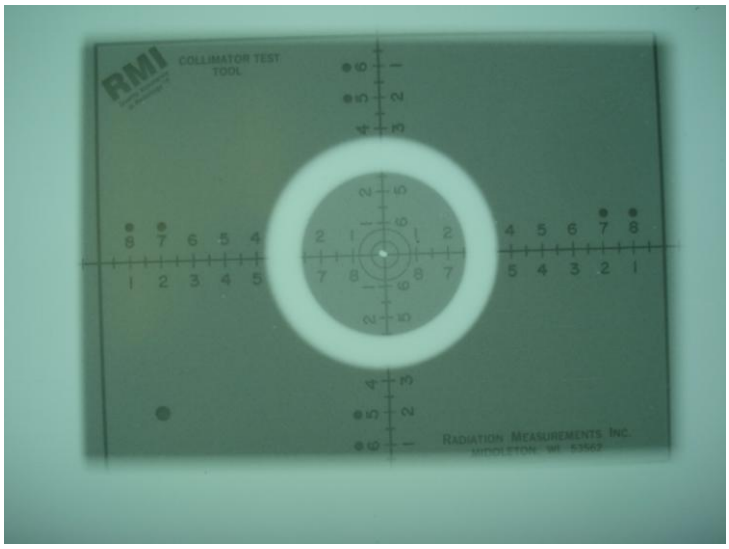

Beam alignment

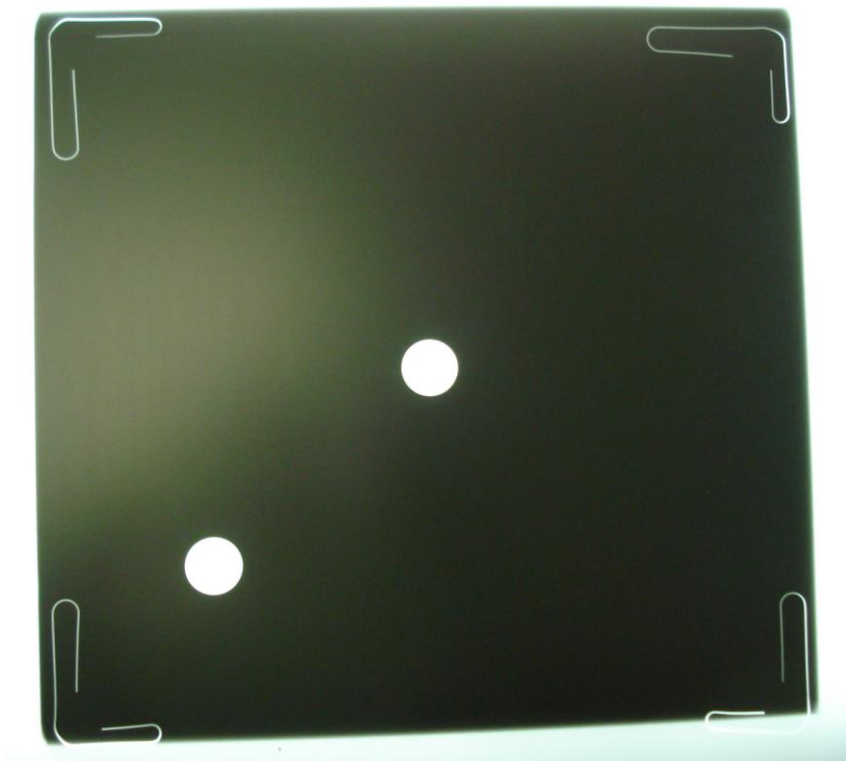

FLUOROSCOPIC UNIT

Set up values: kV=60 mAs=20 ms=100 FSD=100cm

Beam centring

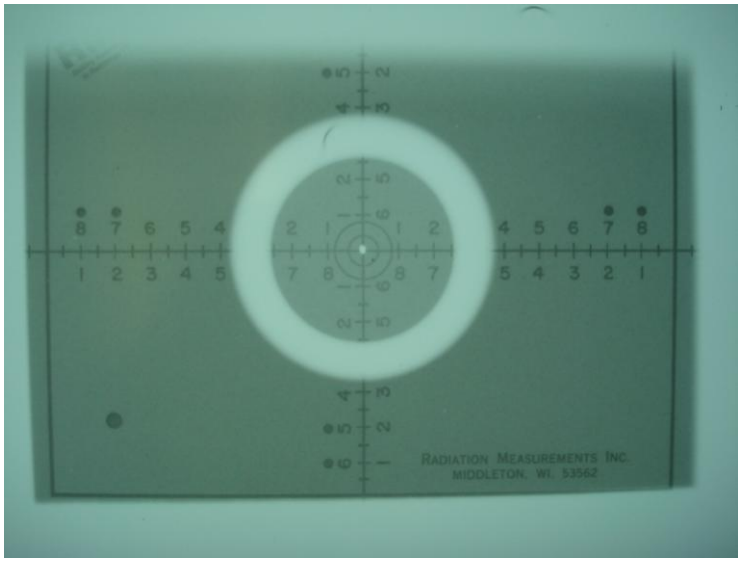

Beam alignment

CHEST UNIT

Set up values: kV=58 mAs=2.8 ms=5.6 FSD=100cm

Beam centring

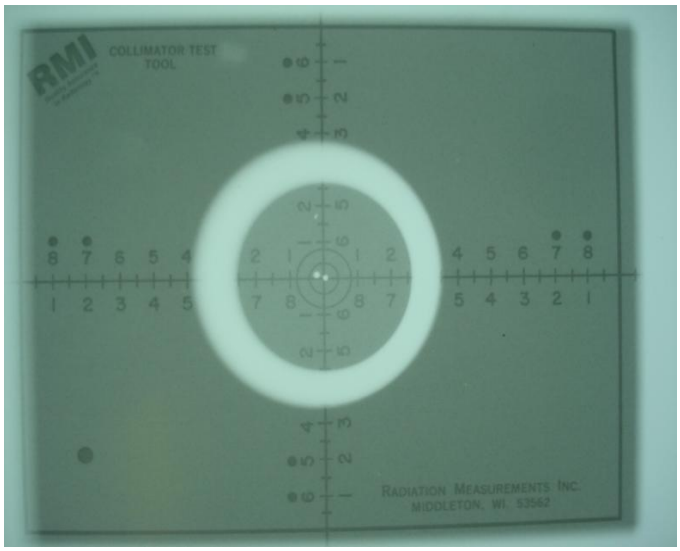

Beam alignment

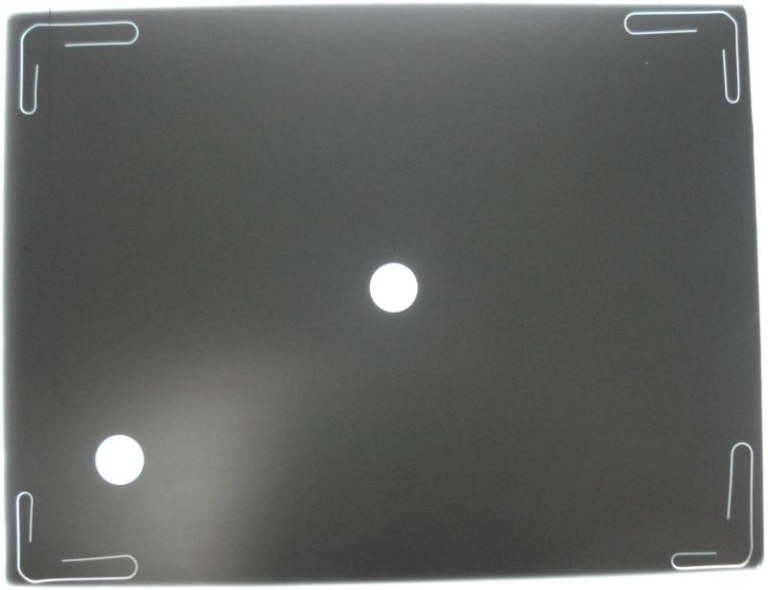

Appendix 2

ENTRANCE SURFACE DOSE TEST

SHIMADZU CID

Exam	TLD NO.	RAD	q_{js}	RCF	ECC_j	Qj	DOSE	ESD
Cervical Spine (AP)	1	1	98.49	106.09	1.08	29.51	0.30	3.00
	2	1	104.60	106.09	1.01	28.66	0.27	2.74
	3	1	98.50	106.09	1.08	25.41	0.26	2.58
	4	1	107.30	106.09	0.99	28.15	0.26	2.62
	5	1	116.80	106.09	0.91	28.01	0.24	2.40
	6	1	107.60	106.09	0.99	28.89	0.27	2.68
	7	1	94.06	106.09	1.13	28.69	0.31	3.05
	8	1	103.50	106.09	1.03	27.46	0.27	2.65
	9	1	101.00	106.09	1.05	28.13	0.28	2.79
Cervical Spine (LAT)	10	1	109.70	106.09	0.97	36.67	0.33	3.34
	11	1	97.78	106.09	1.09	32.78	0.34	3.35
	12	1	103.60	106.09	1.02	38.75	0.37	3.74
	13	1	113.30	106.09	0.94	37.25	0.33	3.29
	14	1	99.52	106.09	1.07	38.67	0.39	3.89
	15	1	110.40	106.09	0.96	33.25	0.30	3.01
	16	1	123.10	106.09	0.86	34.49	0.28	2.80
	17	1	104.20	106.09	1.02	32.37	0.31	3.11
	18	1	104.50	106.09	1.02	34.39	0.33	3.29
Skull (AP)	19	1	100.60	106.09	1.05	37.18	0.37	3.70
	20	1	103.30	106.09	1.03	37.98	0.37	3.68
	21	1	102.30	106.09	1.04	41.78	0.41	4.08
	22	1	105.50	106.09	1.01	42.63	0.40	4.04
	23	1	101.00	106.09	1.05	39.49	0.39	3.91
	24	1	101.70	106.09	1.04	41.77	0.41	4.11
	25	1	103.00	106.09	1.03	41.85	0.41	4.06
	26	1	97.85	106.09	1.08	44.08	0.45	4.50
	27	1	105.40	106.09	1.01	37.77	0.36	3.58
Skull (LAT)	28	1	106.90	106.09	0.99	29.48	0.28	2.76
	29	1	99.37	106.09	1.07	30.74	0.31	3.09
	30	1	105.20	106.09	1.01	33.64	0.32	3.20
	31	1	108.50	106.09	0.98	31.65	0.29	2.92
	32	1	111.80	106.09	0.95	29.48	0.26	2.64
	33	1	96.76	106.09	1.10	28.54	0.29	2.95
	34	1	98.23	106.09	1.08	31.05	0.32	3.16
	35	1	107.30	106.09	0.99	32.31	0.30	3.01
	36	1	120.40	106.09	0.88	28.97	0.24	2.41
Abdomen (AP)	1	1	98.49	106.09	1.08	52.6	0.53	5.34
	2	1	104.60	106.09	1.01	50.96	0.49	4.87
	3	1	98.50	106.09	1.08	50.38	0.51	5.11
	4	1	107.30	106.09	0.99	51.9	0.48	4.84
	5	1	116.80	106.09	0.91	48.45	0.41	4.15
	6	1	107.60	106.09	0.99	49.78	0.46	4.63

	7	1	94.06	106.09	1.13	51.38	0.55	5.46
	8	1	103.50	106.09	1.03	51.44	0.50	4.97
	9	1	101.00	106.09	1.05	50.44	0.50	4.99
Pelvis (AP)	10	1	109.70	106.09	0.97	50.93	0.46	4.64
	11	1	97.78	106.09	1.09	48.34	0.49	4.94
	12	1	103.60	106.09	1.02	48.7	0.47	4.70
	13	1	113.30	106.09	0.94	50.07	0.44	4.42
	14	1	99.52	106.09	1.07	50.41	0.51	5.07
	15	1	110.40	106.09	0.96	49.89	0.45	4.52
	16	1	123.10	106.09	0.86	49.51	0.40	4.02
	17	1	104.20	106.09	1.02	46.45	0.45	4.46
	18	1	104.50	106.09	1.02	48.86	0.47	4.68
Lumber Spine (AP)	19	1	100.60	106.09	1.05	54.25	0.54	5.39
	20	1	103.30	106.09	1.03	52.06	0.50	5.04
	21	1	102.30	106.09	1.04	56.24	0.55	5.50
	22	1	105.50	106.09	1.01	55.31	0.52	5.24
	23	1	101.00	106.09	1.05	54.52	0.54	5.40
	24	1	101.70	106.09	1.04	52.38	0.52	5.15
	25	1	103.00	106.09	1.03	56.39	0.55	5.47
	26	1	97.85	106.09	1.08	59.77	0.61	6.11
	27	1	105.40	106.09	1.01	55.54	0.53	5.27
Lumber Spine (LAT)	28	1	106.90	106.09	0.99	103.3	0.97	9.66
	29	1	99.37	106.09	1.07	98.17	0.99	9.88
	30	1	105.20	106.09	1.01	107.6	1.02	10.23
	31	1	108.50	106.09	0.98	96.68	0.89	8.91
	32	1	111.80	106.09	0.95	104.3	0.93	9.33
	33	1	96.76	106.09	1.10	97.11	1.00	10.04
	34	1	98.23	106.09	1.08	99.82	1.02	10.16
	35	1	107.30	106.09	0.99	98.92	0.92	9.22
	36	1	120.40	106.09	0.88	102	0.85	8.47
Chest (PA)	1	0.125	45.62	296.97	0.81	19.25	0.05	0.53
	2	0.125	32.15	296.97	1.15	19.85	0.08	0.77
	3	0.125	41.54	296.97	0.89	21.64	0.07	0.65
	4	0.125	42.29	296.97	0.88	22.78	0.07	0.67
	5	0.125	38.21	296.97	0.97	19.03	0.06	0.62
	6	0.125	27.82	296.97	1.33	20.14	0.09	0.90
	7	0.125	38.04	296.97	0.98	20.38	0.07	0.67
	8	0.125	33.68	296.97	1.10	19.86	0.07	0.74
	9	0.125	40.33	296.97	0.92	16.44	0.05	0.51
Chest (LAT)	10	0.125	26.77	296.97	1.39	20.13	0.09	0.94
	11	0.125	16.01	296.97	2.32	19.2	0.15	1.50
	12	0.125	30.04	296.97	1.24	19.86	0.08	0.83
	13	0.125	33.29	296.97	1.12	19.83	0.07	0.74
	14	0.125	38.74	296.97	0.96	20.39	0.07	0.66
	15	0.125	47.87	296.97	0.78	20.16	0.06	0.58
	16	0.125	39.15	296.97	0.95	19.99	0.06	0.64
	17	0.125	45.52	296.97	0.82	20.14	0.06	0.55
	18	0.125	33.74	296.97	1.10	20.99	0.08	0.78

PHILIPS DIGITAL DIAGNOST (1)

Exam	TLD NO.	RAD	q_j	RCF	ECC_j	Qj	DOSE	ESD
Skull (AP)	1	1	98.49	106.09	1.08	36.83	0.37	3.74
	2	1	104.60	106.09	1.01	36.44	0.35	3.48
	3	1	98.50	106.09	1.08	38.84	0.39	3.94
	4	1	107.30	106.09	0.99	37.77	0.35	3.52
	5	1	116.80	106.09	0.91	36.13	0.31	3.09
	6	1	107.60	106.09	0.99	36.26	0.34	3.37
	7	1	94.06	106.09	1.13	40.3	0.43	4.28
	8	1	103.50	106.09	1.03	40.6	0.39	3.92
	9	1	101.00	106.09	1.05	40.96	0.41	4.06
Skull (LAT)	10	1	109.70	106.09	0.97	24.9	0.23	2.27
	11	1	97.78	106.09	1.09	23.06	0.24	2.36
	12	1	103.60	106.09	1.02	24.78	0.24	2.39
	13	1	113.30	106.09	0.94	22.98	0.20	2.03
	14	1	99.52	106.09	1.07	24	0.24	2.41
	15	1	110.40	106.09	0.96	25.42	0.23	2.30
	16	1	123.10	106.09	0.86	24.35	0.20	1.98
	17	1	104.20	106.09	1.02	25.4	0.24	2.44
	18	1	104.50	106.09	1.02	25.86	0.25	2.47
Cervical Spine (AP)	19	1	100.60	106.09	1.05	38.86	0.39	3.86
	20	1	103.30	106.09	1.03	34.37	0.33	3.33
	21	1	102.30	106.09	1.04	33.13	0.32	3.24
	22	1	105.50	106.09	1.01	33.34	0.32	3.16
	23	1	101.00	106.09	1.05	30.1	0.30	2.98
	24	1	101.70	106.09	1.04	35.97	0.35	3.54
	25	1	103.00	106.09	1.03	36.17	0.35	3.51
	26	1	97.85	106.09	1.08	34.43	0.35	3.52
	27	1	105.40	106.09	1.01	36.31	0.34	3.44
Cervical Spine (LAT)	28	1	106.90	106.09	0.99	33.07	0.31	3.09
	29	1	99.37	106.09	1.07	36.37	0.37	3.66
	30	1	105.20	106.09	1.01	34.79	0.33	3.31
	31	1	108.50	106.09	0.98	33.77	0.31	3.11
	32	1	111.80	106.09	0.95	35.12	0.31	3.14
	33	1	96.76	106.09	1.10	34.98	0.36	3.62
	34	1	98.23	106.09	1.08	34.78	0.35	3.54
	35	1	107.30	106.09	0.99	33.85	0.32	3.15
	36	1	120.40	106.09	0.88	35.67	0.30	2.96
Pelvis (AP)	1	1	98.49	106.09	1.08	39.09	0.40	3.97
	2	1	104.60	106.09	1.01	43.26	0.41	4.14
	3	1	98.50	106.09	1.08	39.68	0.40	4.03
	4	1	107.30	106.09	0.99	39.34	0.37	3.67
	5	1	116.80	106.09	0.91	38.59	0.33	3.30
	6	1	107.60	106.09	0.99	43.35	0.40	4.03
	7	1	94.06	106.09	1.13	39.56	0.42	4.21
	8	1	103.50	106.09	1.03	42.69	0.41	4.12
	9	1	101.00	106.09	1.05	42.55	0.42	4.21
Abdomen	10	1	109.70	106.09	0.97	49.21	0.45	4.49

(AP)	11	1	97.78	106.09	1.09	48.92	0.50	5.00
	12	1	103.60	106.09	1.02	50.18	0.48	4.84
	13	1	113.30	106.09	0.94	47.69	0.42	4.21
	14	1	99.52	106.09	1.07	49.3	0.50	4.95
	15	1	110.40	106.09	0.96	48.99	0.44	4.44
	16	1	123.10	106.09	0.86	49.57	0.40	4.03
	17	1	104.20	106.09	1.02	49.39	0.47	4.74
	18	1	104.50	106.09	1.02	48.8	0.47	4.67
Lumber Spine (AP)	19	1	100.60	106.09	1.05	54.14	0.54	5.38
	20	1	103.30	106.09	1.03	53.67	0.52	5.20
	21	1	102.30	106.09	1.04	55.1	0.54	5.39
	22	1	105.50	106.09	1.01	53.92	0.51	5.11
	23	1	101.00	106.09	1.05	49.75	0.49	4.93
	24	1	101.70	106.09	1.04	48.93	0.48	4.81
	25	1	103.00	106.09	1.03	49.54	0.48	4.81
	26	1	97.85	106.09	1.08	49.23	0.50	5.03
	27	1	105.40	106.09	1.01	49.99	0.47	4.74
Lumber Spine (LAT)	28	1	106.90	106.09	0.99	87.47	0.82	8.18
	29	1	99.37	106.09	1.07	80.15	0.81	8.07
	30	1	105.20	106.09	1.01	88.56	0.84	8.42
	31	1	108.50	106.09	0.98	86.87	0.80	8.01
	32	1	111.80	106.09	0.95	85.19	0.76	7.62
	33	1	96.76	106.09	1.10	87.23	0.90	9.02
	34	1	98.23	106.09	1.08	86.87	0.88	8.84
	35	1	107.30	106.09	0.99	86.8	0.81	8.09
	36	1	120.40	106.09	0.88	88.9	0.74	7.38
Chest (PA)	1	0.125	45.62	296.97	0.81	19.91	0.05	0.55
	2	0.125	32.15	296.97	1.15	21.01	0.08	0.82
	3	0.125	41.54	296.97	0.89	21.29	0.06	0.64
	4	0.125	42.29	296.97	0.88	21.35	0.06	0.63
	5	0.125	38.21	296.97	0.97	21.24	0.07	0.69
	6	0.125	27.82	296.97	1.33	22.09	0.10	0.99
	7	0.125	38.04	296.97	0.98	20.57	0.07	0.68
	8	0.125	33.68	296.97	1.10	20.15	0.07	0.75
	9	0.125	40.33	296.97	0.92	22.34	0.07	0.69
Chest (LAT)	10	0.125	26.77	296.97	1.39	20.56	0.10	0.96
	11	0.125	16.01	296.97	2.32	22.92	0.18	1.79
	12	0.125	30.04	296.97	1.24	23.6	0.10	0.98
	13	0.125	33.29	296.97	1.12	23.84	0.09	0.90
	14	0.125	38.74	296.97	0.96	22.79	0.07	0.74
	15	0.125	47.87	296.97	0.78	22.03	0.06	0.58
	16	0.125	39.15	296.97	0.95	23.17	0.07	0.74
	17	0.125	45.52	296.97	0.82	23.08	0.06	0.63
	18	0.125	33.74	296.97	1.10	21.86	0.08	0.81

PHILIPS DIGITAL DIAGNOST (2)

Exam	TLD NO.	RAD	q_j	RCF	ECC_j	Qj	DOSE (RAD)	ESD (mGy)
Pelvis (AP)	1	1	98.49	106.09	1.08	43	0.44	4.37
	2	1	104.60	106.09	1.01	42.2	0.40	4.03
	4	1	107.30	106.09	0.99	38.1	0.36	3.55
	5	1	116.80	106.09	0.91	37.8	0.32	3.24
	6	1	98.49	106.09	1.08	38.96	0.40	3.96
	7	1	104.60	106.09	1.01	39.57	0.38	3.78
	9	1	107.30	106.09	0.99	38.18	0.36	3.56
	10	1	116.80	106.09	0.91	41.98	0.36	3.59
	11	1	107.60	106.09	0.99	41.09	0.38	3.82
Abdomen (AP)	12	1	94.06	106.09	1.13	37.72	0.40	4.01
	13	1	101.00	106.09	1.05	42.63	0.42	4.22
	16	1	109.70	106.09	0.97	42.64	0.39	3.89
	17	1	97.78	106.09	1.09	37.61	0.38	3.85
	18	1	103.60	106.09	1.02	37.98	0.37	3.67
	20	1	113.30	106.09	0.94	38.93	0.34	3.44
	21	1	123.10	106.09	0.86	40.35	0.33	3.28
	22	1	104.20	106.09	1.02	42.69	0.41	4.10
	25	1	104.50	106.09	1.02	38.35	0.37	3.67
Lumber Spine (AP)	27	1	103.30	106.09	1.03	47.92	0.46	4.64
	28	1	102.30	106.09	1.04	48.41	0.47	4.73
	29	1	105.50	106.09	1.01	49.14	0.47	4.66
	30	1	103.00	106.09	1.03	49.38	0.48	4.79
	31	1	105.40	106.09	1.01	42.29	0.40	4.01
	32	1	106.90	106.09	0.99	53.41	0.50	5.00
	33	1	99.37	106.09	1.07	54.63	0.55	5.50
	34	1	105.20	106.09	1.01	48.28	0.46	4.59
	35	1	108.50	106.09	0.98	52.45	0.48	4.83
Lumber Spine (LAT)	36	1	111.80	106.09	0.95	97.59	0.87	8.73
	37	1	96.76	106.09	1.10	96.98	1.00	10.02
	38	1	98.23	106.09	1.08	91.98	0.94	9.36
	39	1	107.30	106.09	0.99	93.96	0.88	8.76
	40	1	120.40	106.09	0.88	99.28	0.82	8.25
	1	1	98.49	106.09	1.08	99.67	1.01	10.12
	2	1	104.60	106.09	1.01	100.3	0.96	9.59
	4	1	107.30	106.09	0.99	98.76	0.92	9.20
	5	1	116.80	106.09	0.91	98.19	0.84	8.41
Skull (AP)	36	1	111.80	106.09	0.95	29.84	0.27	2.67
	37	1	96.76	106.09	1.10	30.34	0.31	3.14
	38	1	98.23	106.09	1.08	33.96	0.35	3.46
	39	1	107.30	106.09	0.99	29.1	0.27	2.71
	40	1	120.40	106.09	0.88	28.25	0.23	2.35
	10	1	116.80	106.09	0.91	29.67	0.25	2.54
	11	1	107.60	106.09	0.99	31.38	0.29	2.92
	12	1	94.06	106.09	1.13	29.5	0.31	3.14
	13	1	101.00	106.09	1.05	29.36	0.29	2.91
Skull	27	1	103.30	106.09	1.03	28.49	0.28	2.76

(LAT)	28	1	102.30	106.09	1.04	26.73	0.26	2.61
	29	1	105.50	106.09	1.01	28.37	0.27	2.69
	30	1	103.00	106.09	1.03	29.93	0.29	2.91
	31	1	105.40	106.09	1.01	26.47	0.25	2.51
	32	1	106.90	106.09	0.99	25.28	0.24	2.36
	33	1	99.37	106.09	1.07	27.37	0.28	2.75
	34	1	105.20	106.09	1.01	27.77	0.26	2.64
	35	1	108.50	106.09	0.98	26.94	0.25	2.48
Cervical Spine (AP)	1	1	98.49	106.09	1.08	26.92	0.27	2.73
	2	1	104.60	106.09	1.01	28.41	0.27	2.72
	4	1	107.30	106.09	0.99	29.14	0.27	2.72
	5	1	116.80	106.09	0.91	29.28	0.25	2.51
	6	1	98.49	106.09	1.08	29.29	0.30	2.97
	7	1	104.60	106.09	1.01	31.41	0.30	3.00
	9	1	107.30	106.09	0.99	31.63	0.29	2.95
	10	1	116.80	106.09	0.91	32.28	0.28	2.76
	11	1	107.60	106.09	0.99	31.45	0.29	2.92
Cervical Spine (LAT)	12	1	94.06	106.09	1.13	32.59	0.35	3.46
	13	1	101.00	106.09	1.05	32.98	0.33	3.27
	16	1	109.70	106.09	0.97	31.98	0.29	2.92
	17	1	97.78	106.09	1.09	31.28	0.32	3.20
	18	1	103.60	106.09	1.02	32.98	0.32	3.18
	20	1	113.30	106.09	0.94	33.45	0.30	2.95
	21	1	123.10	106.09	0.86	33.54	0.27	2.72
	22	1	104.20	106.09	1.02	32.45	0.31	3.11
	25	1	104.50	106.09	1.02	31.03	0.30	2.97
Chest (PA)	1	0.125	45.62	296.97	0.81	30.44	0.08	0.83
	2	0.125	32.15	296.97	1.15	19.88	0.08	0.77
	3	0.125	41.54	296.97	0.89	19.53	0.06	0.59
	4	0.125	42.29	296.97	0.88	19.09	0.06	0.56
	5	0.125	38.21	296.97	0.97	18.59	0.06	0.61
	6	0.125	27.82	296.97	1.33	20.49	0.09	0.92
	7	0.125	38.04	296.97	0.98	20.51	0.07	0.67
	8	0.125	33.68	296.97	1.10	20.51	0.08	0.76
	9	0.125	40.33	296.97	0.92	20.52	0.06	0.64
Chest (LAT)	10	0.125	26.77	296.97	1.39	29.3	0.14	1.37
	11	0.125	16.01	296.97	2.32	28.6	0.22	2.23
	12	0.125	30.04	296.97	1.24	27.58	0.11	1.15
	13	0.125	33.29	296.97	1.12	27.81	0.10	1.04
	14	0.125	38.74	296.97	0.96	28.78	0.09	0.93
	15	0.125	47.87	296.97	0.78	27.27	0.07	0.71
	16	0.125	39.15	296.97	0.95	27.14	0.09	0.87
	17	0.125	45.52	296.97	0.82	28.2	0.08	0.77
	18	0.125	33.74	296.97	1.10	28.04	0.10	1.04

FLUOROSCOPIC UNIT

Exam.	TLD NO.	RAD	q_j	RCF	ECC_j	Qj	DOSE (RAD)	ESD (mGy)
Lumber Spine (AP)	1	1	98.49	106.09	1.08	42.4	0.43	4.31
	2	1	104.60	106.09	1.01	42.28	0.40	4.04
	4	1	107.30	106.09	0.99	41.71	0.39	3.89
	5	1	116.80	106.09	0.91	41.92	0.36	3.59
	6	1	98.49	106.09	1.08	36.54	0.37	3.71
	7	1	104.60	106.09	1.01	38.12	0.36	3.64
	9	1	107.30	106.09	0.99	42.76	0.40	3.99
	10	1	116.80	106.09	0.91	36.75	0.31	3.15
	11	1	107.60	106.09	0.99	36.21	0.34	3.37
Lumber Spine (LAT)	12	1	94.06	106.09	1.13	71.25	0.76	7.57
	13	1	101.00	106.09	1.05	82.4	0.82	8.16
	16	1	109.70	106.09	0.97	85.69	0.78	7.81
	17	1	97.78	106.09	1.09	70.6	0.72	7.22
	18	1	103.60	106.09	1.02	75.43	0.73	7.28
	20	1	113.30	106.09	0.94	76.8	0.68	6.78
	21	1	123.10	106.09	0.86	82.19	0.67	6.68
	22	1	104.20	106.09	1.02	82.25	0.79	7.89
	25	1	104.50	106.09	1.02	82.43	0.79	7.89
Abdomen (AP)	27	1	103.30	106.09	1.03	35.93	0.35	3.48
	28	1	102.30	106.09	1.04	32.53	0.32	3.18
	29	1	105.50	106.09	1.01	39.63	0.38	3.76
	30	1	103.0	106.09	1.03	41.11	0.40	3.99
	31	1	105.40	106.09	1.01	35.8	0.34	3.40
	32	1	106.90	106.09	0.99	31.79	0.30	2.97
	33	1	99.37	106.09	1.07	41.1	0.41	4.14
	34	1	105.20	106.09	1.01	32.38	0.31	3.08
	35	1	108.50	106.09	0.98	37.21	0.34	3.43
Pelvis (AP)	36	1	111.80	106.09	0.95	36.06	0.32	3.23
	37	1	96.76	106.09	1.10	34.63	0.36	3.58
	38	1	98.23	106.09	1.08	38.07	0.39	3.88
	39	1	107.30	106.09	0.99	34.92	0.33	3.25
	40	1	120.40	106.09	0.88	38.86	0.32	3.23
	1	1	98.49	106.09	1.08	38.05	0.39	3.86
	2	1	104.60	106.09	1.01	40.95	0.39	3.91
	4	1	107.30	106.09	0.99	42.32	0.39	3.94
	5	1	116.80	106.09	0.91	39.29	0.34	3.36
Chest (PA)	1	0.125	45.62	296.97	0.81	20.65	0.06	0.57
	2	0.125	32.15	296.97	1.15	20.2	0.08	0.79
	3	0.125	41.54	296.97	0.89	19.97	0.06	0.60
	4	0.125	42.29	296.97	0.88	20.68	0.06	0.61
	5	0.125	38.21	296.97	0.97	20.23	0.07	0.66
	6	0.125	27.82	296.97	1.33	19.99	0.09	0.90
	7	0.125	38.04	296.97	0.98	19.89	0.07	0.65
	8	0.125	33.68	296.97	1.10	19.96	0.07	0.74
	9	0.125	40.33	296.97	0.92	20.9	0.06	0.65
Chest	10	0.125	26.77	296.97	1.39	27.61	0.13	1.29

(LAT)	11	0.125	16.01	296.97	2.32	29.5	0.23	2.30
	12	0.125	30.04	296.97	1.24	24.71	0.10	1.03
	13	0.125	33.29	296.97	1.12	30.89	0.12	1.16
	14	0.125	38.74	296.97	0.96	31.65	0.10	1.02
	15	0.125	47.87	296.97	0.78	31.66	0.08	0.83
	16	0.125	39.15	296.97	0.95	28.68	0.09	0.92
	17	0.125	45.52	296.97	0.82	30.33	0.08	0.83
	18	0.125	33.74	296.97	1.10	27.46	0.10	1.02

CHEST UNIT

Exam	TLD NO.	RAD	q_j	RCF	ECC_j	Qj	DOSE (RAD)	ESD (mGy)
Chest	1	0.125	45.56	269.2494	0.184647	23.44	0.02	0.16
(PA)	2	0.125	42.51	269.2494	0.791724	24.59	0.07	0.72
	3	0.125	33.24	269.2494	1.01252	23.93	0.09	0.90
	4	0.125	37.85	269.2494	0.889199	23.03	0.08	0.76
	5	0.125	28.62	269.2494	1.175967	24.76	0.11	1.08
	6	0.125	35.14	269.2494	0.957774	24.06	0.09	0.86
	7	0.125	30.59	269.2494	1.100235	24.32	0.10	0.99
	8	0.125	35.89	269.2494	0.937759	23.94	0.08	0.83
	9	0.125	29.30	269.2494	1.148675	24.44	0.10	1.04
Chest	10	0.125	32.59	269.2494	1.032715	25.5	0.10	0.98
(LAT)	11	0.125	15.85	269.2494	2.123418	24.99	0.20	1.97
	12	0.125	28.75	269.2494	1.17065	24.96	0.11	1.09
	13	0.125	31.14	269.2494	1.080802	25.37	0.10	1.02
	14	0.125	30.58	269.2494	1.100594	25.53	0.10	1.04
	15	0.125	35.06	269.2494	0.959959	26.16	0.09	0.93
	16	0.125	30.28	269.2494	1.111499	26.28	0.11	1.08
	17	0.125	31.25	269.2494	1.076998	25.26	0.10	1.01
	18	0.125	38.96	269.2494	0.863865	26.27	0.08	0.84

Appendix 3

FREQUENCY DISTRIBUTION FOR EACH EXAMINATION

ABDOMEN (AP)

ESD (mGy) range	Frequency	Cumulative frequency	Relative frequency (% frequency)
2.01-2.55	0	0	0
2.56-3.00	1	1	3
3.01-3.55	7	8	19
3.56-4.00	6	14	17
4.01-4.55	9	23	25
4.56-5.00	10	33	28
5.01-5.55	3	36	8
TOTAL	36		100

PELVIS (AP)

ESD (mGy) range	Frequency	Cumulative frequency	Relative frequency (% frequency)
3.01-3.55	6	6	17
3.56-4.00	13	19	36
4.01-4.55	11	20	30
4.56-5.00	5	35	14
5.01-5.55	1	36	3
TOTAL	36		100

LUMBER SPINE (AP)

ESD (mGy) range	Frequency	Cumulative frequency	Relative frequency (% frequency)
3.01-3.55	2	2	6
3.56-4.00	5	7	14
4.01-4.55	3	10	8
4.56-5.00	11	21	30
5.01-5.55	14	35	39
5.56-6.00	1	36	3
TOTAL	36		100

LUMBER SPINE (LAT)

ESD (mGy) range	Frequency	Cumulative frequency	Relative frequency (% frequency)
6.01-6.55	0	0	0
6.56-7.00	2	2	6
7.01-7.55	3	5	8
7.56-8.00	5	10	14
8.01-8.55	9	19	25
8.56-9.00	4	23	11
9.01-9.55	5	28	14
9.56-10.00	3	31	8
10.01-10.55	5	36	14
TOTAL	36		100

CHEST (PA)

ESD (mGy) range	Frequency	Cumulative frequency	Relative frequency (% frequency)
0.11-0.30	1	1	2
0.31-0.50	0	1	0
0.51-0.70	23	24	51
0.71-0.90	17	41	38
0.91-1.20	4	4	9
TOTAL	45		100

CHEST (LAT)

ESD (mGy) range	Frequency	Cumulative frequency	Relative frequency (% frequency)
0.51-0.80	12	12	27
0.81-1.10	24	36	53
1.11-1.30	3	39	7
1.31-1.50	2	41	4
1.51-1.80	1	42	2
1.81-2.10	1	43	2
2.11-2.30	2	45	4
TOTAL	45		100

CERVICAL SPINE (AP)

ESD (mGy) range	Frequency	Cumulative frequency	Relative frequency (% frequency)
2.01-2.55	2	2	7
2.56-3.00	16	18	59
3.01-3.55	8	26	30
3.56-4.00	1	27	4
TOTAL	27		100

CERVICAL SPINE(LAT)

ESD (mGy) range	Frequency	Cumulative frequency	Relative frequency (% frequency)
2.01-2.55	1	1	4
2.56-3.00	10	11	37
3.01-3.55	13	24	48
3.56-4.00	3	27	11
TOTAL	27		100

SKULL (AP)

ESD (mGy) range	Frequency	Cumulative frequency	Relative frequency (% frequency)
2.01-2.55	2	2	7
2.56-3.00	4	6	15
3.01-3.55	7	13	26
3.56-4.00	7	20	26
4.01-4.55	7	27	26
TOTAL	27		100

SKULL (LAT)

ESD (mGy) range	Frequency	Cumulative frequency	Relative frequency (% frequency)
1.01-1.55	0	0	0
1.56-2.00	1	1	4
2.01-2.55	12	13	45
2.56-3.00	10	23	37
3.01-3.55	2	25	7
3.56-4.00	2	27	7
TOTAL	27		100

Appendix 4

TECHNIQUES USED IN THE X-RAY UNITS CONSIDERED

SHIMADZU CID

Examination	Cervical spine		Skull		Abdomen	Pelvis	Lumber spine		chest	
	AP	LAT	AP	LAT	AP	AP	AP	LAT	PA	LAT
kV	64	66	63	60	64	66	66	70	84	96
mAs	16	20	25	25	32	25	32	80	3.2	5
ms	63	50	48	50	160	125	63	200	16	32
FFD (cm)	110	110	110	110	110	110	110	110	180	180
FSD (cm)	96	84	88	83	85	85	88	80	155	146

PHILIPS DIGITAL DIAGNOST (1)

Examination	Cervical spine		Skull		Abdomen	Pelvis	Lumber spine		Chest	
	AP	LAT	AP	LAT	AP	AP	AP	LAT	PA	LAT
kV	66	66	77	73	81	77	77	90	117	125
mAs	30.3	18.8	23.4	26.6	16.6	14	14.6	20.7	2.56	12.0
ms	80.2	48.5	59.9	64.8	12.9	15.3	30.3	16.6	4.04	21.6
FFD (cm)	110	110	110	110	110	110	110	110	180	180
FSD (cm)	88	84	88	81	83	83	83	73	158	146

PHILIPS DIGITAL DIAGNOST (2)

Examination	Cervical spine		Skull		Abdomen	Pelvis	Lumber spine		Chest	
	AP	LAT	AP	LAT	AP	AP	AP	LAT	PA	LAT
kV	66	66	77	73	81	77	77	90	117	125
mAs	9	70.3	7.04	55.7	15.6	10.9	19.4	22.2	1.88	10.9
ms	24.5	186	18.3	142	19.1	12.7	30.2	30.2	3.35	20.3
FFD (cm)	110	110	110	110	110	110	110	110	180	180
FSD (cm)	89	85	88	82	83	83	82	73	149	141

FLUOROSCOPIC UNIT

Examination	Abdomen	Pelvis	Lumber spine		Chest	
	AP	AP	AP	LAT	PA	LAT
kV	80	84	78	90	117	125
mAs	10	20	5	16.6	8	1
ms	11.4	-	-	20.7	0.4	0.4
FFD (cm)	110	110	110	110	180	180
FSD (cm)	86	87	89	76	157	143

CHEST UNIT

Examination	Chest	
	PA	LAT
kV	125	125
mAs	56	34
ms	180	106
FFD (cm)	180	180
FSD (cm)	155	146

FIELD SIZE AT EACH EXAMINATION

Examination	Field size (cm^2)
Cervical spine (AP)	17 X 29
Cervical spine (LAT)	17 X 29
Skull (AP)	30 X 22
SSkull (LAT)	22 X 30
Abdomen (AP)	35 X 43
Pelvis (AP)	35 X 43
Lumber spine (AP)	18 X 40
Lumber spine (LAT)	18 X 40
Chest (PA)	43 X 35
Chest (LAT)	35 X 43

Appendix 5

EQUIPMENT USED

For quality assurance

- RMI Quality assurance in radiology collimator test tool
  Radiation measurements Inc
  Serial no: 800422-10290

- Glass Cylinder
  Gammex RMI
  Serial no: 800423-8654

- Full Function Meter
  Gammex RMI
  Serial no: 801913-1472

- Paper clips and coins

X-ray units used

- Company: Energy X-ray
  Three phase-12 pulse
  Machine: Shimadzu UD 150L-R11
  Max tube kVp: 150
  AL. equivalent: 1.0 mm
  Serial no: x0162262004

- Digital diagnost (1)
  Constant potential
  Company: Philips

Machine: Optimus 65
Inherent filtration: 0.22AL/75 kV
Serial no: 0602057

- Digital diagnost (2)
  Constant potential
  Company: Philips
  Machine: Optimus 65
  Inherent filtration: 0.22AL/75 kV
  Serial no: 0602056

- Fluorex fine scope 800
  Constant potential
  Company: TECMED (Toshiba)
  Machine: KX0-80N
  Max tube kVp: 150
  AL. equivalent: 1.2 mm
  Serial no: A759381

- Chest unit
  Constant potential
  Company: Shimadzu
  Machine: R30H
  Max tube kVp: 150
  AL. equivalent: 1.0 mm
  Serial no: 011x723102

Equipments used for TLD's

- Ultrasound cleaner
  Julabo
  Type: USR 1
  Serial no: 8336086

- Suction tweezer
  Charles Austen pumps LTD
  Serial no: N3467

- 623 Dosemeter Irradiator
  Pitman instruments
  Type: 6231C
  Serial no: 4-7

- TLD reader (47900 Furnace)
  Thermolyne
  Model: F47920-80
  Serial no: 1057970376487